UTILITY OF TWO DISTINCT MACROMOLECULAR CARRIERS FOR NUCLEIC ACID DELIVERY

John An

A dissertation submitted to the faculty of the University of North Carolina at Chapel Hill in partial fulfillment of the requirement for the degree of Doctor of Philosophy in the Division of Molecular Pharmaceutics at the School of Pharmacy.

Chapel Hill
2008

Approved by:

Moo J. Cho, Ph.D., Advisor

Anthony J. Hickey, Ph.D., Chair

Philip C. Smith, Ph.D., Reader

Michael B Jarstfer, Ph.D., Reader

Rudy Juliano, Ph.D., Reader

ABSTRACT

John An: Utility of Two Distinct Macromolecular Carriers for Nucleic Acid Delivery

(Under the direction of Moo J. Cho, PhD)

The major crux of nucleic acid-based therapy is that nucleic acids are not naturally occurring outside the cell. The systems biology of humans has evolved to detect exogenous nucleic acids as a part of foreign pathogens with efficient mechanisms to destroy and eliminate the threat. Therefore, exogenous naked or unmodified nucleic acids are restricted to the site of their administration and hence are of limited clinical value. A means of delivering therapeutic concentrations of these macromolecules to the target site for a desirable period of time is, thus, an essential component in their development as medicines.

This dissertation describes the origination of two differing approaches to achieve one specific goal, deliver nucleic acid based medicine to cancer cells. The first approach is a gold nanoparticle-based delivery carrier to actively target human derived nasopharyngeal carcinoma specifically over-expressing the folate receptor. Two derivatives were studied which led to the successful synthesis and characterization of the gold nanoparticle-based carrier. A new modular strategy was also developed utilizing some of the therapeutic oligonucleotide as a linker to attach folic acid targeting ligands for increased efficiency. Preliminary in vitro experiments failed to elicit a pharmacologic response. Further in vitro studies focusing on time-dependant uptake and cellular localization may identify the lack of efficacy.

The second approach utilized endogenous albumin as a carrier for therapeutic oligonucleotides. Unlike exogenous macromolecular carriers that must undergo stringent testing to ensure human safety, binding to albumin using its natural ligand, fatty acid, ensures that the carrier is inert and nontoxic. It was proposed that preservation of both ionic and hydrophobic interactions of fatty acids is necessary to bind with high affinity to albumin. An amino (palmitic) acid analog was designed and synthesized in order to produce a handle to attach the therapeutic oligomer while preserving the ionic charge. Initial binding studies reveal a loss of affinity compared to the free palmitic acid, but superior to the currently marketed fatty acylated delivery system. Currently, studies are focusing on the affect of charge interactions in binding to albumin in order to develop a fatty acid analog with enhanced binding properties.

In Loving Memory of my Mother,
who should have been here to share in this achievement.

My trials and tribulations are miniscule compared to her battle against cancer.

ACKNOWLEDGEMENTS

My graduate student life started in the summer of 2001. I had a PharmD, a PhRMA fellowship, and made more money than I ever had with a graduate student stipend. I entered the PhD program with great enthusiasm and a drive that could move mountains, although I had to first learn to use a pipette. Once acclimated to the rigors of school, I quickly developed a new family with many brothers and sisters for support. Through Dr. Cho, I learned what tough love really was, but most importantly, what good science is. I aged in his lab, learned from his knowledge, and developed an ethic that will carry me throughout my scientific career. I tried to beat him by coming in earlier and staying later, only to lose after a month of sleep deprivation. He always had his door open to everyone, so I left my door open but found there to be too much distraction. As I gained experience and independence, I was able to challenge others and answer questions that others could not. Most importantly, I learned to convey knowledge and communicate difficult explanations so others may benefit what I have learned. I know what I know, but most importantly I know what I don't know, or so I believe.

I have many brothers and sisters in science who deserve more gratitude than just an acknowledgement. Listing this family would double the dissertation size, so I will only acknowledge those who guided me. As a teaching assistant for three years, I learned how to present and lecture under the guidance of Professor Boka Hadzija, who rightfully holds more teaching awards than there is space on her office wall. I am deeply grateful to Professor Tony Hickey, my dissertation chair and supportive guide through my graduate studies. To Professor Philip Smith, I still have your *All About Albumin* book. I have passed it along to

Michael Hackett, who is continuing my work. I am also deeply grateful to Professor Michael Jarstfer, who taught me molecular biology and analytical techniques that I have passed on to countless others.

As time moves on, the division changed from Drug Delivery and Disposition to Molecular Pharmaceutics. Professor Leaf Huang needs no introduction as chair of our division and as a distinguished scientist. Incorporation of his knowledge and teaching has only expanded my realization that I have a lot more to learn. I am indebted to Dean Rudy Juliano, the new mayor in town. As director of graduate studies and member of my committee, he also guided me through difficult times. It is a triumph for the School to acquire such a scientist and mentor to both students and professors.

The final acknowledgements are to my family outside of school. After discussing the strenuous times in my graduate studies, my father laughed and reminded me of harder times others faced and I would be blessed if this was the hardest time in my life. Thanks for the kick Dad. To my brother, Andrew, get a job. I will always be there to help give you a kick, an organ, or the shirt off my back. Most importantly, to the pharmacy student and now wife, who did not think I could speak English when we first met in Beard 202, I love you Sarah. I do not dedicate this dissertation to you because I devote my life and future to us.

TABLE OF CONTENTS

Page

LIST OF FIGURES

Page

LIST OF ABBREVIATIONS

AuNP	colloidal gold nanoparticle
BODIPY FL	dipyrromethene boron difluoride
BSA	bovine serum albumin
CPG	controlled-pore glass
DCC	dicyclohexylcarbodiimide
DCM	dichloromethane
DIEA	*N*-diisopropylethylamine
DMAP	4-(dimethylamino)pyridine
DMF	dimethylformamide
dH_2O	distilled water
DMSO	dimethylsufoxide
DNA	deoxyribonucleic acid
cDNA	carrier deoxyribonucleic acid
gDNA	gold-complexed deoxyribonucleic acid
sDNA	thiolated deoxyribonucleic acid
DNAse	deoxyribonuclease
ds	double stranded
DSP	dithiobis(succinimidyl propionate)
DTT	dithiothreitol
EDC	1-ethyl-3-(3-dimethylaminopropyl)carbodi*imide*
EDTA	ethylenediaminetetraacetic acid
EGFP	enhanced green fluorescent protein

EPR	enhanced permeability and retention
EtOAc	ethyl acetate
EtOH	ethanol
FA	folic acid
Fab	fragment antigen binding
FBS	fetal bovine serum
FA-cDNA	Folic acid-PEG_{3350}-DNA
FDA	Food and Drug Administration
FL-cDNA	BODIPY-PEG_{900}-cDNA
FITC	fluorescein isothiocyanate
GSH	reduced glutathione
HBSS	Hanks' Balanced Salt Solution
HBTU	tetramethyl-*O*-(1*H*-benzotriazol-1-yl)uronium hexafluorophosphate
HPLC	high performance liquid chromatography
HSA	human serum albumin
ICP-MS	inductively coupled plasma mass spectroscopy
ITC	isothermal titration calorimetry
kDa	kiloDalton
MALDI-TOF	matrix-assisted laser desorption/ionization, time of flight
MC	microcentrifuge
mRNA	messenger ribonucleic acid
MTX	methotrexate
NHS	*N*-hydroxysuccinimide

ODN	oligodeoxynucleotide
PA	palmitic acid
PAGE	polyacrylamide gel electrophoresis
PCR	polymerase chain reaction
PEG_x	poly(ethylene glycol)$_{\text{molecular weight}}$
RBF	round-bottom flask
RES	reticuloendothelial system
RISC	RNA-induced silencing complex
RNAi	RNA interference
RNAse	ribonuclease
RPMI	Roswell Park Memorial Institute
RT	room temperature
SDS	sodium dodecylsulfate
SEC	Size Exclusion Chromatography
SEM	scanning electron microscope
SELEX	systemic evolution of ligands by exponential enrichment
siRNA	short interfering RNA duplexes
SPARC	secreted protein acid and rich in cysteine
ss	single stranded
SSO	splice shifting oligonucleotide
TEA	triethylamine
TEAA	triethylammonium acetate
THF	tetrahydofuran

TNFα	tumor necrosis factor alpha
UV	ultraviolet

Chapter I

INTRODUCTION

The advancement of nucleic acid-based gene modulation is one of mankind's greatest achievements in science. This technology is utilized with great success in the laboratory, but unfortunately has failed to produce ground-breaking changes in medicine and gene therapy. Nucleic acid-based therapy is heavily reliant on the successful delivery of therapeutic amounts of drug to the target site of action, a crucial complexity encountered in animals and humans. Both the physical properties of nucleic acids unfavorable for in vivo delivery and the systemic defense mechanisms of the host contribute to difficulties associated with development of nucleic acid-based treatment modality. In addition, due to their high intrinsic potency, successful therapy is critically dependant upon increased residence time of a small quantity of drug in systemic circulation (de Fougerolles et al. 2007). To mitigate these shortcomings, numerous carrier and particle-based systems have been tested. The type of carrier strategy exploited for such nucleic acid-based therapy must depend on the properties of therapeutic agent as well as its mechanism of action.

1.1 Nucleic Acid-Based Therapies

Archetypal nucleic acid-based medicine can be broadly separated into gene replacement or gene silencing therapy. Of the gene therapy field, gene and plasmid delivery is beyond the scope of this dissertation. The topic involves a broad range of delivery

techniques and divergent complications in humans (de Fougerolles et al. 2007). Most gene silencing, or in certain cases gene altering therapies, utilize short oligonucleotides, commonly 18-25 nucleic acid sequences, as the main therapeutic component. These agents and their mechanism of actions can be further broken into several broad nucleic acid-based therapies discussed below; anti-gene, anti-sense, and RNA interference.

1.1.1 Anti-Gene Therapy

Slow progress in the anti-gene field appear to have limited development of potential therapeutic application. In common with typical in vivo delivery barriers, anti-gene oligonucleotides, known as triple helix-forming oligodeoxynucleotides (ODN), must further penetrate the nucleus, hybridize to condensed double stranded deoxynucleic acid (dsDNA) via homologous recombination, and form stable Hoogsteen bonds that will block gene transcription or to elicit gene mutation. In theory, knowledge of the genetic code is the minimum requirement in developing a pool of sequence specific triple helix-forming oligodeoxynucleotides that targets the gene of interest. However, ideal gene hybridizing sites are unknown and pose another obstacle in developing disease modifying anti-gene agents. These additional barriers result in poor gene modulation typically resulting in low efficacy and limited use outside the research laboratory (Opalinska and Gewirtz. 2002).

1.1.2 Anti-Sense Therapy

The oldest and most thoroughly studied nucleic acid-based therapy is anti-sense or anti-mRNA therapy. Similar to anti-gene therapy, the therapeutic oligonucleotide hybridizes to its complement sequence to inhibit gene regulation by blocking downstream at the mRNA

level. Knowledge of the mRNA code is also the minimum necessity, although certain sequences may provide higher inhibition of translation than others. Although blocking protein expression at the gene level is stoichiometrically superior, mRNA is more accessible for targeting in the nucleus and often available in the cytosol during transport as well as during translation. Inhibition at the mRNA level is also more efficient than inhibiting protein replicates post-translation as with most current small molecule therapies.

Originally utilized in 1977 to exogenously block translation, the first therapeutic anti-sense study used a 13-mer oligodeoxynucleotide to inhibit in vitro viral replication (Zamecnik and Stephenson. 1978). Upon binding to the complement mRNA, the stable double stranded region inhibits translational machinery from reading the complete mRNA sequence thus down-regulating protein expression. Next generation anti-sense ODNs can also destroy target mRNA using one of two mechanisms, either RNase H-mediated or as a ribozyme.

Chemically modified oligonucleotides, especially those with phosphorothioate backbones can activate RNase H. This intracellular enzyme recognizes the RNA strand in its duplex to hybridizing oligonucleotide as a foreign molecule similar to that of viral genome and specifically cleaves the mRNA strand. Destruction of the complement mRNA also regenerates the active oligonucleotide for further gene knockdown.

Ribozymes are ribonucleotide sequences with a defined structure and intrinsic enzymatic activity, similar to that of enzymes but composed of nucleic acids. Most ribozymes form a similar structure composed of a catalytic motif flanked by specific targeting sequences (Phylactou. 2000). The catalytic motif coordinates with a divalent cation and RNA folds to further stabilize the structure. DNAzymes are a similar class of catalytic

nucleotides designed for improved stability in biological milieu over that of RNA-based ribozymes. Currently this fledgling technology is limited to the laboratory and has not yielded a clinical therapeutic agent (Opalinska and Gewirtz. 2002).

1.1.3 RNA Interference Strategy

In recent years RNA interference (RNAi) has gained tremendous utility in basic research as well as in the development of potential therapeutic agents for post-translational gene knockdown. Initially thought to combat invading viral RNA, it is now known that small non-coding RNA are also potent mediators of gene regulation (Chiu et al. 2004). RNAi is a naturally occurring cellular process using transcribed double stranded RNA (dsRNA) from intragenic regions and introns to target and control mRNA translation. The 0.5 to 1.0 kilo base pair dsRNA is processed by a RNase-III family of nucleases, known as DICER, and truncated into short 21-25 base pair duplexes consistently with two nucleotide 3'-overhangs. These short interfering RNA duplexes (siRNA) are incorporated into a large, multi-protein complex to form a RNA-induced silencing complex (RISC). The nuclease complex discards one strand of siRNA and utilizes the other strand to target the complement mRNA for destruction (Dykxhoorn et al. 2006, Chakraborty. 2007).

After 30 years of advances, only a few anti-sense based oligonucleotides have reached clinical approval with many more in the drug development pipeline. Approximately two to three orders of magnitude more potent than anti-sense, siRNA based therapeutics have also blossomed in the biotechnology field with several RNAi-based medicines undergoing clinical studies for FDA approval (de Fougerolles et al. 2007). Unlike conventional medicines consisting of small molecules, nucleic acid-based medicines are less affected by

upregulated transporters and metabolizing enzymes in cells, are not converted to active metabolites, and produce differing toxicity than conventional therapy therefore avoiding additive dose limiting toxicity in multi-drug therapies. Unfortunately, the first generation of nucleic acid-based medicine is proven to be less superior to conventional therapies, mainly due to poor pharmacokinetic and biodistribution properties in humans (Braasch et al. 2004, Soutschek et al. 2004).

1.2 Macromolecular Delivery Benefits and Strategies

Past failures in clinical studies have revealed the limitations to using non-modified nucleic acid for development. Non-modified oligonucleotides are rapidly degraded in the biological milieu and also eliminated from the body through renal and hepatic mechanisms. Nonspecific uptake into healthy cells and sequestration by the reticuloendothelial system (RES) also decreases circulating concentrations of active drug. Oligonucleotides are highly anionic and are several thousand daltons in molecular mass, limiting the drugs' ability to penetrate target cells. These unfavorable physical properties and its inadequate delivery are the main limitations in establishing a nucleic acid-based therapeutic agent.

To overcome these limitations, numerous specialized carriers have been developed to protect and deliver nucleic acids to the site of pathology. Since "one size does not fit all," carrier systems are typically optimized to deliver a specific nucleic acid cargo for a particular disease state. Alterations of the carrier and its cargo may induce differing properties and characteristics, therefore classifying the system as a new chemical entity. The core assembly is most often synthetic, derived from natural products, or inorganic. All carriers can be categorized as nanoparticles, due to their nanometer size. The trends in therapeutic carriers

converge with other technologies being developed for medicine and other applications such as robotics and lithography devices. For the sake of simplicity, macromolecular carriers and nanoparticles are synonymous and used interchangeably throughout this dissertation.

The National Science Foundation defines nanotechnology as the development of science and technology "at the atomic, molecular, or macromolecular range of approximately 1-100 nanometers to create and use structures, devices, and systems that have novel properties" (NSET, February 2000). The application of nanotechnology for medicine has become a priority of the NIH with its vast potential and benefit over conventional small molecule therapies. Among the long term objectives of the NIH in nanomedicine are goals to use nanoparticles to specifically target cancer cells and to design molecular-sized biological devices or systems to deliver medicine when and where it is needed within the body. As a nucleic acid delivery carrier, nanotechnology imparts the ability to confer multiple advantages. It not only protects the cargo from degradation and elimination but also target specific cells or environments resulting in decreased systemic toxicity.

1.2.1 Biological and Chemical Stability

Compared to conventional therapeutics consisting of small molecules, nucleic acids are highly charged with negative ions. They are large molecules that lose functional activity upon degradation or changes in higher-order structure. Native oligonucleotides are subject to rapid enzymatic attack primarily through the action of 3'-exonucleases in circulation, but also as a result of endonuclease attack as in the case of RNA.

To overcome these limitations, chemically altering the inter-nucleotide backbone and modifying the oligonucleotide with nuclease-resistant bases are typical methods to improve

enzymatic stability (Weyermann et al. 2004). Altering the structure of the oligonucleotide by incorporating analogs resembling DNA and RNA maintains hybridization capacity but are less recognized by nucleases and scavenger receptors. However, another set of limitations arise from these customized oligonucleotides. Modifications in structure using nucleic acid analogs should be prudently selected to avoid possible changes in physical properties and therapeutic potential. Phosphorothioates are prone to nonspecific protein binding, peptide nucleic acid analogs do not possess an anionic backbone and, thus, are less soluble, and some analogs do not activate RNase H (Lochmann et al. 2004). Certain chemical modifications of siRNA abolish RNAi activity (Jackson et al. 2006). The loss in activity may be sequence- or position-specific and is a major focus of contemporary research (Jackson et al. 2006, Chiu et al. 2005, Judge et al. 2006). These analogues proved effective when administered directly at the desired site of action, but are much less effective upon systematic administration. This is a result of RES sequestration and renal elimination from the body (Chiu et al. 2004).

Alternatively, covalent conjugation or ionic complexation to nanoparticles can further protect nucleic acids from biochemical degradation. Nanoparticle incorporation, encapsulation or simple shielding from degrading conditions can increase bioavailability and sustain extended circulation by isolating the oligonucleotide from the hostile environment. Macromolecular carriers can also deliver multiple copies of oligonucleotide in a concentrated fashion, increasing delivery efficiency and improving potency even when only a few carriers reach the intended target site.

1.2.2 Biodistribution at the Organ-Tissue Level

The "tunability" or ability to control the chemical composition, size, morphology, and surface characteristics of nanoparticles is a potentially major advantage in improving pharmacokinetic properties of its nucleic acid cargo. Incorporation of oligonucleotides into nanoparticles increases the overall mass and apparent size beyond the capability of glomerular filtration. Without a macromolecular carrier, free oligonucleotides and siRNA, with average molecular weights between five to 14 kiloDaltons (kDa), are efficiently eliminated through the kidney yielding a short systemic half-life. The renal molecular weight cut-off is approximately 70 kDa corresponding to soluble molecules less than 4 nm in diameter (Caliceti and Veronese. 2003). Thus nanoparticles larger than 70 kDa are mainly subject to other routes of elimination such as liver and the RES (Torchilin and Lukyanov. 2003). To circumvent hepatic uptake and opsonization, nanoparticles are usually coated with poly(ethylene glycol) (PEG) or other inert hydrophilic polymers to form a steric shield around the core and oligonucleotide.

A unique ability of macromolecular drug carriers is to passively accumulate in areas of leaky endothelium. The large mass and size restricts extravasation of nanoparticles, confining the majority in blood circulation. Inflammatory disease states and cancer can disrupt the vasculature, forming large gaps along the endothelium, allowing nanoparticles to escape into diseased sites. Since there is no selective permeability or specific uptake, this process is passive in nature (Matsumura and Maeda. 1986).

In cancer, as solid tumors develop within the body, enzymes and regulating factors are released to remodel the extracellular environment. Key alterations in the vasculature structure as well as physiological changes surrounding the tumor mass include angiogenesis

leading to defective hypervasculature with increased vascular permeability along with impaired lymphatic drainage of extracellular fluid. The enhanced permeability and retention (EPR) of macromolecules at the tumor periphery is unique to nanoparticles in cancer therapy (Matsumura and Maeda. 1986). Unfortunately heterogeneity in tumor growth limits EPR as a global approach and presents further complications. The vasculature surrounding the tumor is chaotic with limited permeability into the tumor mass. Compromised lymphatic drainage retains fluid load increasing interstitial pressure. Since macromolecules move by convection, increased pressure surrounding the tumor limits nanoparticle penetration through the thick extracellular matrix (Netti et al. 1999). The same physical property allowing macromolecules to bypass renal clearance also excludes diffusion of oligonucleotide into the tumor. Utilizing only passive accumulation may deliver nanoparticles to the tumor periphery but subsequent penetration into the tumor mass and into cancer cells is another delivery issue (Brown et al. 2004). For anti-sense and siRNA, the next hurdle is intracellular delivery.

1.2.3 The Cellular Transport Barrier

The final obstacle to successful nucleic acid based therapy is the inescapable cellular barriers. The very design and nature of the cell membrane is to limit penetration of exogenous particles, including those used in drug delivery. Therefore, successful pharmacokinetics and in vivo delivery of nanoparticle carriers to the diseased tissue does not translate to potential pharmacodynamic effects. The final destination of nucleic acid based therapy must be accessible to target mRNA within cells. Upon reaching the target site, the macromolecular carrier must selectively penetrate into the target cell and efficiently release the oligonucleotide to exert a pharmacologic effect (Schmajuk et al. 1999). This two step

process, uptake and release mechanism is the essential foundation of macromolecular delivery if an efficient and stable therapeutic response is to be achieved.

The ability to modify and incorporate a targeting strategy greatly enhances the pharmacodynamics of macromolecular delivery carriers (Asokan and Cho. 2005). Unfortunately, strategies designed to escape RES clearance, such as incorporating a steric or hydrophilic shield around the nanoparticle also hinders cellular uptake (Cullis and Chonn. 1998). Without a specific mechanism of uptake, cellular endocytosis is typically limited to random fluid phase pinocytosis in cells (Najlah and D'Emanuele. 2006). This uptake process is altered during cellular growth leading to variable uptake and response in target cells. To overcome poor uptake, various transfection technologies have been employed for in vivo applications. Positively charged nanoparticles interact with the anionic backbones of oligonucleotides, forming strong ionic bonds that retain the cargo during systemic circulation and protect against enzymatic digestion. The cationic charge also interacts with anionic glycoproteins on cell surfaces causing adsorptive endocytosis (Opalinska and Gewirtz. 2002). The ability for cationic delivery carriers to non-covalently bind oligonucleotides and penetrate the cell membrane yields a potent in vitro transfection system. However, it often fails to deliver nucleic acids in animals (Duncan and Izzo. 2005). The same strong cationic charge that binds to both oligonucleotides also binds to circulating proteins, causing aggregation and opsonization with increased toxicity (Cullis et al. 1998). Charge interaction with cells is nonspecific, causing systemic transfection in non-disease state cells, and considerable filtration by the RES and the liver macrophages (Moghimi and Hunter. 2001).

To increase specificity, active targeting strategies are combined with the macromolecular carrier to selectively bind to receptors on the target cells after extravasation.

The current targeting strategy standard is to modify the nanoparticle with a ligand directed toward a specific receptor expressed on the surface of the affected cell (Brannon-Peppas and Blanchette. 2004). Identification of any receptor or structure on targeted cells not available or in lower quantity on normal healthy cells can be utilized as a mechanism to increase delivery specificity. Antibody generation and combinatorial techniques such as phage display, systemic evolution of ligands by exponential enrichment (SELEX), or mRNA display can develop new targeting molecules against a vast array of surface proteins or complexes with relatively high affinity (Baggio et al. 2002, Lorsch and Szostak. 1994, Carothers et al. 2006). Similar types of targeting ligands can be protein, nucleic acid based, or small molecule such as folic acid.

Nucleic acid-based targeting ligands, also known as aptamers, are oligonucleotide sequences capable of folding into highly structured tertiary structures via hydrogen bonds and electrostatic interactions (Jayasena. 1999). Most aptamers isolated through SELEX attain very high affinity toward the target protein or carbohydrate with binding constants comparable to that of antibodies, producing a highly specific targeting ligand (Wilson and Szostak. 1999). One application is an aptamer against prostate specific membrane antigen developed from SELEX that is shown to specifically deliver nanoparticles to malignant prostate tumors (McNamara et al. 2006).

The architecture surrounding the disease site expressing a unique target can also be exploited to accumulate nanoparticles onto target cells. Nanoparticles conjugated with RGD sequences selectively bind to $\alpha_V\beta_3$ integrins exposed only in the angiogenic extracellular matrix of solid tumors (Boswell et al. 2008). These targeting mechanisms and many more improve delivery and retention of many macromolecular delivery carriers. As in the case of

the cationic uptake systems, these targeting methods must utilize random adsorptive endocytosis to internalize the nanoparticle, which may or may not escape into the cytosol.

Biological ligands for upregulated receptors on affected cells create a natural targeting mechanism for macromolecular delivery carriers. Vitamin B_9, also known as folic acid, is necessary for de novo purine synthesis of amino acids. Normally dividing cells recycle metabolites to reform purines, acquiring basal levels of exogenous folic acid for growth. In rapidly dividing cells, this essential nutrient is absorbed in higher quantities by means of folate receptors overexpressed on the surface of cells. In cancer, biopsies from human ovarian, colorectal, breast, lung, renal, and endometrial tumors were found to overexpress the folate receptor (Sudimack and Lee. 2000). Unique to folate uptake, the nutrient is transferred from endosomes directly to cytosol by means of receptor-mediated endocytosis (Sabharanjak and Mayor. 2004). This strategy circumvents the necessity of an endosomal release mechanism and often utilized in various strategies for cellular drug delivery (Salazar and Ratnam. 2007).

Subsequent to endocytic entry, the macromolecular delivery carrier must release the therapeutic oligonucleotide for a pharmacological affect. Many endocytic processes lead to lysosomal fusion of the endosome and subsequent enzymatic degradation. Within the process of uptake and maturation of the endosome, two general mechanisms of release are widely exploited to release cargo from nanoparticles, an enzymatic process or chemical hydrolysis. Delivery systems based on enzymatic hydrolysis require a labile peptide bond cleaved by early lysosomal enzymes such as cathepsin B, urokinase-type-plasminogen activator, and matrix metalloproteinase 2 (Pechar et al. 2005). Utility of enzymatic release for

nucleotide carriers may be limited unless the peptide bond is broken before hydrolysis of the oligonucleotide in endosomal conditions. (Bareford and Swaan. 2007).

Hydrolysis to liberate nucleic acids from nanocarriers can offer a variety of release profiles. Novel approaches involving photolabile linkers and ultrasound technology offer unique release mechanisms, but most strategies rely on a pH-driven or a reductive environment for release (Karagiannis et al. 2006). Acid-labile bonds are the most prominent release strategy utilized in macromolecular delivery systems. As the endosome matures, ATP-driven proton pumps activate, causing a decrease in pH to as low as five (Mukherjee et al. 1997). Widespread knowledge of endosomal acidification has produced a vast array of linkers designed to decompose within the endosomal acidity while stable at physiological pH. Linkers such as hydrazone bonds, orthogonal esters, and ketal or acetal bonds are typical chemical modifications employed in nanoparticles (Asokan and Cho. 2005).

Differences in redox potential between intracellular and extracellular milieu are also exploited for intracellular delivery of oligonucleotides. The greater reductive environment of cytosol and certain organelles can reduce disulfide bonds, providing an innate mechanism to release the therapeutic cargo. The presence of reactive oxygen species in extracellular space forms an oxidizing environment, preserving disulfide bonds of carrier proteins, such as albumin. The reductive environments in cells are produced mainly from high concentrations of reduced γ-glutamyl-cysteinylglycine (GSH). Also known as glutathione, this molecule is a critical regulator regenerating enzymatic activity, regulates metabolism, and stabilizes homeostasis. Intracellular concentrations of GSH vary from 5 mM in mitochondria to as high as 20 mM (Oupicky and Diwadkar. 2003) in the nucleus, compared to 1.5 μM concentrations encountered in circulation (Oupicky et al. 2001). This distinctive redox gradient produces a

simple mechanism of release by attaching the oligonucleotide cargo to the nanoparticle using disulfide bonds (Oupicky et al. 2001). Multiple macromolecular carriers utilize this controlled release mechanism, but one critical issue must be addressed using this strategy. Recent studies suggest the route of endocytosis and downstream transport of endosomes can lead to either an oxidative or reductive environment (Austin et al. 2005). Therefore, reductive release from the nanoparticle may vary from confounding variables influenced by size, type or quantity of targeting ligands, and cellular variances in cells (Saito et al. 2003) .

Escape from the endosome is necessary for gene-modulating nucleic acid based therapy. In vitro studies show that cationic charge can disrupt the cell and endosomal membrane, but delivery efficiency is limited. To avoid the limitations of cationic charge in circulation, weak bases, with pKa ranging between neutral pH and pH 5.0 encountered in late endosomes, are incorporated into nanoparticles to disrupt the membrane. These weak bases are uncharged during circulation and protonated in the endosomal environment. The increase in charge on the membrane impermeable nanoparticle disrupts the ionic balance, producing an influx of chloride counter ions into the endosome. Water then enters the endosome increasing osmotic pressure and causing the endosome to swell. Increased endosomal pressure causes rupture of the membrane permitting the nanoparticle to escape into the cytosol. This strategy, commonly referred to as proton sponge effect (Sonawane et al. 2003) is intrinsic in many weak bases and applied on multiple macromolecular carriers, such as polymer based scaffolds like dendrimers (Guillaudeu et al. 2008), polyethyleneimine (Brissault et al. 2006) and carbohydrate vectors like chitosan (Bowman and Leong. 2006).

1.3 Research Focus

Nanotechnology and development of macromolecular drug carriers have been recently promoted to overcome current delivery-related limitations in gene therapy and nucleic acid-based medicine. As the complexity of the nanoparticle increases with integration of diverse strategies, the global application of the technology becomes limited due to complications in preparation and analysis of a multi-faceted approach. A careful balance between systems application and simplicity is required to develop a clinically applicable and therapeutically superior vector based medicine. The ongoing studies utilize two dissimilar delivery vectors to arrive at one endpoint, to efficiently deliver oligonucleotides to solid tumors. The first vector is formulating stable particulate gold nanoparticles into an ODN carrier with a simple targeting mechanism. This subject is described in **Chapters II** and **III**. The second strategy does not incorporate a release mechanism or a targeting strategy. It exploits only the normal functions of the most abundant protein in the body of humans. Albumin is a nutrient and a natural systemic carrier of small molecules, hence a natural endogenous delivery carrier. **Chapter IV** describes this specific approach.

1.4 References

A. Asokan and M. J. Cho. Cytosolic delivery of macromolecules: 4. Head group-dependent membrane permeabilization by pH-sensitive detergents. Journal of Controlled Release. 106:146-153 (2005/8/18).

C. D. Austin, X. Wen, L. Gazzard, C. Nelson, R. H. Scheller, and S. J. Scales. Oxidizing potential of endosomes and lysosomes limits intracellular cleavage of disulfide-based antibody-drug conjugates. Proc Natl Acad Sci U S A. 102:17987-17992 (2005).

R. Baggio, P. Burgstaller, S. P. Hale, A. R. Putney, M. Lane, D. Lipovsek, M. C. Wright, R. W. Roberts, R. Liu, J. W. Szostak, and R. W. Wagner. Identification of epitope-like consensus motifs using mRNA display. J Mol Recognit. 15:126-134 (2002).

L. M. Bareford and P. W. Swaan. Endocytic mechanisms for targeted drug delivery. Adv Drug Deliv Rev. 59:748-758 (2007).

C. A. Boswell, P. K. Eck, C. A. Regino, M. Bernardo, K. J. Wong, D. E. Milenic, P. L. Choyke, and M. W. Brechbiel. Synthesis, Characterization, and Biological Evaluation of Integrin alphavbeta3-Targeted PAMAM Dendrimers. Mol Pharm. (2008).

K. Bowman and K. W. Leong. Chitosan nanoparticles for oral drug and gene delivery. Int J Nanomedicine. 1:117-128 (2006).

D. A. Braasch, Z. Paroo, A. Constantinescu, G. Ren, O. K. Oz, R. P. Mason, and D. R. Corey. Biodistribution of phosphodiester and phosphorothioate siRNA. Bioorg Med Chem Lett. 14:1139-1143 (2004).

L. Brannon-Peppas and J. O. Blanchette. Nanoparticle and targeted systems for cancer therapy. Adv Drug Deliv Rev. 56:1649-1659 (2004).

B. Brissault, A. Kichler, C. Leborgne, O. Danos, H. Cheradame, J. Gau, L. Auvray, and C. Guis. Synthesis, characterization, and gene transfer application of poly(ethylene glycol-b-ethylenimine) with high molar mass polyamine block. Biomacromolecules. 7:2863-2870 (2006).

E. B. Brown, Y. Boucher, S. Nasser, and R. K. Jain. Measurement of macromolecular diffusion coefficients in human tumors. Microvasc Res. 67:231-236 (2004).

P. Caliceti and F. M. Veronese. Pharmacokinetic and biodistribution properties of poly(ethylene glycol)-protein conjugates. Adv Drug Deliv Rev. 55:1261-1277 (2003).

J. M. Carothers, S. C. Oestreich, and J. W. Szostak. Aptamers selected for higher-affinity binding are not more specific for the target ligand. J Am Chem Soc. 128:7929-7937 (2006).

C. Chakraborty. Potentiality of small interfering RNAs (siRNA) as recent therapeutic targets for gene-silencing. Curr Drug Targets. 8:469-482 (2007).

Y. L. Chiu, A. Ali, C. Y. Chu, H. Cao, and T. M. Rana. Visualizing a correlation between siRNA localization, cellular uptake, and RNAi in living cells. Chem Biol. 11:1165-1175 (2004).

Y. L. Chiu, C. U. Dinesh, C. Y. Chu, A. Ali, K. M. Brown, H. Cao, and T. M. Rana. Dissecting RNA-interference pathway with small molecules. Chem Biol. 12:643-648 (2005).

P. R. Cullis, A. Chonn, and S. C. Semple. Interactions of liposomes and lipid-based carrier systems with blood proteins: Relation to clearance behaviour in vivo. Adv Drug Deliv Rev. 32:3-17 (1998).

P. R. Cullis and A. Chonn. Recent advances in liposome technologies and their applications for systemic gene delivery. Adv Drug Deliv Rev. 30:73-83 (1998).

A. de Fougerolles, H. P. Vornlocher, J. Maraganore, and J. Lieberman. Interfering with disease: a progress report on siRNA-based therapeutics. Nat Rev Drug Discov. 6:443-453 (2007).

R. Duncan and L. Izzo. Dendrimer biocompatibility and toxicity. Adv Drug Deliv Rev. 57:2215-2237 (2005).

D. M. Dykxhoorn, D. Palliser, and J. Lieberman. The silent treatment: siRNAs as small molecule drugs. Gene Ther. 13:541-552 (2006).

S. J. Guillaudeu, M. E. Fox, Y. M. Haidar, E. E. Dy, F. C. Szoka, and J. M. Frechet. PEGylated dendrimers with core functionality for biological applications. Bioconjug Chem. 19:461-469 (2008).

A. L. Jackson, J. Burchard, D. Leake, A. Reynolds, J. Schelter, J. Guo, J. M. Johnson, L. Lim, J. Karpilow, K. Nichols, W. Marshall, A. Khvorova, and P. S. Linsley. Position-specific chemical modification of siRNAs reduces "off-target" transcript silencing. RNA. 12:1197-1205 (2006).

S. D. Jayasena. Aptamers: an emerging class of molecules that rival antibodies in diagnostics. Clin Chem. 45:1628-1650 (1999).

A. D. Judge, G. Bola, A. C. Lee, and I. MacLachlan. Design of noninflammatory synthetic siRNA mediating potent gene silencing in vivo. Mol Ther. 13:494-505 (2006).

T. C. Karagiannis, P. N. Lobachevsky, B. K. Leung, J. M. White, and R. F. Martin. Receptor-mediated DNA-targeted photoimmunotherapy. Cancer Res. 66:10548-10552 (2006).

D. Lochmann, V. Vogel, J. Weyermann, N. Dinauer, H. von Briesen, J. Kreuter, D. Schubert, and A. Zimmer. Physicochemical characterization of protamine-phosphorothioate nanoparticles. J Microencapsul. 21:625-641 (2004).

J. R. Lorsch and J. W. Szostak. In vitro selection of RNA aptamers specific for cyanocobalamin. Biochemistry. 33:973-982 (1994).

Y. Matsumura and H. Maeda. A new concept for macromolecular therapeutics in cancer chemotherapy: mechanism of tumoritropic accumulation of proteins and the antitumor agent smancs. Cancer Res. 46:6387-6392 (1986).

J. O. McNamara 2nd, E. R. Andrechek, Y. Wang, K. D. Viles, R. E. Rempel, E. Gilboa, B. A. Sullenger, and P. H. Giangrande. Cell type-specific delivery of siRNAs with aptamer-siRNA chimeras. Nat Biotechnol. 24:1005-1015 (2006).

S. M. Moghimi and A. C. Hunter. Capture of stealth nanoparticles by the body's defences. Crit Rev Ther Drug Carrier Syst. 18:527-550 (2001).

S. Mukherjee, R. N. Ghosh, and F. R. Maxfield. Endocytosis. Physiol Rev. 77:759-803 (1997).

M. Najlah and A. D'Emanuele. Crossing cellular barriers using dendrimer nanotechnologies. Curr Opin Pharmacol. 6:522-527 (2006).

P. A. Netti, L. M. Hamberg, J. W. Babich, D. Kierstead, W. Graham, G. J. Hunter, G. L. Wolf, A. Fischman, Y. Boucher, and R. K. Jain. Enhancement of fluid filtration across tumor vessels: implication for delivery of macromolecules. Proc Natl Acad Sci U S A. 96:3137-3142 (1999).

J. B. Opalinska and A. M. Gewirtz. Nucleic-acid therapeutics: basic principles and recent applications. Nat Rev Drug Discov. 1:503-514 (2002).

D. Oupicky, R. C. Carlisle, and L. W. Seymour. Triggered intracellular activation of disulfide crosslinked polyelectrolyte gene delivery complexes with extended systemic circulation in vivo. Gene Ther. 8:713-724 (2001).

D. Oupicky and V. Diwadkar. Stimuli-responsive gene delivery vectors. Curr Opin Mol Ther. 5:345-350 (2003).

M. Pechar, K. Ulbrich, T. Etrych, A. Fabra, M. Stevenson, and L. Seymour. Oligopeptides as targeting structures in cancer theraPY. J Control Release. 101:376-379 (2005).

L. A. Phylactou. Ribozyme and peptide-nucleic acid-based gene therapy. Adv Drug Deliv Rev. 44:97-108 (2000).

S. Sabharanjak and S. Mayor. Folate receptor endocytosis and trafficking. Adv Drug Deliv Rev. 56:1099-1109 (2004).

G. Saito, J. A. Swanson, and K. D. Lee. Drug delivery strategy utilizing conjugation via reversible disulfide linkages: role and site of cellular reducing activities. Adv Drug Deliv Rev. 55:199-215 (2003).

M. D. Salazar and M. Ratnam. The folate receptor: what does it promise in tissue-targeted therapeutics? Cancer Metastasis Rev. 26:141-152 (2007).

G. Schmajuk, H. Sierakowska, and R. Kole. Antisense oligonucleotides with different backbones. Modification of splicing pathways and efficacy of uptake. J Biol Chem. 274:21783-21789 (1999).

J. Soutschek, A. Akinc, B. Bramlage, K. Charisse, R. Constien, M. Donoghue, S. Elbashir, A. Geick, P. Hadwiger, J. Harborth, M. John, V. Kesavan, G. Lavine, R. K. Pandey, T. Racie, K. G. Rajeev, I. Rohl, I. Toudjarska, G. Wang, S. Wuschko, D. Bumcrot, V. Koteliansky, S. Limmer, M. Manoharan, and H. P. Vornlocher. Therapeutic silencing of an endogenous gene by systemic administration of modified siRNAs. Nature. 432:173-178 (2004).

J. Sudimack and R. J. Lee. Targeted drug delivery via the folate receptor. Adv Drug Deliv Rev. 41:147-162 (2000).

V. P. Torchilin and A. N. Lukyanov. Peptide and protein drug delivery to and into tumors: challenges and solutions. Drug Discov Today. 8:259-266 (2003).

J. Weyermann, D. Lochmann, and A. Zimmer. Comparison of antisense oligonucleotide drug delivery systems. J Control Release. 100:411-423 (2004).

D. S. Wilson and J. W. Szostak. In vitro selection of functional nucleic acids. Annu Rev Biochem. 68:611-647 (1999).

P. C. Zamecnik and M. L. Stephenson. Inhibition of Rous sarcoma virus replication and cell transformation by a specific oligodeoxynucleotide. Proc Natl Acad Sci U S A. 75:280-284 (1978).

Chapter II

COLLOIDAL GOLD-BASED siRNA DELIVERY SYSTEM

Colloidal gold nanoparticles (AuNP) have recently been used as particulate drug carriers utilized in macromolecular drug delivery. Several unique characteristics about colloidal gold make this scaffold an excellent prospect for the delivery of small and large therapeutic agents (Ghosh et al. 2008a, Paciotti et al. 2004). Reproducible formation of nearly monodisperse and nanometer sized colloidal gold from gold salts are major advantages over other comparable nanocarriers. Indeed stable gold nanoparticles with average sizes from one to 100 nm with little variance and consistent spherical shape can be produced using established protocols (Frens 1972, Horisberger 1979).

The surface of colloidal gold is easily functionalized through charge, hydrophobic and dative interactions (Ghosh et al. 2008b, Han et al. 2007). The dative binding between mercaptans and gold permits multiple thiolated drugs, proteins and oligonucleotides to stably conjugate to the small carrier (Farma et al. 2007, Seferos et al. 2007). Most importantly, dative binding is reversible and provides an innate capability for gold nanoparticles to release agents once reaching reductive intracellular conditions (Chompoosor et al. 2008). This non-enzymatic release strategy utilizes thiol exchange with intracellular GSH to displace the dative binding from the surface of gold (Hong et al. 2006). The three orders of magnitude difference between extracellular and intracellular thiol concentration has been shown to displace both hydrophobic and datively bound fluorophores on gold carriers (Han et al.

2005). Oligonucleotides complexed onto the surface of gold are also protected from nuclease activity (Han et al. 2006).

Gold particles have a long history of therapeutic and diagnostic use in the field of medicine (Hainfeld et al. 2008, Sage et al. 1964). Gold, as colloidal solids, are inert and non-toxic when administered in cell culture (Connor et al. 2005). Gold colloids can be ingested in large quantities and are often used as decoration on food and drinks. Gold salts are FDA approved for injection with doses up to 50 mg per month and therapeutic responses after a 1 gm. cumulative dose for rheumatoid arthritis (Finkelstein et al. 1977). Injectable gold particles are also a major formulation component utilized to efficiently inject plasmids via gene gun (Robinson and Pertmer. 2001, Yang et al. 2001). As a delivery carrier, tumor necrosis factor (TNF-α) conjugated to 33 nm pegylated gold colloids passively accumulate in solid tumors, while avoiding hepatic and RES elimination. Disulfide conjugation to gold colloid also sequestered the dose limiting systemic toxic effects of interferon used for anticancer therapy (Farma et al. 2007).

2.1 Statement of Purpose

Gold nanoparticles are stably dispersed colloidal suspensions with an innate and modifiable ability to bind, retain, and release cargo molecules, thus serving as a carrier scaffold. Colloidal gold can be modified with ODNs to form stable conjugates (Cardenas et al. 2006). The conjugates can be hybridized with complementary oligonucleotides carrying a targeting ligand, polymeric shield, or therapeutic cargo.

To investigate the utility of colloidal gold as a carrier, the theoretical loading capacity was determined based on surface area calculations for spherical particles with diameters

ranging from five to fifty nanometers, shown in **Figure 2-1**. Two methods were employed to calculate the total number of possible dsDNA that could fit onto the surface of a spherical gold colloid. Surface Plasmon resonance systems utilize a gold coated sensor in which thiolated molecules are datively bound to the surface (Peterson et al. 2001). The number of dsDNA per surface area was found and used as a crude reference. Also, assuming that dsDNA is a cylinder, the cross-sectional diameter of 2.8nm was used to quantitively calculate the amount of possible binding for ODN onto the surface of gold. Both calculations do not take into account the change in surface contour of differing diameter spheres, which would impact the steric hinderance of surface. Interestingly, all calculations over-estimated the actual number of single stranded ODN binding to gold spheres based on published literature (Demers et al. 2000).

This study focuses on the surface modification of colloidal gold nanoparticles in order to target folate receptor-expressing cancer cells, deliver, and release oligonucleotide cargo after internalization. Two plausible strategies were examined; an siRNA delivery system depicted in **Figure 2-2**, and a splice shifting oligonucleotide (SSO) delivery system discussed in **Chapter III**. The development of the siRNA carrier system is separated into three stepwise specific aims.

Aim 1**:** *Conjugate and characterize 5'-thiol modified ssDNA to AuNP*. Colloidal gold is inherently unstable to salt conditions and must be coated with the hydrophilic oligonucleotide to prevent aggregation. Successful DNA adsorption onto AuNP must be reproducible and stable in physiological milieu. Here, the siRNA carrier system starts with conjugating non-

therapeutic 18-mer DNA, designated gDNA, to the AuNP. The resulting gDNA-AuNP is analyzed in the first set of experiments.

Aim 2*: Conjugate either folic acid or dipyrromethene boron difluoride* (*BODIPY FL*) *to ODN that is complementary to gDNA.* For active targeting, pegylated folic acid is conjugated to the complement oligonucleotide (cDNA) to target tumor cells.

Aim 3: *Hybridize and quantify the cDNA on the gDNA-AuNP.*

The targeting ligand or cargo must not interfere with complement strand in hybridizing to the DNA modified AuNP, gDNA-AuNP. In the case of siRNA carrier system, for proof of principle, the pegylated fluorescent marker BODIPY FL was substituted for siRNA to characterize binding and loading efficiency.

2.2 Materials and Methods

The siRNA delivery strategy is based upon a modular approach, which would enable convenient optimization of targeting and siRNA components to achieve a successful delivery vehicle. A specific number of gDNA sequences radiate from the AuNP core, surface bound via dative binding through a 5'-thiol DNA modifier. The gDNA-AuNP serves as the modular component, with the ability to hybridize its cDNA that is conjugated to any therapeutic cargo or targeting ligand. Varying the stoichiometry of the components prior to hybridization is the basis for the versatile platform. The complete macromolecular assembly is comprised of a 10-nm gold core carrier passivated with ODN and hybridized to a mixture of BODIPY FL and the folic acid targeting ligand.

2.2.1 Materials

Colloidal gold particles in suspension were purchased from BB International (10 nm, Cat. Code EM.GC10, Madison, WI) and Sigma (10 nm and 20 nm, Cat. #G1527/G1652, St. Louis, MI). All custom-synthesized ODNs; 5'-thiol-C6-CTGTCCCTCTGCAGCAGC, 5'-amino-C6-GCTGCTGCAGAGGGACAG, were purchased from IDT (Coralville, IA) with the exception of controlled-pore glass (CPG) support-bound DNA (Lineberger Cancer Center, Chapel Hill, NC). Cell culture media were obtained from Gibco (Grand Island, NY) and charcoal-filtered fetal bovine serum from Gemini Bioproducts (Cat. # 100-119, Atlanta, GA). SybrGold (Cat. # S11494) and BODIPY FL C_5 SE (Cat. # D1684) was obtained from Molecular Probes (Eugene, OR). Inorganic salts, folic acid, 1-ethyl-3-(3-dimethylaminopropyl)carbodiimide (EDC), dithiothreitol (DTT) (Cat. # D5545), *N*-hydroxysuccinimide, and various organic solvents were obtained from Aldrich (Milwaukee, WI). Dithiobis(succinimidyl propionate) (DSP) was obtained from Pierce (Cat. #22585, Rockford, IL). Sephadex G-25 resin (Sigma Cat. # G25150), bisamine PEG_{3350} (Cat. # P9906), bisamine PEG_{900} (Fluka Cat. # 06703), and α-hydroxyl, ω-amino PEG_{3000} (Fluka Cat. # 07969) were obtained through Sigma (St. Louis, MI). General chemicals and organic solvents were also obtained from Sigma (St. Louis, MI).

2.2.2 General Methods and Procedures

All nucleic acid samples were quantified using UV/visible extinction coefficients and purity was determined by reverse-phase HPLC or polyacrylamide gel electrophoresis (PAGE). Size exclusion purification of DNA and conjugates were routinely performed through a Sephadex G-25 resin (Sigma-Aldrich, St. Louis, MI).

HPLC Method

Purification of DNA and conjugates was carried out by HPLC using an Agilent ZORBAX 300SB-C18 column (9.4mm x 25 cm, Santa Clara, CA) on a Shimadzu SCL-10A/LC-8A HPLC system (Columbia, MD) with a Rainin Dynamax UV detector (Oakland, CA). The column was heated to 37°C using an Eldex CH-150 enclosed heater (Napa,CA). HPLC conditions were as follows: 3 ml/min linear gradient; and % buffer B, 10–20%/10 min; 20-40%/10 min, 40-80%/10 min, 100%/5 min. Pump A contained 0.1 M triethylammonium acetate (TEAA) whereas pump B contained acetonitrile. The eluent was continuously monitored at 260 nm. Peak fractions were combined, vacuum concentrated, G-25 desalted (see below), lyophilized, and ethanol (EtOH) precipitated.

Size Exclusion Purification and Desalting Technique

Commercially obtained Sephadex G-25 was swollen overnight in dH_2O. The slurry (30 ml) was loaded into a one fluid ounce Becton Dickinson syringe preloaded with wet glass wool (Thermo Fisher Cat. # 11-390, Waltham, MA) and capped with a Teflon flow control valve (Baxter Cat. # 9433, Muskegon, MI). Samples were loaded and eluted with dH_2O and fractions analyzed using the Nanodrop ND-1000 spectrophotometer (Wilmington, DE). The resin was washed until no eluting absorbance was detected and reused throughout the study.

2.2.3 Attachment of Thiolated DNA (gDNA) to Gold Nanoparticle (AuNP)

Initial AuNP studies were performed with 10-nm and 20-nm colloidal gold. Commercially obtained 5'-thiol modified 18mer ssDNA (IDT, Coralville, IA) was dissolved in dH_2O and used without purification. The stock citrate-stabilized colloidal gold (4 ml) was

passed through a Whatman 0.22 um syringe filter (Cat. # 6900-2502, Clifton, NJ), rinsed with 0.25 ml of dH_2O, and collected in four siliconized Fisher Scientific 1.65 ml microcentrifuge (MC, Cat. # 02-681-320, Pittsburgh, PA) tubes. The tubes were centrifuged at 16,100 G for 30 min at 25°C. The supernatant and subsequent fractions were collected in a 20-ml scintillation vial. The pellets were quickly redispersed in 1 ml of dH_2O by repeat pipeting and vigorous vortexing. The tubes were centrifuged again at 16,100 G for 30 min at 25°C. The supernatants were transferred to the collection vial and pellets resuspended again with 450 µl of 10 mM phosphate buffer (pH 7.5). AuNP aliquots were combined into two final tubes containing 0.9 ml each.

Conventional terminology of gold colloid suspensions is expressed similar to molecules in solution, that is one particle of AuNP may be composed of numerous atoms of Au, but is considered as one molecule. The concentration of recovered AuNP was determined using ε_{max} of 9.55 x 10^7 $M^{-1}cm^{-1}$ for 10nm AuNP and 9.41 x 10^8 $M^{-1}cm^{-1}$ for 20nm AuNP, referring to one AuNP particle as one molecule.

To each tube, 300-fold molar excess of 5'-thiol modified gDNA was added to each tube in less than 10 µl total volume. The gDNA was added to the inside cap of the open tube, gently closed, and vortexed to rapidly mix the gDNA with AuNP. The tubes were rocked for 30 minutes then adjusted to a final concentration of 0.05 M NaCl and 0.1% sodium dodecylsulfate (SDS). The sol was rocked overnight at room temperature (RT) in the dark. Over the course of two days, 25 µl of 2 M NaCl is rapidly mixed to each tube until the final NaCl concentration reached 0.3 M. After another overnight incubation, the gDNA-AuNP particles were pelleted and resuspended in 0.5 ml dH_2O. The sol was centrifuged again and redispersed in 10 mM phosphate buffer (pH 7.5) with 0.1 % SDS.

To quantify gDNA bound to AuNP, an aliquot of each gDNA-AuNP was scanned using a Shimadzu UV-2401PC spectrophotometer. As seen in **Figure 2-3**, the concentration of AuNP was calculated from peak absorbance at 520 nm, while DNA concentration was calculated after AuNP absorbance was subtracted at 260 nm using ε_{260} value of 1.54×10^5 $M^{-1}cm^{-1}$.

2.2.4 Synthesis of Complement DNA (cDNA) Ligands

The pegylated BODIPY FL was linked to cDNA through a labile disulfide linker and labeled FL-cDNA. Similarly, folic acid modified cDNA was labeled FA-cDNA. The general synthesis scheme is depicted in **Figure 2-4,** outlining shared intermediates and the final structure. Individual syntheses are presented below.

HPLC purified 5'-amino-cDNA was dissolved in dH_2O and absorbance at 260 nm was measured with the Nanodrop ND-1000. The solution was adjusted to a final concentration of 0.1 M imidazole buffer (pH: 6.0) in 200 µl total volume. In a 3 ml reaction vial, 50-fold molar excess DSP was dissolved in 800 µl dimethylformamide (DMF). While stirring, the DNA solution was added dropwise into the vial. The reaction mixture was purged with argon and stirred at RT overnight. The reaction mixture was passed through a 0.22 um filter to remove suspended DSP and loaded onto a G-25 desalting. Fractions containing cDNA absorbance were pooled and concentrated under vacuum. The DSP-modified cDNA was purified by HPLC using previously stated methods and conditions. Several batches of DSP-modified cDNA thus prepared were combined and purified using HPLC to form one stock batch.

Synthesis of PEG_{3000}-cDNA Ligand (PEG-cDNA)

DSP-modified cDNA (0.5 mg, 83 nmol) and α-hydroxyl-ω-amino PEG_{3000} (3 mg, 1 μmol) was dissolved in 0.6 ml of 0.1M imidazole buffer (pH: 6.0). A fresh solution of 5 mg/ml EDC in imidazole buffer was prepared and 0.2 ml (1 mg, 5.2 μmol) was transferred to the reaction vial. The reaction mixture was stirred at RT overnight. The hydroxy-PEG_{3000}-DNA solution was G-25 desalted and HPLC purified.

Synthesis of Bodipy-PEG_{900}-cDNA Ligand (FL-cDNA)

In a 3-ml Pierce Reacti-Vial (Cat. # 13222, Rockford, IL), DSP-modified cDNA (0.5 mg, 83 nmol) was dissolved in 0.1 ml of 0.1M imidazole buffer (pH:6.0). A fresh solution of EDC (2 mg) in 1 ml of imidazole buffer was prepared and 0.1 ml (1.0 μmol) was transferred to the reaction vial. The reaction was stirred for 1 hour. The bis-amino PEG_{900} (4 mg, 4.4 μmol) was dissolved in 1.0 ml of 0.1M imidazole buffer (pH: 6.0) and added to the reaction mixture. The reaction was stirred again for 1 hour. Another 100 μl aliquot of EDC was added to the reaction solution and stirred overnight at RT. The H_2N-PEG_{900}-cDNA solution was G-25 desalted and HPLC purified.

Fluorescent labeling of H_2N-PEG_{900}-cDNA with BODIPY-C5-SE was preformed following manufacturer's recommended protocol (Invitrogen, Carlsbad, CA). The H_2N-PEG_{900}-cDNA was HPLC purified, G-25 desalted, lyophilized prior to the conjugation reaction. The lyophilized intermediate (115 μg, 18 nmol) was dissolved in 86 μl of freshly made 0.1 M borate buffer (pH:8.5) contained in a 1.6 ml microcentrifuge (MC) tube with a small stir bar. The commercially obtained bottle containing BODIPY FL-C_5-SE (5 mg) was dissolved in 280 μl of anhydrous dimethylsufoxide (DMSO) and capped with argon. Only

250 μg (600 nmol) of BODIPY FL in 14 μl DMSO was transferred into the MC tube containing DNA and stirred at RT overnight. The suspension was centrifuged and supernatant transferred to a new MC tube. The pellet was rinsed with 100 μl dH_2O, centrifuged again, and supernatant combined with the previous fraction. The reaction mixture was G-25 desalted and HPLC purified.

Folic acid-PEG_{3350}-DNA Ligand (FA-cDNA)

Folic acid was conjugated to bis-amino PEG_{3350} prior to attachment to DSP-modified cDNA. In a 25 ml round-bottom flask (RBF), bis-amino PEG_{3350} (1.0 gm, 0.3 mol) was dissolved in 5 ml anhydrous DMSO. The folic acid (120 mg, 0.27 mmol) was dissolved in 2 ml anhydrous DMSO in a 7 ml scintillation vial with trace *N*-hydroxysuccinimide (NHS) and activated with a 1:1.1 molar equivalent of EDC (57 mg, 0.3 mmol). The activated folic acid was transferred to the RBF and stirred overnight at RT.

The reaction mixture was precipitated using 50/50 cold ether with acetone at a 2:1 reaction volume ratio. The pellet was dissolved in 50 mM ammonium bicarbonate buffer (pH:8.0) and filtered through a 0.45 um filter. To separate excess cationic bisamino-PEG_{3350} from neutral folic acid-PEG_{3350}-amine, the solution was loaded on a S-Sepharose cation exchange (GE Healthcare Cat. #17-0511-01 Piscataway, NJ) column and eluted with 50 mM bicarbonate buffer. The fastest yellow product band is collected and concentrated under vacuum. The product is then passed through a Q-Sepharose anion exchange (GE Healthcare Cat. #17-0510-01 Piscataway, NJ) column to remove unreacted free folic acid and recovered product band is concentrated under vacuum. The folic acid-PEG_{3350}-amine is desalted

through a G-15 column and lyophilized in a tared vial. A sample was dissolved in $CDCl_3$ and analyzed via proton nuclear magnetic resonance (Varian ^{1}H-NMR, Palo Alto, CA).

In a 3-ml Recti-Vial, dithiopropionate-modified cDNA (0.5 mg, 83 nmol) was dissolved in 0.1 ml of 0.1M imidazole buffer (pH: 6.0). In a separate vial, EDC (21 μmol, 4 mg) and NHS (17.4 μmol, 2 mg) were dissolved in 1.0 ml of imidazole buffer (pH: 6.0). A 0.25 ml aliquot of the activating agent was transferred to the reaction vial and stirred for one hour. Another 0.25 ml of activating solution is added to the reaction vial followed by 10 mg of folic acid-PEG-amine (2.63 μmol) for 32x molar excess to dithiopropionate-modified cDNA. The reaction vial protected from light and stirred overnight at RT. The reaction mixture was desalted and HPLC purified.

2.2.5 Ligand Hybridization to gDNA-AuNP

In a 1.65-ml siliconized MC tube, gDNA-AuNP sol was centrifuged and redispersed in 500 μl of 0.3 M NaCl/10 mM phosphate buffer (pH:7.5). The concentration of AuNP was determined at 520 nm and gDNA concentration calculated based from past batch hybridization efficiency of DNA to AuNP. A 1,000-fold molar excess FL-cDNA to gold bound DNA was added to the sol and vortexed (vol~10 μl). To anneal the DNA, the solution was placed in a 65° C water bath, rocked for 15 minutes, and allowed to cool to RT while standing on the bench top. The annealing step was repeated again. The stably suspended gold solution, otherwise known as sol, was centrifuged and resuspended in 1.0 ml of 10 mM phosphate buffer. The sol was pelleted again and reconstituted in 100 μl of phosphate buffer. The concentration of AuNP was determined at 520 nm and equal volume of 1.0 M dithiothreitol (DTT) in 10 mM phosphate buffer added to the tube. The solution was

vortexed and incubated overnight at 37° C in a water bath. The solution was centrifuged again and aliquot of supernatant transferred to a new tube. The BODIPY FL fluorescence with λ_{em} of 485 nm and λ_{ex} of 504 nm was measured using a Nanodrop ND-3300 spectrofluorometer (Wilmington, DE) and the concentration determined from a standard fluorescence curve.

2.3 Results and Discussion

Thiol modified gDNA was attached to both 10 and 20-nm diameter gold colloid and quantified the loading efficiency. The 10-nm particles were more stable to initial oligonucleotide modifications albeit with lower recovery yield than the larger 20-nm particles. The 10-nm AuNP was chosen for further developed throughout the rest of the study.

2.3.1. Attachment to AuNP

Stable gold nanoparticles were formed by the incorporation of 5'-thiol modified 18-mer gDNA or 20-mer SSO (in **Chapter III**) using the salt conditioning technique developed by the Mirkin Lab (Hill and Mirkin. 2006). If the surface modification failed during conjugation, the reaction color changed from red to blue or precipitate, often occurring with the 20-nm gold colloid. Successful surface coating required all solutions to be filtered through a Whatman 0.22 um disposable syringe filter, with glass containers that were acid-washed, and clean of dust. Any foreign particulate introduced during the AuNP conjugation triggered gold aggregation on the particulate significantly decreasing the recovery. Multiple centrifugation of the AuNP solution was also necessary to pellet the sol. Frequently, at least

four 30-minute high speed centrifuge spins were necessary to collect ~95% of the starting concentration. Supernatant from every centrifugation was collected and analyzed to quantify loss during conjugation or incomplete recovery. For these reasons, batch yield dropped to 30% recovery of 10-nm AuNP and 50% recovery of 20-nm AuNP. Surface binding of gDNA produced 66 strands to one 10-nm AuNP characterized by UV spectroscopy, while the 20-nm AuNP produced 260:1 ratio of DNA to particle, as depicted in **Figure 2-3**.

2.3.2 Synthesis of DNA Ligands

As illustrated in **Figure 2-4**, three complement strand constructs were developed for the gDNA-AuNP system. All cDNA ligands consisted of a 5'-amino-modified 18-mer oligonucleotide conjugated to disulfide containing crosslinker, DSP. To produce PEG-cDNA, the DSP-modified cDNA was further pegylated with α-hydroxyl-ω-amino PEG_{3000} with thoughts to increase circulation stability as seen in TNF_{α}-AuNP (Farma et al. 2007a). As a surrogate of siRNA, pegylated BODIPY FL was used. Bisamine PEG_{900} was conjugated to dithiopropionate-modified cDNA then heterofunctionalized with activated BODIPY FL, forming the final construct FL-cDNA. The ligand was HPLC purified and analyzed by UV/visible spectrophotometry. BODIPY FL was quantified at 504 nm, and background subtracted DNA absorbance at 260 nm, resulting in 90% expected absorbance ratio between BODIPY FL and cDNA. The FL-cDNA was used without further purification.

Limited solubility of folic acid hindered direct conjugation to heterofunctional bisamine PEG_{3350}-cDNA used to synthesize FL-cDNA. To increase solubility, bisamine-PEG was initially conjugated to folic acid then attached directly to DSP-modified cDNA. The pegylated folic acid was also conjugated to FITC and used as a probe to assess folate

receptor expression in KB and OVCAR3 cells. All conjugated cDNA were purified using HPLC and analyzed via UV/visible spectrometry or PAGE, as shown in **Figure 2-5**, **Figure 2-6**, and **Figure 2-7** respectively. HPLC purification of PEG containing cDNA was facile due to the long retention time and the characteristic broad peak due to the heterogeneity of the PEG starting material. The FA-cDNA was used without further purification.

2.3.3 Ligand Hybridization Efficiency

To quantify hybridization efficiency, excess FL-cDNA was mixed with gDNA-AuNP and annealed twice by heating to 65°C and slowly cooling to RT. Free FL-cDNA was removed by repeated centrifugation until fluorescence was not detected in the supernatant (Connor et al. 2005, Demers et al. 2000) . The concentration of AuNP was determined using absorbance at 520 nm prior to extraction. As shown in **Figure 2-8**, hybridized FL-cDNA to gDNA-AuNP was extracted using 1.0 M DTT to thiol exchange with AuNP. The solution became clear and AuNP precipitate was pelleted. The supernatant fluorescence was analyzed against a standard curve containing known concentrations of BODIPY FL in 1.0 M DTT and 10 mM phosphate buffer. Fluorescence calculations indicated that approximately 6.2 FL-cDNA were attached to every AuNP, resulting in 9.4% hybridization efficiency toward gDNA immobilized on the particle. The experimentally determined substitution ratio is 6:66:1 FL-cDNA to gDNA to AuNP, for 10 nm particles.

2.4 Conclusion

As stated previously in **Section 2.2.3**, conventional terminology of gold particles in suspension is expressed similar to molecules in solution. One particle of gold colloid is

equivalent to one molecule when analyzed using ε_{max} of 9.55 x 10^7 $M^{-1}cm^{-1}$ for 10nm AuNP and 9.41 x 10^8 $M^{-1}cm^{-1}$ for 20nm AuNP. Surface conjugation causes a slight red-shift in peak absorbance compared to stock citrate-stabilized AuNP with max absorbance at 520 nm, but the excitation coefficient is not altered.

Initial gold colloid studies utilized commercially obtained 10 and 20-nm diameter particles to characterize the loading efficiency of 5'thiolated DNA through dative binding. Difficulty preparing large volumes of gDNA bound 20-nm AuNP limited its production compared to the smaller 10-nm particle. While the 20-nm AuNP supplied 260 possible hybridizing sites, the larger AuNP was prone to aggregation overnight during the salt aging process. Unlike the 10-nm particle, the 20-nm gDNA complexed colloidal suspension required daily mixing to prevent settling. For these reasons, the 10-nm AuNP was chosen for future studies.

Three cDNA ligands were successfully synthesized to hybridize to the complement gDNA; folic acid-PEG_{3350}-DNA, bodipy-PEG_{900}-cDNA, and PEG_{3000}-cDNA. The PEG_{3000}-cDNA was designed to increase PEGylation coverage of AuNP and its therapeutic cargo during systemic delivery. The FA targeting ligand was designed to carry the longest PEG chain (3350 mw), in order to avoid steric hinderance from HO-PEG_{3000}-cDNA while binding to the folate receptor. The bodipy-PEG_{900} was used as a surrogate to mimic siRNA incorporated into the AuNP delivery system.

The DSP disulfide crosslinker incorporated into each cDNA conjugate should cleave in cytosolic conditions, releasing the pegylated BODIPY FL or siRNA. The surface of the AuNP is also able to exchange thiols, similarly releasing the cargo. This redundancy is necessary or the carrier cDNA attaching the targeting ligand would still be hybridized to the

therapeutic cargo, which may inhibit RNAi activity of the therapeutic cargo. It is unknown whether the 5'-thiol modification on the sense strand of siRNA would alter the silencing activity and needs to be addressed in future siRNA studies.

Unfortunately, the low hybridization efficiency of six hybridizing sites out of 66 immobilized gDNA sequences limits the carrier's utility to transport both therapeutic ODN and a targeting ligand. If half the hybridizing sites contain the folic acid targeting ligand, only three sites can be utilized to carry siRNA, resulting in a costly and inefficient delivery vehicle for the development of a gold-based carrier. Without additional PEG containing cDNA, PEG_{3000}-cDNA, stability and protection of siRNA would be in question.

To overcome the low hybridization efficiency, two strategies can be incorporated into future studies. Initial passivation using a hydrophilic molecule, such as short thiolated polyethelyene oxide, can stabilize the gold nanoparticle in organic and aqueous solutions (Agasti et al. 2007). Addition of larger thiolated compounds, and possibly oligonucleotides, can place exchange with the small polyethelyene oxide molecule in a concentration dependant procedure, also known as Murray exchange method (Templeton et al. 2000). The short polyethelyene oxide between the surface bound gDNA molecules separates the strands while stabilizing the AuNP. Although the substitution ratio of gDNA to AuNP will decrease, less steric hindrance during hybridization should improve the binding capacity of the AuNP carrier. The second strategy also focuses on lowering steric hindrance during hybridization, but may preserve the substitution ratio between gDNA and AuNP. Extension of the gold-bound oligonucleotide with a PEG chain or addition of poly-thymidine nucleic acids between the thiol and hybridizing sequence will distance the modular linker further away from the constrictive surface of gold, possibly decreasing steric hindrance during hybridization. The

increased distance from the crowded surface would enable the cDNA to hybridize with less restriction. This method is utilized on surface plasmon resonance biochips and gold nanoparticles for biosensors to increase binding or hybridization efficiency (Hurst et al. 2006).

Instead of incorporating an extended gDNA or attempting Murray exchange to prepare gDNA-AuNP, the delivery strategy was significantly altered to a simpler design for further studies, discussed in **Chapter III**. This strategy utilizes the SSO as the therapeutic agent and also the modular linker to hybridize the targeting ligand. Only the targeting ligand was necessary to hybridize to the linker, assuming similar hybridization efficiency is encountered in the colloidal gold-based SSO delivery system.

Diameter (nm)	Radius (nm)	S.A./particle (nm2)	# dsDNA/ particle[A]	#dsDNA/ particle[B]	#ssDNA/ particle[B]
5	2.5	78.5	14	2	9
10	5	314	55	9	35
15	7.5	706.5	123	20	78
20	10	1256	218	35	138
30	15	2826	491	79	311
40	20	5024	872	141	553
50	25	7850	1363	220	864

Figure 2-1. Surface area calculations for various diameter spheres. (A) Calculations based on a 2.8nm cross-sectional diameter of dsDNA. (B) Calculations based on SPR chip capacity

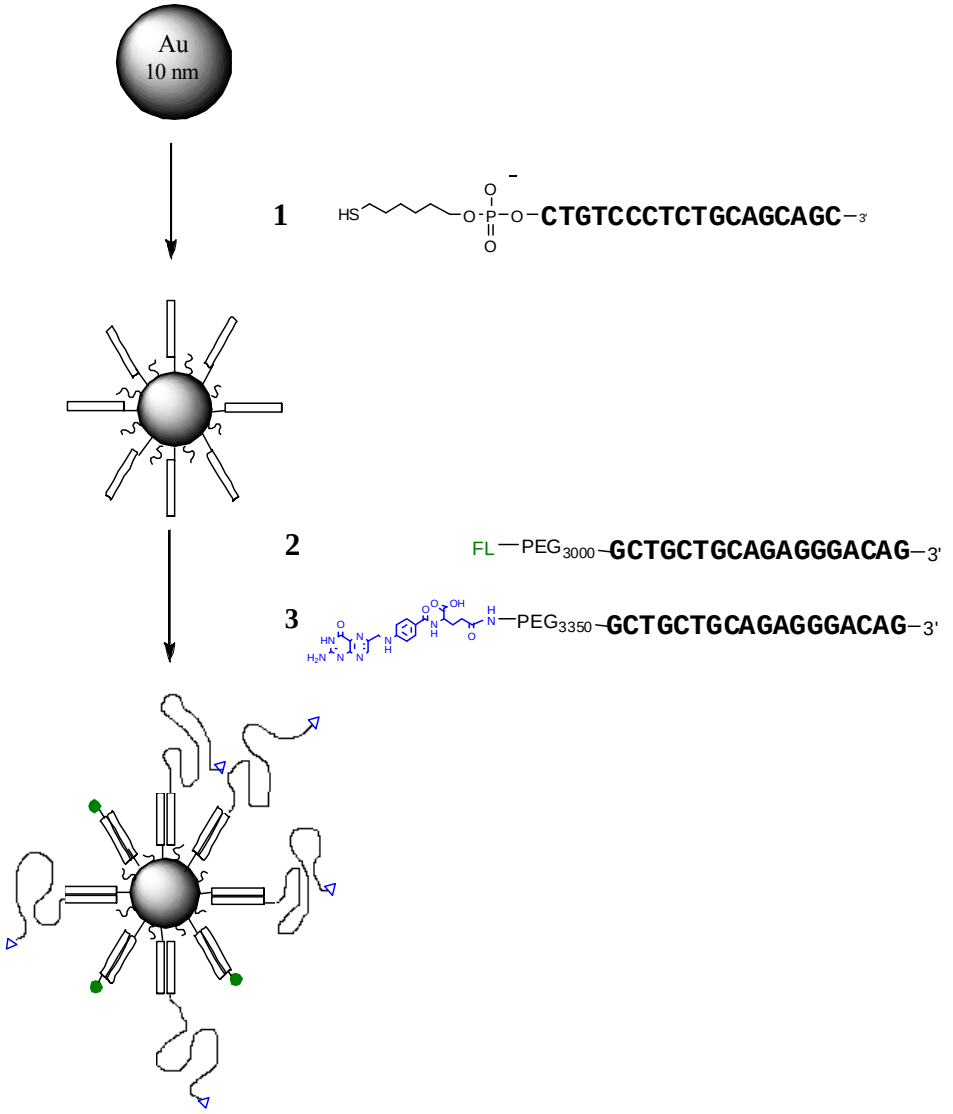

Figure 2-2. The siRNA delivery system is composed of a AuNP surface conjugated with non-therapeutic oligonucleotides for hybridization. Various ligands and cargo, such as siRNA, can be hybridized using the complement strand. This figure depicts a fluorophore (2 and green spheres) and folic acid (3 and blue triangles) conjugated to the complement oligonucleotide and complexed to the modular carrier.

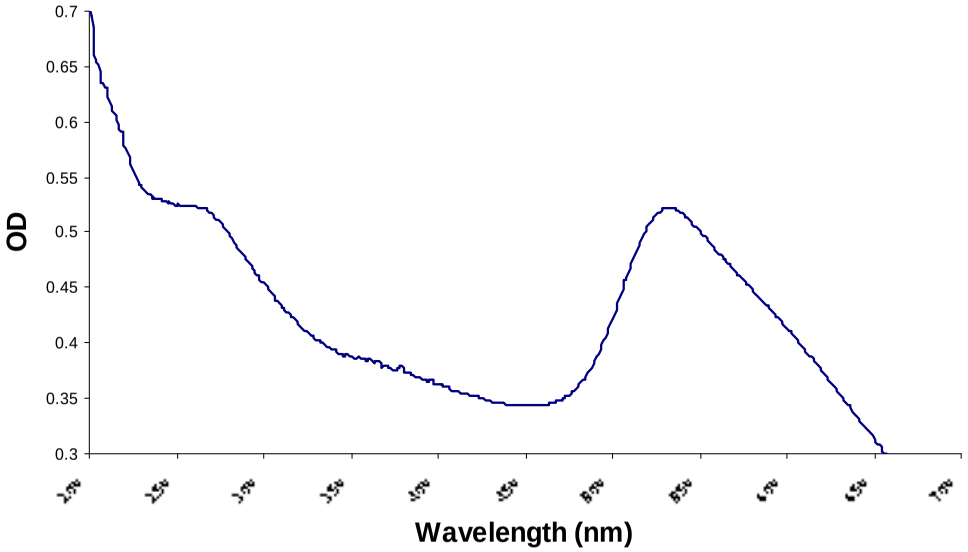

A

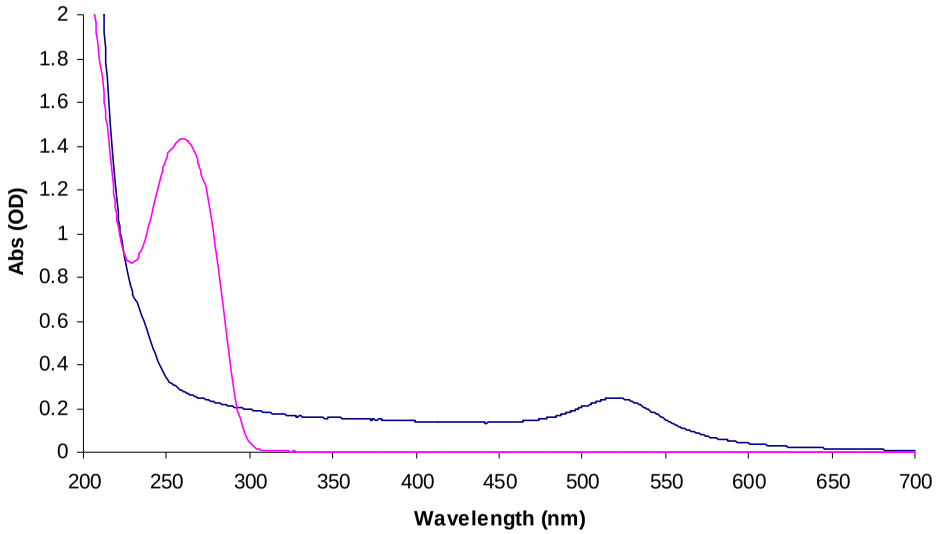

B

Figure 2-3. Complexation of cDNA and 20 nm AuNP produced an overlapping UV/visible spectrum. (A) Spectrum of cDNA-AuNP. A slight red-shift in AuNP is observed due to surface modification. (B) Combined spectrum of cDNA and AuNP.

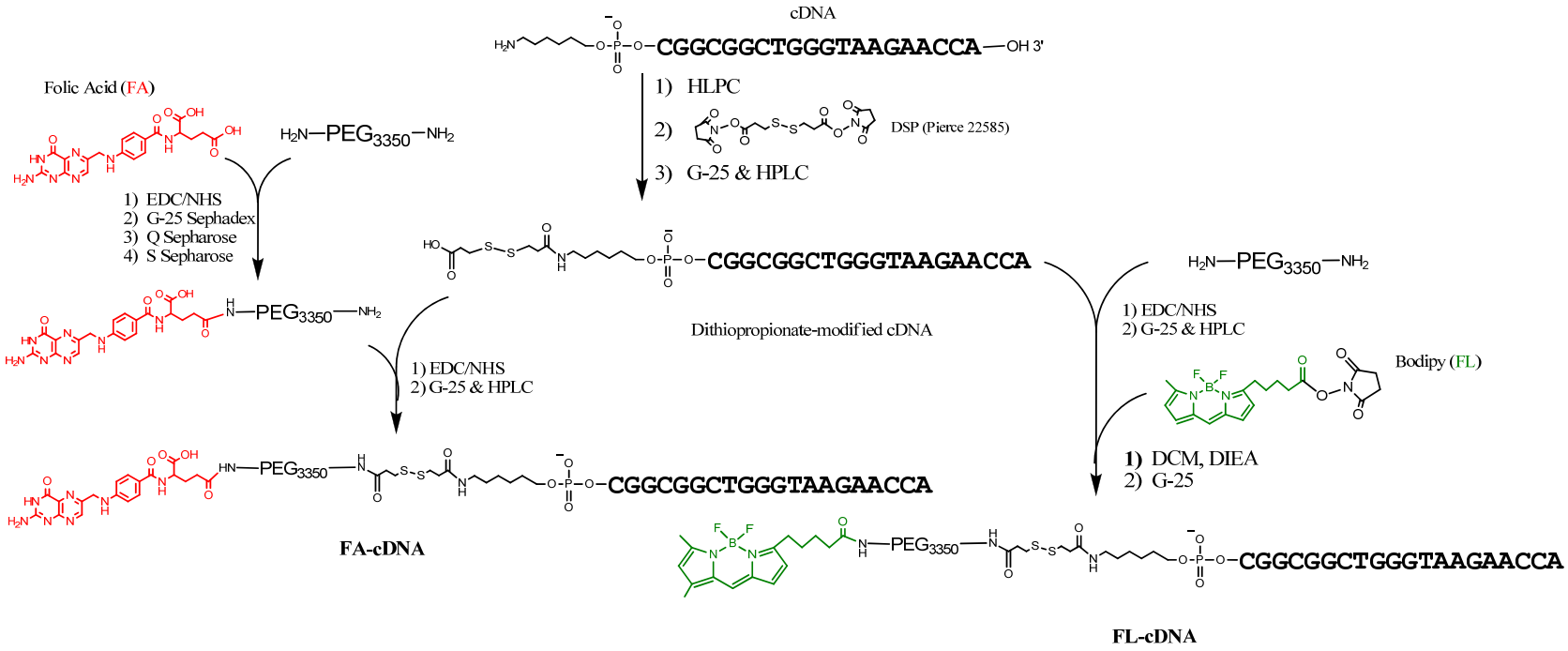

Figure 2-4. General synthetic scheme outlying intermediates combined to produce FA-cDNA

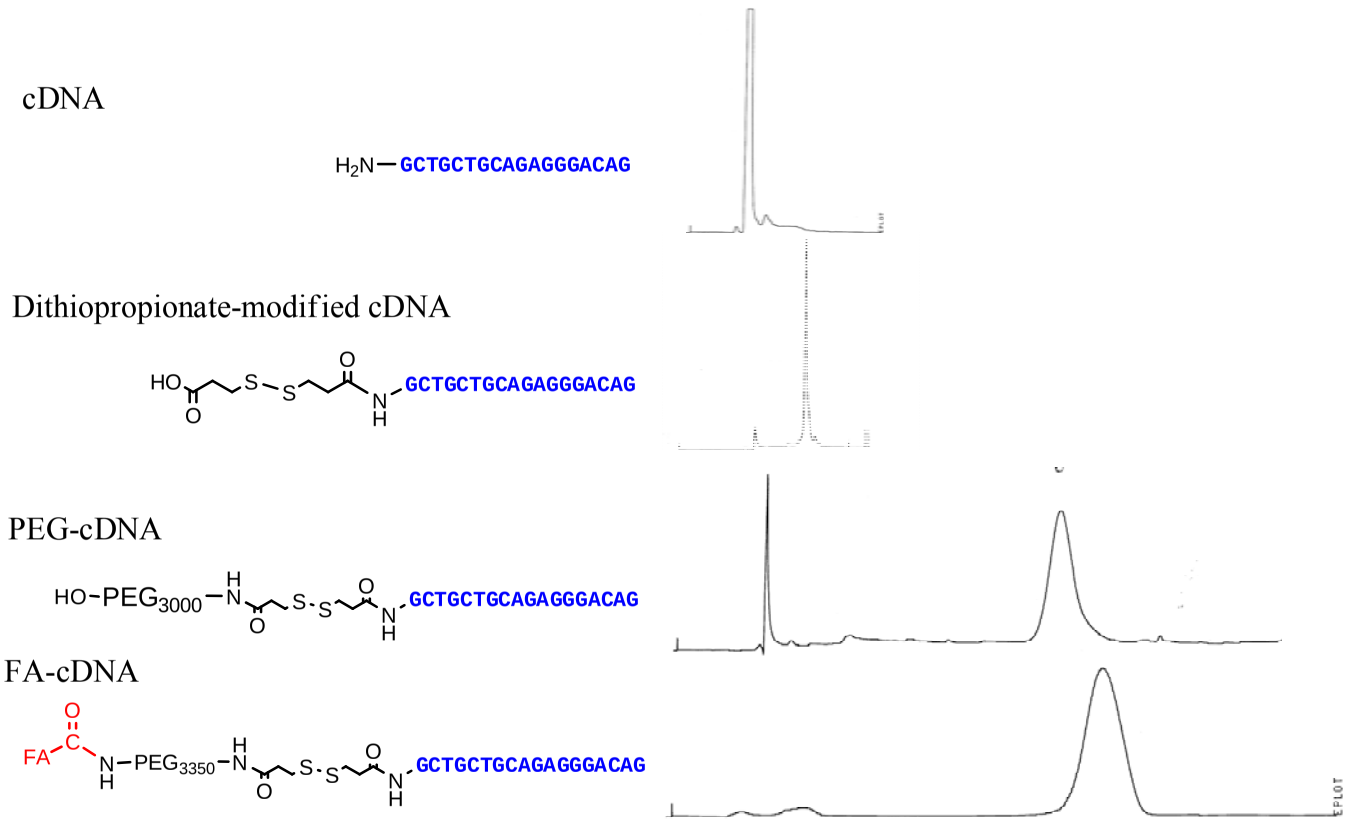

Figure 2-5. HPLC chromatogram of starting material cDNA and intermediate dithiopropionate-modified cDNA were purified prior to conjugation with PEG. Heterogeneity of stock PEG resµlted in peak broadening as seen in PEG-cDNA and FA-cDNA. FL-cDNA chromatogram not shown.

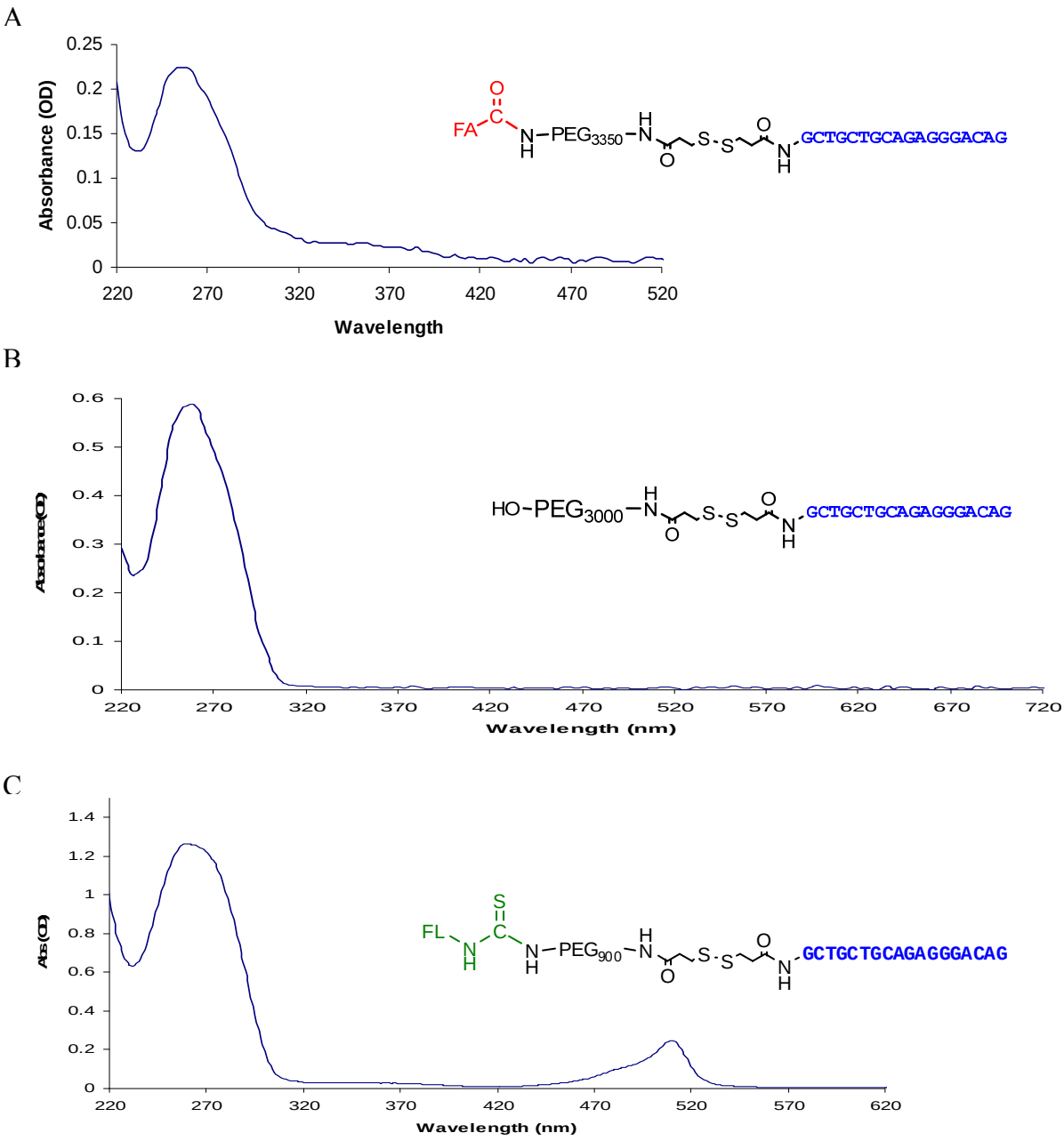

Figure 2-6. UV/visible spectrum of cDNA conjugates. (A) FA-PEG-ss-DNA. Folic acid ϵ282: 2.52 x 10^4 M^{-1} cm^{-1} & ϵ350: 6.77 x 10^3 M^{-1} cm^{-1}, (B) HO-PEG-ss-DNA. DNA ϵ260: 1.76 x 10^5 M^{-1} cm^{-1} (C) BODIPY -PEG-ss-DNA ϵ504: 6.80 x 10^4 M^{-1} cm^{-1}

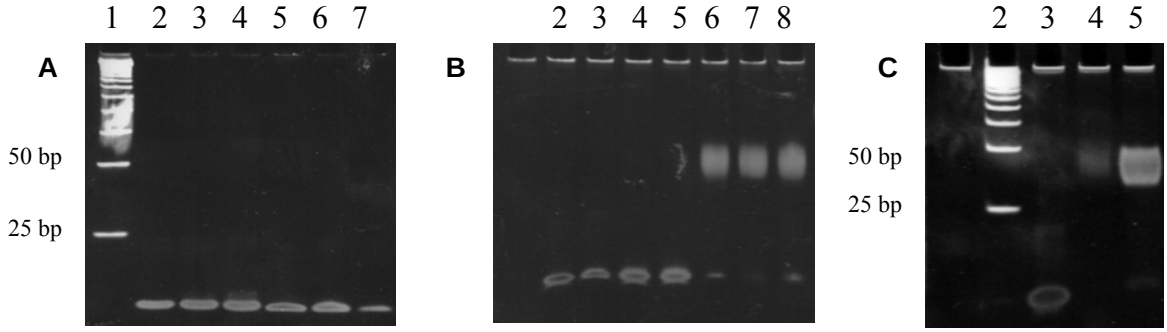

Figure 2-7. Non-denaturing 15% PAGE analysis of PEG-cDNA and FA-cDNA to confirm HPLC results. The DNA was visualized using SybrGold® stain. (A) The starting cDNA and dithiopropionate-modified cDNA was visualized for purity. Lane 1 contains a 25 bp ladder. Lanes 2 - 4 contain 50, 100, and 250 ng of HPLC purified 5' amine-DNA. Lanes 5 -7 contain three separate batches of HPLC purified dithiopropionate-modified cDNA. (B) Excess α,ω bisamine-PEG was reacted to NHS/EDC activated dithiopropionate modified cDNA and HPLC purified. Lane 2 contained starting bisamine-PEG material. Lanes 3 - 5 contain 50, 100, and 250 ng of dithiopropionate-modified cDNA. Lanes 6 - 8 contain three separate batches of PEG-cDNA. (C) Excess FA-PEG-NH_2 was reacted to NHS/EDC activated dithiopropionate modified cDNA to produce FA-cDNA. Lane 2 contains a 25 bp ladder. Lane 3 contains the dithiopropionate modified cDNA intermediate. Lane 4 contains previously synthesized PEG-cDNA and Lane 5 contains HPLC purified FA-cDNA.

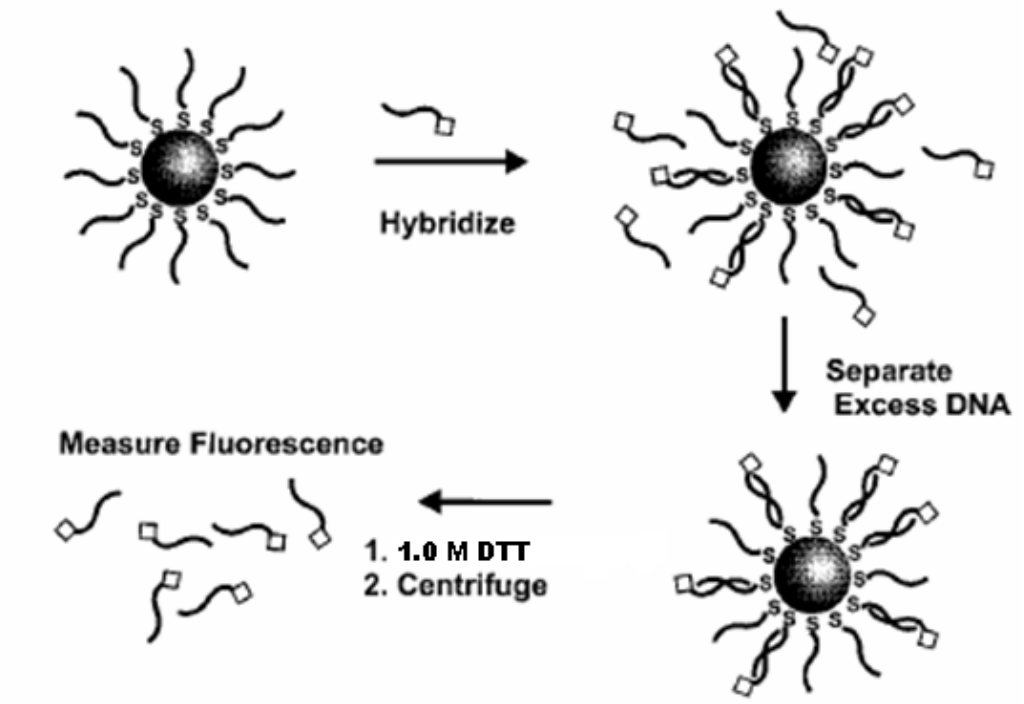

Figure 2-8. Hybridization efficiency was calculated using 1.0 M DTT to thiol exchange onto the surface of DNA coated AuNP releasing BODIPY FL labeled DNA. The resulting complex is unstable and precipitates from solution. The supernatant fluorescence was compared to a standard curve to calculate hybridization efficiency, resulting in 9.3% for the siRNA delivery system and 11.8% for the SSO delivery system. Adapted from *Demers et al 2000*.

2.5 References

S. Agasti, Chang-Cheng You, Palaniappan Arumugam and Vincent M. Rotello. Structural control of the monolayer stability of water-soluble gold Nanoparticles. J. Mater. Chem. 18; 70–73 (2008).

M. Cardenas, J. Barauskas, K. Schillen, J. L. Brennan, M. Brust, and T. Nylander. Thiol-specific and nonspecific interactions between DNA and gold nanoparticles. Langmuir. 22:3294-3299 (2006).

A.W. Peterson, R.J. Heaton, and R.M. Georgiadis. The effect of surface density on DNA hybridization. Nuc. Acid Res. 29;24:5163-5168 (2001)

A. Chompoosor, G. Han, and V. M. Rotello. Charge dependence of ligand release and monolayer stability of gold nanoparticles by biogenic thiols. Bioconjug Chem. 19:1342-1345 (2008).

E. E. Connor, J. Mwamuka, A. Gole, C. J. Murphy, and M. D. Wyatt. Gold nanoparticles are taken up by human cells but do not cause acute cytotoxicity. Small. 1:325-327 (2005).

L. M. Demers, C. A. Mirkin, R. C. Mucic, R. A. Reynolds 3rd, R. L. Letsinger, R. Elghanian, and G. Viswanadham. A fluorescence-based method for determining the surface coverage and hybridization efficiency of thiol-capped oligonucleotides bound to gold thin films and nanoparticles. Anal Chem. 72:5535-5541 (2000).

J. M. Farma, M. Puhlmann, P. A. Soriano, D. Cox, G. F. Paciotti, L. Tamarkin, and H. R. Alexander. Direct evidence for rapid and selective induction of tumor neovascular permeability by tumor necrosis factor and a novel derivative, colloidal gold bound tumor necrosis factor. Int J Cancer. 120:2474-2480 (2007a).

A. E. Finkelstein, F. R. Roisman, and D. T. Walz. Effect of auranofin, a new antiarthritic agent, on immune complex-induced release of lysosomal enzymes from human leukocytes. Inflammation. 2:143-150 (1977).

G. Frens. Controlled nucleation for the regulation of particle size in monodisperse gold suspensions. Nature Phys. Sci. 241: 20-22. (1972).

P. Ghosh, G. Han, M. De, C. K. Kim, and V. M. Rotello. Gold nanoparticles in delivery applications. Adv Drug Deliv Rev. (2008a).

J. F. Hainfeld, F. A. Dilmanian, D. N. Slatkin, and H. M. Smilowitz. Radiotherapy enhancement with gold nanoparticles. J Pharm Pharmacol. 60:977-985 (2008).

G. Han, N. S. Chari, A. Verma, R. Hong, C. T. Martin, and V. M. Rotello. Controlled recovery of the transcription of nanoparticle-bound DNA by intracellular concentrations of glutathione. Bioconjug Chem. 16:1356-1359 (2005).

G. Han, P. Ghosh, and V. M. Rotello. Functionalized gold nanoparticles for drug delivery. Nanomed. 2:113-123 (2007).

G. Han, C. T. Martin, and V. M. Rotello. Stability of gold nanoparticle-bound DNA toward biological, physical, and chemical agents. Chem Biol Drug Des. 67:78-82 (2006).

H. D. Hill and C. A. Mirkin. The bio-barcode assay for the detection of protein and nucleic acid targets using DTT-induced ligand exchange. Nat Protoc. 1:324-336 (2006).

R. Hong, G. Han, J. M. Fernandez, B. J. Kim, N. S. Forbes, and V. M. Rotello. Glutathione-mediated delivery and release using monolayer protected nanoparticle carriers. J Am Chem Soc. 128:1078-1079 (2006).

M. Horisberger. Evaluation of colloidal gold as a cytochemical marker for transmission and scanning electron microscopy. Biol. Cellulaire 36: 253-258 (1979).

S. J. Hurst, A. K. Lytton-Jean, and C. A. Mirkin. Maximizing DNA loading on a range of gold nanoparticle sizes. Anal Chem. 78:8313-8318 (2006).

G. F. Paciotti, L. Myer, D. Weinreich, D. Goia, N. Pavel, R. E. McLaughlin, and L. Tamarkin. Colloidal gold: a novel nanoparticle vector for tumor directed drug delivery. Drug Deliv. 11:169-183 (2004).

H. L. Robinson and T. M. Pertmer. Nucleic acid immunizations. Curr Protoc Immunol. Chapter 2:Unit 2.14 (2001).

H. H. Sage, B. K. Sinha, D. Kizilay, and R. Toulon. Radioactive Colloidal Gold Measurements of Lymph Flow and Functional Patterns of Lymphatics and Lymph Nodes in the Extremities. J Nucl Med. 5:626-642 (1964).

D. S. Seferos, D. A. Giljohann, N. L. Rosi, and C. A. Mirkin. Locked nucleic acid-nanoparticle conjugates. Chembiochem. 8:1230-1232 (2007).

A. C. Templeton, W. P. Wuelfing, and R. W. Murray. Monolayer-protected cluster molecules. Acc Chem Res. 33:27-36 (2000).

N. S. Yang, J. Burkholder, D. McCabe, V. Neumann, and D. Fuller. Particle-mediated gene delivery in vivo and in vitro. Curr Protoc Hum Genet. Chapter 12:Unit 12.6 (2001).

Chapter III

COLLOIDAL GOLD-BASED OLIGONUCLEOTIDE DELIVERY SYSTEM

An intriguing class of anti-sense based medicines that do not fit any of the nucleic-acid based therapies discussed in **Section 1.1** are those that alter the code of mRNA (Opalinska and Gewirtz. 2002). Resembling that of classical anti-sense, but utilizing the advances in molecular biology in the past 30 years, oligonucleotides can be targeted toward specific sequences involving splice sites of unedited or pre-mRNA to alter the sequence of mRNA and its translational product (Sierakowska et al. 1999).

Post-transcriptional modifications of pre-mRNA require introns to be removed from the messenger to form functional genetic codes for protein translation. Alterations in splicing of one gene can produce multiple isoforms of mRNA, significantly increasing the repertoire in the human proteome (Schmajuk et al. 1999). At least 60% of the genome undergoes multiple splicing and is directly implicated in sex determination, apoptosis, antibody production, and neuronal development (Modrek and Lee. 2002).

Point mutations at genomic splice sites are known to cause dramatic deletions and frame shift, resulting in truncated or non-functioning protein expression (Xu et al. 2002, Hachem and Gartenhaus. 2005). Subsequent aberrant splicing is associated with a plethora of diseases such as cancer, Parkinson's disease, cystic fibrosis, muscular dystrophy, and β-Thalassemia (Kole et al. 2004). In β-Thalassemia, a genetic human blood disease marked with low oxygen capacity, the β-globin is mutated affecting functional hemoglobin formation. Although hundreds of mutations on the globin gene can cause Thalassemia,

several severe forms are due to point mutations along the intron creating non-natural splice sites (Sierakowska et al. 1999). This generates non-coding introns to be included in the edited mRNA, some with premature stop codons, translating into mutant globins that cannot combine and form hemoglobin. Anti-sense oligonucleotides hybridized to these mutations cause the post-transcriptional machinery to skip the site and splice further upstream at the correct genomic splice sites, forming functional globins (Sazani and Kole. 2003a). These splice shifting oligonucleotides (SSO) must not activate RNase H and must gain access to pre-mRNA located in the nucleus (Sazani and Kole. 2003b)

The ability to truncate mRNA sequences with oligonucleotides is utilized in a functional assay system with a positive readout, unlike that of typical anti-sense which can only down-regulate mRNA (Kang et al. 1998, Paroo et al. 2004). A long-standing limitation with studies involving complex delivery systems utilizing anti-sense oligonucleotides stem from the variable pharmacodynamics and analyzing anti-sense directed down-regulation of the target protein. Results can be affected by nonspecific anti-sense mechanisms, carrier effects, and environmental variability in biological systems, causing cell growth inhibition and variable protein activity (Lin et al. 2001).

By incorporating the abnormal intron #2, with the 705 or 654 nucleotide site mutation from Thalassemia, into the code of any gene, the resulting mRNA then transcribes the incorporated non-coding fragment. This insert contains a cryptic stop codon causing translational arrest and ubiquitous elimination of the protein portion (Schmajuk et al. 1999, Sierakowska et al. 1999). For upregulation assays, the 705 or 654 mutant intron was incorporated in either the luciferase (luc-705) or green fluorescence protein (EGFP-654)

gene. Successful therapy with splice shifting oligonucleotides will produce functional luciferase activity or emit green fluorescence in a positive readout (Schmajuk et al. 1999).

Recently, splice switching technology has been applied to therapeutically alter oncogene activity in a two-prong approach to sensitize cancer cells against conventional chemotherapeutic agents (Mercatante et al. 2001). The B-cell lymphoma (bcl-2) class of oncogenes regulates apoptosis and is implicated in resistance to chemotherapy (Wilusz et al. 2005). Certain members in the Bcl-2 family undergo gene splicing that produces either pro- or anti-apoptotic factors. The Bcl-x gene is an oncogenic member existing as two isoforms with opposing effects as depicted in **Figure 3-1**. The long form, Bcl-xL, contains four conserved Bcl-2 homology (BH) domains. Increased production of this Bcl-xL oncoprotein stabilizes mitochondrial function, promoting cell survival and causing chemotherapy resistance (Hachem and Gartenhaus. 2005). The short sequence, Bcl-xS, is formed when the 5'-splice site of Bcl-xL is bypassed by the splicosome and regulated to a site further downstream, removing the BH-1 and BH-2 domains. The loss of the BH4 domain exposes the BH3 "death domain" to promote apoptosis. The Bcl-xS isoform is also expressed in low amounts in cancer cells (Hachem and Gartenhaus. 2005). Directed SSO toward the 5'-conserved splice site in pre-mRNA converts the anti-apoptotic isoform to the pro-apoptotic, thus causing both down-regulation of the oncogene and upregulation of an apoptotic signal (Mercatante et al. 2001, Mercatante et al. 2002). Normal cells expressing basal levels of Bcl-xL are less affected by SSO chemo-sensitizers but long-lived post-mitotic cells with naturally high levels Bcl-xL may be affected using this therapy.

3.1 Statement of Purpose

Oligonucleotides containing 2'-*O*-methyl modified bases are more stable in biological milieu than siRNA based therapies and may not require complex pegylation to protect the surface bound cargo. A simplified approach containing SSO complexed to AuNP as the modular scaffold is developed as a delivery carrier as seen in **Figure 3-2**. This approach also employs folic acid conjugated to the complement stand as a targeting mechanism. Similar to the siRNA approach, the development of the SSO delivery carrier is separated to three stepwise specific aims.

Aim 1: *Conjugate and characterize 5'-thiol modified SSO to AuNP*. The SSO carrier system consists of a therapeutic 20-mer SSO which is directly conjugated to the surface of AuNP resulting in the formation of SSO-AuNP. This serves as both therapeutic cargo and modular linker.

Aim 2: *Conjugate folic acid to DNA that is complementary to SSO (sDNA)*. For the SSO carrier system, the folic acid targeting ligand is directly conjugated to the complement of the SSO sequence. This sequence is referred to as sDNA throughout this chapter. To characterize hybridization efficiency, BODIPY FL was separately conjugated to the sDNA.

Aim 3: *Characterize and test in an in vitro model to knock down mRNA activity using SSO targeting Bcl-xL oncogene*. Only the SSO-AuNP is tested for in vitro efficacy. The folic acid targeting gold carrier systems should preferentially accumulate and alter mRNA activity in cell culture.

3.2 Materials and Methods

The SSO delivery system is a simplified version of the siRNA delivery system. The complexation of SSO to AuNP, the HPLC and SEC purification procedure, and the hybridization technique utilized in this chapter are identical to the methods used in **Chapter II**. Deviations and differences between methods are stated in each section and similar analytical techniques are referenced to the initial study.

3.2.1 Materials

Colloidal gold in suspension was purchased from BB International (10 nm, Cat. Code EM.GC10, Madison, WI) and Sigma (10 nm, Cat. #G1527, St. Louis, MI). All custom synthesized oligonucleotides were purchased from IDT (Coralville, IA); 5' thiol-C6-TGGTTCTTACCCAGCCGCCG, 5' amino-C6-CGGCGGCTGGGTAAGAACCA, with the exception of controlled pore glass (CPG) bound DNA (Lineberger Cancer Center, Chapel Hill, NC). Cell culture media were obtained from Gibco (Grand Island, NY) and charcoal filtered fetal bovine serum from Gemini Bioproducts (Cat. # 100-119, Atlanta, GA). SybrGold (Cat. # S11494) and BODIPY FL C_5 SE (Cat. # D1684) was obtained from Molecular Probes (Eugene, OR). Folic acid (Cat. # F7876), 1-ethyl-3-(3-dimethylaminopropyl)-carbodiimide (Cat. # E7750), *N*-hydroxysuccinimide (Cat. # 130672), and various organic solvents were obtained from Aldrich (Milwaukee, WI). Fluorescein isothiocyanate (FITC, Cat. # F7250), general chemicals and inorganics were also obtained from Sigma (St. Louis, MI).

3.2.2 Attachment of Splice-Shifting Oligonucleotides (SSO) to AuNP

The commercially obtained 5'-thiol modifier SSO was HPLC purified, concentrated under vacuum, and G-25 desalted prior to conjugation to only the 10 nm AuNP. The identical procedure utilized for the siRNA strategy in **Section 2.3.1** was employed for SSO (ε_{260} =1.80 x 10^5 $M^{-1}cm^{-1}$) binding to AuNP.

3.2.3 Synthesis of SSO Complementary DNA (sDNA) Conjugates

To increase synthetic yield of sDNA conjugates, solid-phase synthesis was employed to conjugate folic acid to the oligonucleotide (Habus et al. 1998). This technique also avoids the solubility limitation and side-product formation encountered when linking folic acid to the sDNA using solution based methods.

Solid-Phase Synthesis of CPP-bound 5'-Amino Modified sDNA

Four batches of CPG-bound oligonucleotide were synthesized by Dr. Rowshon Alam, (mohammed_alam@med.unc.edu) using phosphoramidites with ultraMILD-protected bases in a 1-μmol scale on a CPG support (500˚A) on a AB 3400 DNA synthesizer (Applied Biosystems, Foster City, CA). The coupling times for the phosphoramidites and final 5'-amino linker were 360 and 600 sec, respectively. 5-Ethylthio-1H tetrazole was used as an activator (0.25M solution in acetonitrile) and 5% phenoxyacetic anhydride in tetrahydrofuran/pyridine as a blocking solution during oligonucleotide synthesis. The monomethoxytrityl protected 5'-amino linker was introduced at the 5'-end of the oligonucleotide at the last step of synthesis and stored in small reaction vials. To deprotect the 5'-amine while preserving ultraMILD-protected bases, the support was treated with 80%

aqueous acetic acid for 1h at 55˚C in a water bath. The support was then transferred to a synthesis cartridge and subsequently washed twice with 3 ml water, then acetonitrile, and finally ether.

Synthesis of Folic Acid-sDNA (FA-sDNA)

CPG-bound 5'-amino DNA (50 mg) was transferred to an empty Poly-Pak synthesis cartridge (Cat. # 60-1100-01, Glen Research), graciously supplied by Dr. Rowshon Alam, and rinsed with 3 ml of 0.1% triethylamine (TEA) in DMSO. In a 7 ml scintillation vial, folic acid (0.1 mmol, 44 mg) was dissolved in 1 ml of anhydrous DMSO. To the DMSO solution, 0.5 mmol of EDC (96 mg) and 0.01 mmol of 4-(*N,N*-dimethylamino)pyridine (DMAP, 1.2 mg) were dissolved and 10 µl of TEA introduced to the reaction mixture. The DMSO solution was loaded into a reaction cartridge (0.5 ml total volume) and capped with empty tuberculin syringes (Sigma Cat. # Z230723, St. Louis, MI). The cartridge was protected from light and rotated for 24 hours at RT.

The cartridge was rinsed twice with 3 ml of DMSO, acetonitrile, ether, and finally air dried. The resin bound folic acid-DNA was transferred to a 3 ml reaction vial and suspended in 0.5 ml of concentrated NH_4OH. The vial was incubated at 55˚C for 6 hours. After cleavage, the supernatant was transferred to another vial and resin rinsed with 1 ml dH_2O. The rinse solution was combined with supernatant and immediately evaporated to near dryness. The DNA solution was diluted to 400 µl with 0.1 M TEAA and purified via HPLC. The DNA fractions were pooled, concentrated, G-25 desalted and lyophilized. The folic acid-DNA was analyzed with UV/visible spectrometry and Bruker Ultraflex I matrix-assisted

laser desorption/ionization-time of flight spectrometer **(**MALDI-TOF, Fremont, CA) shown in **Figure 3-3**.

Synthesis of BODIPY FL-sDNA (FL-sDNA)

One batch of CPG-bound DNA (1 μmol scale synthesis) was cleaved from the CPG support using standard deprotection and cleavage technique described during the synthesis of FA-sDNA in **Section 3.2.3**. BODIPY-labeling of H_2N-sDNA with BODIPY FL was performed following the manufacturer's recommended protocol. Briefly, 36 nmol of H_2N-sDNA (230 μg) was lyophilized in a 1.6 ml MC tube then redissolved in 200 μl of 0.1 M borate buffer (pH:8.5). A stock bottle of BODIPY-C_5-SE (5 mg) dissolved in 280 μl of anhydrous DMSO, from the FL-cDNA synthesis described in **Section 2.2.4**, along with 28 μl (1.2 umol, 500 ug) of BODIPY FL was transferred to the MC tube containing sDNA. The reaction mixture was protected from light and stirred for 72 hours at RT. The suspension was centrifuged and supernatant transferred to a new MC tube. The pellet was rinsed with 100 μl dH_2O, centrifuged again, and supernatants were combined. The reaction solution was desalted and purified via HPLC described in the General Methods and Procedures (**Section 2.2.2**). The FL-sDNA peak was concentrated, G-25 desalted and lyophilized.

3.2.4 Ligand Hybridization to SSO-AuNP

Folic acid or BODIPY FL labeled sDNA was hybridized and quantified using the same procedure as DNA hybridization for gDNA-AuNP. Refer to **Section 2.2.4** for specific methods and analytical techniques.

3.2.5 Splice Shifting in Folate Receptor Expressing KB Cell Culture

Both human KB and OVCAR3 cells have been shown to over-express folate receptor when cultured in folic acid-deficient medium, which must be verified with the current cultured cell lines. The cell lines were passaged for two months in folate-free Roswell Park Memorial Institute (RPMI)-1640 medium supplemented with 5% charcoal filtered fetal bovine serum (FBS) and 1% penicillin/streptomycin (pen/strep) to condition the cells. Folate receptor expressing cells was studied after conditioning for splice correction studies.

Folate Receptor Validation

Folate receptor was verified on human KB and OVCAR3 cell lines using flow cytometry with antibody against folate receptor or folic acid-PEG_{3350}-FL as described below. The folic acid-PEG_{3350}-FL (FA-FL) was prepared using folic acid-PEG_{3350}-amine synthesized previously in **Section 2.2.4**. Refer specifically to the folic acid-PEG_{3350}-DNA ligand synthesis. The folic acid-PEG_{3350}-amine (2.63 μmol, 10 mg) and 20-fold FITC (52.6 μumol, 20.5 mg) was dissolved in 0.25 ml of 100 mM bicarbonate buffer (pH 9.0). The reaction was protected from light and stirred overnight at RT. The reaction solution was desalted and lyophilized. The product was analyzed with TLC and ^{1}H-NMR.

Human KB and OVCAR3 cells were then cultured in folate-free RPMI-1640 medium supplemented with 5% FBS and 1% pen/strep. Non-conditioned KB cells were cultured standard RPMI-1640 medium supplemented with 10% FBS and 1% pen/strep. Both cell lines were maintained under 5% CO_2 and at 37°C. The complete medium was replaced every other day. At 50-75% confluency, the cells were seeded into a 6-well plate at 5 x 10^5/well in 0.5 ml complete media and allowed to adhere overnight. To harvest the cells, each well was

rinsed twice with HBSS and incubated with 1 mM EDTA in PBS. Detached cells were pipetted to disperse aggregates and each well transferred to individual 1.65-ml MC tubes. Cells were twice rinsed by centrifugation at 100 G for 5 minutes and medium was replaced with 0.5 ml of BD staining buffer (Cat. # 554656, Franklin Lakes, NJ), redispersed, and placed in ice.

For non-treated samples (n=2), the cells in MC tubes were stored on ice while treated cells were stained with either FA-FL or anti-folate receptor antibodies. For FA-FL (n=2), cells were resuspended in 98 µl of staining buffer. The FA-FL was reconstituted to 1 mg/ml in PBS and 2 µl added to the cell suspension. The cells were incubated in ice for 30 minutes then diluted with 400 µl of staining buffer to each tube. Cells were centrifuged and supernatant replaced with 0.5 ml of new buffer, twice. For FR antibody binding samples (n=2), cells were resuspended in 95 µl of staining buffer. The murine, anti-folate receptor MOV18 antibody (Axxora Cat. # ALX-804-439, San Diego, CA) was diluted to 0.1 mg/ml and 5 µl added to the cell suspension. . The cells were incubated in ice for 30 minutes then diluted with 0.4 ml of staining buffer to each tube. Cells were centrifuged and supernatant replaced with 0.5 ml of new buffer, centrifuged again, and resuspended in 95 µl staining buffer. The fluorescein-labeled goat anti-mouse polyclonal antibody (Axxora Cat. # ALX-211-200, San Diego, CA) was diluted to 0.1 mg/ml with PBS and 5 µl of the diluted antibody gently mixed into the cell suspension. The cells were incubated in ice for 30 minutes and rinsed using the same method employed with the primary MOV18 antibody. Untreated KB and OVCAR3 cells were gated on a BD FACSCanto system (San Jose, CA) using manufacturers flow cytometer techniques. Roughly 5 x 10^4 cells passing through the gated region were analyzed for green fluorescence in each treated sample.

Splice Switching in KB cells

Conditioned KB cells were harvested at 50-75% confluency and seeded in a 24-well plate at 1 x 10^5 cells/well using folate-free RPMI-1640 medium supplemented with 5% FBS and 1% pen/strep. After 24 hours of incubation, the media was replaced with folate-free RPMI-1640 medium supplemented with 10% charcoal filtered FBS and incubated overnight. HeLa cells were incubated overnight in RPMI-1640 medium supplemented with 10% FBS and 1% pen/strep prior to the start of the study.

Both folic acid and BODIPY labeled SSO-AuNP were adjusted to 100 nM SSO using folate-free RPMI-1640 medium supplemented with 10% charcoal filtered FBS. KB and HeLa cell culture media were replaced with folic acid labeled SSO-AuNP (n=2), BODIPY labeled SSO-AuNP (n=2), or normal growth media. The cells were incubated for 24 hours, rinsed with folate-free RPMI-1640 medium supplemented with 10% charcoal filtered FBS, incubated for another 24 hours and RNA harvested using a Qiagen RNeasy Mini Kit (Cat. # 74104, Valencia, CA) following the manufacturer's instructions. Extracted RNA from cells were amplified by reverse transcription-PCR with Applied Biosystems r*Tth* polymerase (Cat. # N8080187, Foster City, CA) in the presence of Bcl-xL forward (CATGGCAGCAGTAAAGCAAG), reverse (GCATTGTTCCCATAGAGTTCC) primers, and Cy 5-labeled dCTP (GE Healthcare Cat. # PA53521, Piscataway, NJ) for visualization (0.1 nmol per 50 μL PCR). The reverse transcription proceeded at 70 ^{o}C for 15 min followed by PCR steps: 1 cycle of 95 ^{o}C for 3 min; 22 cycles of 95 ^{o}C for 30 sec; 56 ^{o}C for 30 sec; and 72 ^{o}C for 1 min; and final extension at 72 ^{o}C for 7 min. The PCR products were separated on a 10% non-denaturing PAGE and bands were visualized using Typhoon 9400 Variable Mode Imager (GE Healthcare, Piscataway, NJ, USA).

3.3 Results and Discussion

To increase loading efficiency compared to the siRNA delivery system in **Chapter II**, therapeutic SSO was directly conjugated to the surface of AuNP using similar techniques employed with gDNA-AuNP. Replacing the non-therapeutic gDNA developed in **Chapter II** with the therapeutic SSO increased the delivery capacity for therapeutic ODN from six molecular binding sites to 60 molecules of oligonucleotides. The complement oligonucleotide to SSO, designated as sDNA, was successfully conjugated to either a fluorescent marker or folic acid as a targeting ligand.

3.3.1 Attachment of SSO to AuNP

Conjugation using the 5'-thiol modified 20-mer SSO resulted in a slightly lower substitution ratio than seen in **Chapter II**. During the study, saturation of the surface of gold with the SSO using methods described in **Section 2.2.3**, produced batches with reproducible substitution ratios. **Figure 3-3** shows three batches that were produced with a 58:1, 60:1, and 61:1 substitution ratio. Alterations in salt aging technique have been shown to change the substitution ratio on AuNP, causing batch variability (Peterson et al. 2001).

3.3.2 Synthesis of sDNA Ligands

Folic acid is only soluble in DMSO or alkaline conditions and is also difficult to purify using size exclusion techniques. The aromatic rings of folic acid may stack or hydrogen bond forming molecular interactions between molecules strong enough to elute as a larger entity during standard G-25 purification described in the General Methods and Procedures **Section 2.2.2**. Initial attempts to conjugate folic acid to the sDNA failed to

produce the desired product, usually resulting in the formation of multiple byproducts eluting as broad bands during HPLC. Purified fractions analyzed using UV/visible spectroscopy revealed strong folic acid absorbance (ϵ282: 2.52 x 10^4 M^{-1} cm^{-1}) concealing the sDNA signal (sDNA ϵ260: 1.97 x 10^5 M^{-1} cm^{-1}). The activated folic acid may be conjugating to cyclic amines on nucleotide bases or polymerizing onto the secondary amine of folic acid.

To overcome repeated failures in solution-phase chemistry to attach folic acid to sDNA, the targeting ligand was directly conjugated to the sDNA using solid-phase synthesis (Habus et al. 1998, Alam et al. 2008). UltraMILD-protected nucleotides were used to protect the bases from folic acid conjugation. The 5' amino C6 modifier purchased from Glen Research (Cat. # 10-1906, Sterling, VA) was deprotected first, conjugated to activated folic acid, and cleaved from the CPG. The cleavage conditions also deprotected the bases in the final step. HPLC purified FA-sDNA was validated using UV/visible spectroscopy and MALDI-TOF analysis. The MALDI-TOF analysis does reveal some impurities not removed from HPLC purification. The purified FA-sDNA did not produce 1:1 absorbance ratios between folic acid absorbance compared to the DNA absorbance. Based on absorbance results, 88% of sDNA was conjugated with folic acid, although HPLC shows one clear peak far removed from starting material. This may be due to chemical decomposition of folic acid during alkaline cleavage conditions. The FA-sDNA was used as is for in vitro studies.

A BODIPY FL labeled sDNA was synthesized as a probe to quantify hybridization efficiency. Unlike the problems encountered with folic acid, BODIPY FL was not successfully conjugated to CPG-supported sDNA. After repeated failures with solid-phase synthesis, the sDNA was cleaved from the CPG and HPLC purified. Successful synthesis of FL-sDNA was performed in solution is described in **Section 3.2.3**. The product was HPLC

purified and validated using UV/visible spectroscopy and MALDI-TOF analysis. BODIPY FL was quantified at 504 nm, and background subtracted DNA absorbance at 260 nm, resulting in 85% expected absorbance ratio between BODIPY and sDNA, as seen **in Figure 3-4** and **3-5**. The FL-sDNA was used as is for hybridization studies.

3.3.3 Ligand Hybridization Efficiency

The FL-sDNA was hybridized and analyzed using the same methodology described in Section 2.2.5. Fluorescence calculations indicated that approximately 7.1 FL-sDNA were attached to every AuNP, resulting in 11.8% hybridization efficiency, slightly higher than the siRNA delivery system in Chapter II. The experimentally determined molar ratios are 7:60:1 FL-sDNA to SSO per AuNP. One deviation occurred during the experiment, the fluorescence standard curve did not contain 1.0 M DTT as in the sample solution. Later experiments with DTT-corrected fluorescence standards produced in a slightly decreased relative fluorescence intensity compared to the original standard curve. The 11.8% hybridization efficiency may be a slight underestimate of the actual value.

3.3.4 Splice Shifting Response in Folate Receptor Expressing KB Cells

In vitro experiments required two validation studies prior to testing in vitro folic acid targeting SSO-AuNP. The cell line to be used must express the folate receptor and Bcl-xL oncogene. Two cell lines, OVCAR3 and KB cells overexpress folate receptor after conditioning using folate depleted culture media and charcoal filtered FBS (Sudimack and Lee. 2000, Sabharanjak and Mayor. 2004). Previously, it was unknown if either cell lines expressed sufficient quantities of the Bcl-xL oncogene.

Folate receptor expression was analyzed using flow cytometry and shown in **Figure 3-6**. Conditioned and non-conditioned cell lines were harvested using non-enzymatic conditions and incubated at 4°C with either FL-FA or MOV18/FL secondary antibody. Control cells were gated and samples counted to 5 x 10^4 events. As anticipated, the conditioned KB and OVCAR3 cells produced a fluorescence shift past baseline, while non-conditioned cells did not express observable levels of folate receptor.

Total RNA from conditioned KB and OVCAR3 cell lysates were extracted and the Bcl-x mRNA PCR amplified. Equal amounts of mRNA were analyzed on PAGE, shown in **Figure 3.7**, revealing similar Bcl-xL oncogene expression and basal levels of apoptotic Bcl-xS expression (Mercatante et al. 2001) in both cell lines. Due to higher levels of folate receptor expression seen in **Figure 3-6**, the KB cell was chosen for in vitro splice alteration studies.

Conditioned KB cells and HeLa cells grown in complete media were seeded onto a 12-well plate. Wells were incubated with 100 nM equivalents of SSO in folic acid targeting SSO-AuNP or BODIPY FL modified SSO-AuNP. Controls were incubated in SSO free study media. After 24 hours, the media was replaced without SSO and incubated for another 24 hours. Total RNA was extracted and PCR amplified using methodology stated in **Section 2.4.4**. Unfortunately, treated and non-treated cells expressed similar levels of Bcl-xS, indicating little splice alteration seen in **Figure 3.8**. The FA-sDNA hybridized to SSO-AuNP did not significantly alter the Bcl-xL to Bcl-xS expression. Unsuccessful treatment of KB cells using folic acid targeted SSO-AuNP may be due to slow kinetics of oligonucleotide exchange with reduced glutathione in the cytosol. Assuming the carrier particle is endocytosed via the folate mediated route, sufficient quantities of SSO must be released to

exert pharmacologic response. Longer incubation periods than the 48 hour in vitro study may be necessary to alter Bcl-xL splicing.

3.4 Conclusion and Future Studies

Compared to the AuNP delivery system discussed in **Chapter II**, substation of the non-therapeutic gDNA with the therapeutic SSO increased the delivery capacity for therapeutic ODN from six molecular binding sites to 60 molecules of therapeutic oligonucleotide. Although the siRNA delivery system contained 66 gold-bound DNA sequences, three batches of SSO-AuNP produced an average of 60 gold-bound SSO per particle. The 10% drop in substitution ratio compared to the siRNA delivery system is presumably due to the two nucleotide longer sequence of SSO causing a slight increase in steric hindrance at the surface of AuNP (Steel et al. 2000). Shortening the therapeutic ODN may increase the substitution ratio as long as therapeutic activity is maintained.

Two sDNA ligands were successfully synthesized to hybridize to the complement sDNA; FL-sDNA and FA-sDNA. A proof of concept for hybridization and in vitro studies, these conjugates did not contain PEG chains between the sDNA and either BODIPY or folic acid. Also, in contrast to the siRNA delivery method, ligands synthesized for SSO-AuNP may not require an additional reductive mechanism to assist in releasing SSO. Therefore, a disulfide bond was not incorporated to the design of the sDNA conjugates. The direct conjugation of SSO to the AuNP should protect the oligonucleotide and should have better biochemical stability than siRNA compared to the delivery system discussed in **Chapter II**.

Differences in hybridization efficiency were also detected between the siRNA delivery system and that of the SSO strategy. The SSO-AuNP was able to hybridize seven

FL-sDNA sequences compared to six FL-PEG_{900}-cDNA on gDNA-AuNP. Longer oligonucleotides bound to the surface of AuNP does increase the steric hinderance encountered by complementary strands while annealing. The 18-mer gDNA used in **Chapter II** also contained a PEG_{900} linker which would dramatically increase its hydrodynamic radius and possibly steric hinderance during hybridization. This may explain the lower hybridization efficiency observed in 18-mer FL-PEG_{900}-cDNA compared to the 20-mer FL-sDNA.

A key experimental control was missing in the preliminary in vitro experiment. The therapeutic SSO contains the 5'-thiol modification necessary to complex to AuNP. Whether this modification alters the splice shifting ability was not validated. As a positive control, free thiol-SSO should be scrape loaded or transfected into the KB cells, to verify pharmacodynamic activity during the next study.

Failure of splice alteration with the folic acid targeting SSO-AuNP may be linked to other explanations. The hybridization efficiency of FL-sDNA was used to calculate the number of FA-sDNA ligands per SSO-AuNP carrier. The assumption is that FL-sDNA and FA-sDNA exhibit similar binding to SSO-AuNP. The difference in molecular structure between folic acid and BODIPY (shown in **Figure 3-4**) may cause changes in hybridization efficiency. Also, the folic acid ligand is linked to sDNA through a short C-6 linker. If the linker is too short, the folic acid interaction with the folate receptor can be compromised. Uptake and binding studies may elucidate whether folate targeted AuNP does not bind to the folate receptor or do not follow the classical receptor mediated mechanism. Scanning electron microscopy (SEM) may further elucidate whether the carrier does not enter the cells

or is sequestered away from cytosol. Also, analysis using inductively coupled plasma mass spectrometry (ICP-MS) can quantify the magnitude of AuNP particles endocytosed in cells.

Overall, the synthesis of targeting ligands and hybridization to SSO complexed AuNP was accomplished in this dissertation. All components to produce the final folic acid targeting SSO-AuNP were characterized and produced a stable delivery carrier. The dual modality of SSO as a modular scaffold developed for this system is a novel strategy with broad applications using other nanoparticles.

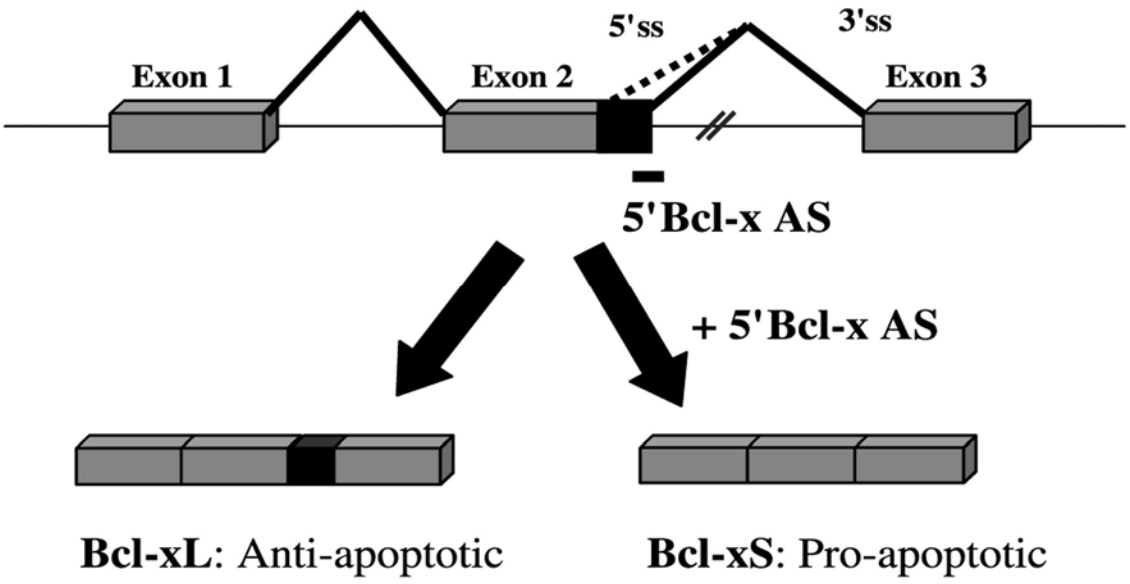

5'Thiol Modified SSO: HS-O-P(=O)(-O)-O- **TGGTTCTTACCCAGCCGCCG** 3'

Figure 3-1. Splice Modulation between Bcl-xL and Bcl-xS mRNA with SSO.

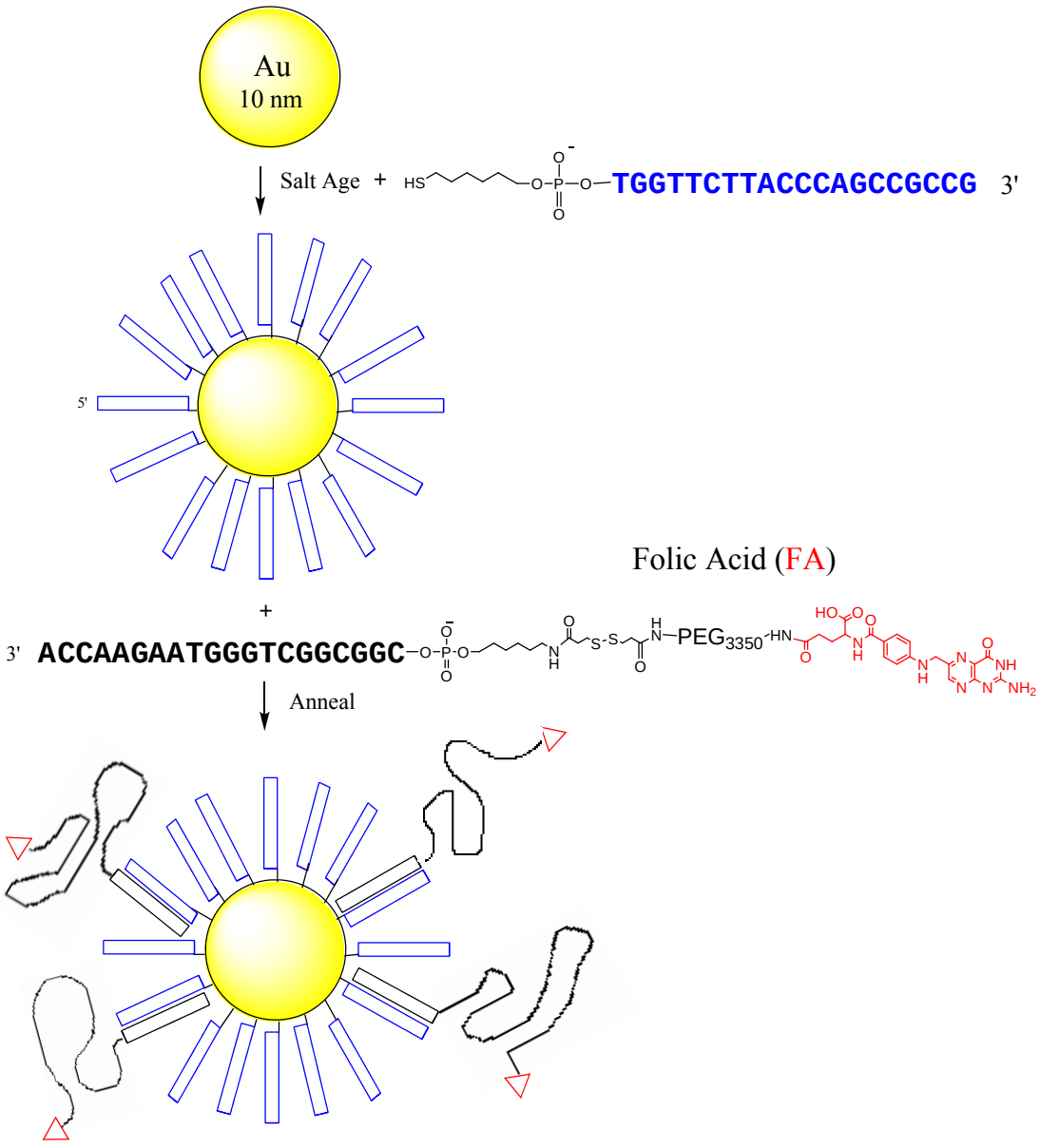

Figure 3-2. The SSO delivery system is a simplified version with SSO conjugated to the surface of the AuNP. This serves as therapeutic cargo as well as modular linker. The folic acid (red triangles) or other targeting ligand is hybridized to the carrier using the complement strand.

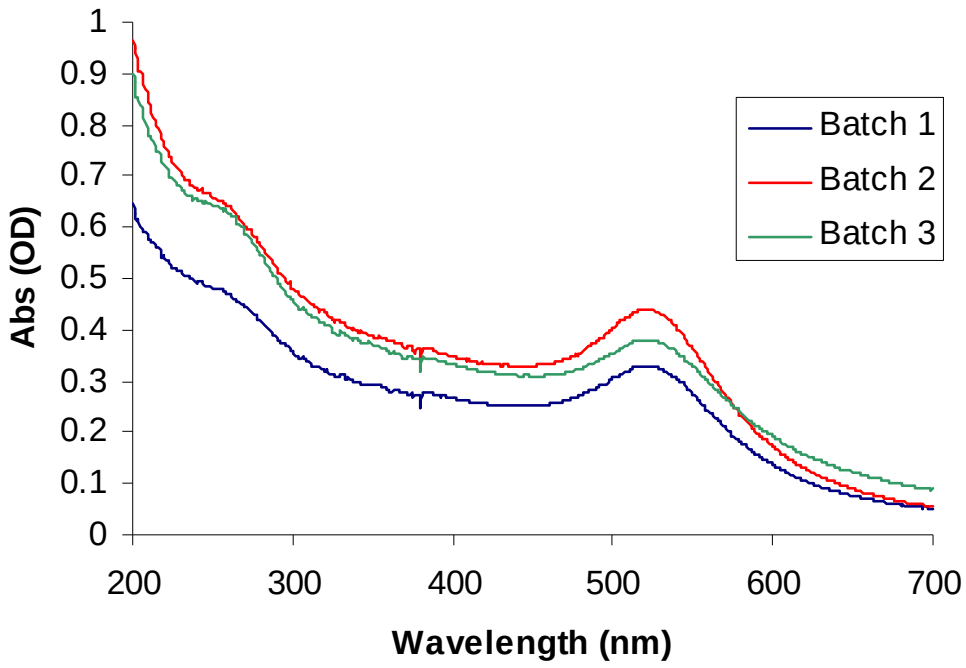

Figure 3-3. Combined spectrums of three purified SSO-AuNP batches. The AuNP causes an increase in baseline absorbance throughout the spectrum, with a peak at 520 nm. The complexed SSO absorbance is seen at 260 nm. The three batches produced a 61:1, 60:1, and 58:1 substitution ratio. Batch three is shown with a slight right shoulder due to AuNP aggregation.

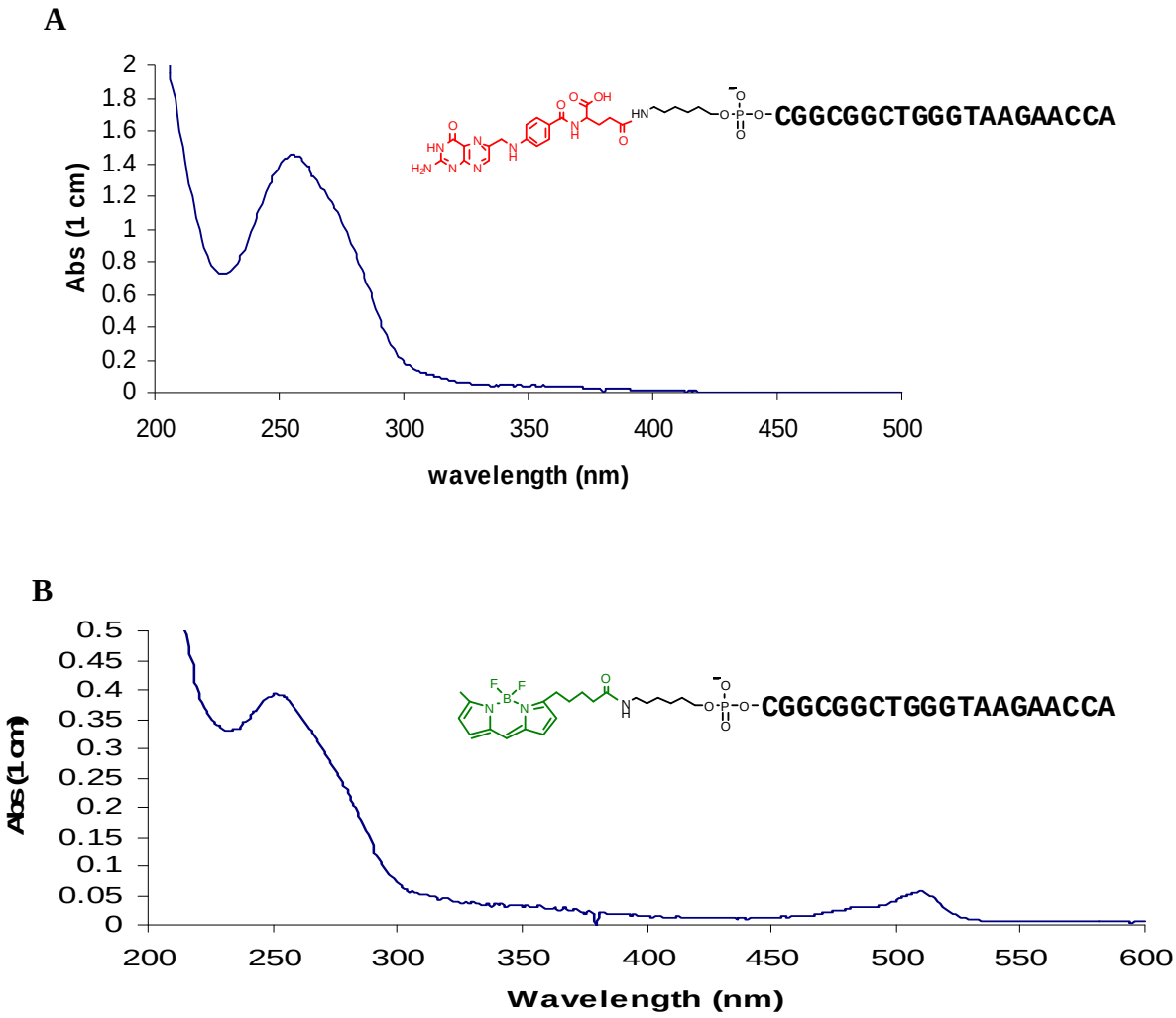

Figure 3-4. UV/visible spectrum of HPLC purified FA-sDNA and FL-sDNA. (A) Calculated folic acid to DNA resulted in 88% expected absorbance ratio. (B) Calculated BODIPY FL to DNA resulted in 85% absorbance ratio. sDNA ϵ260: 196600 $M^{-1}cm^{-1}$, folic acid ϵ282: 25220 M^{-1} cm^{-1} and ϵ350: 6765 M^{-1} cm^{-1}, BODIPY FL ϵ504: 68000 M^{-1} cm^{-1}.

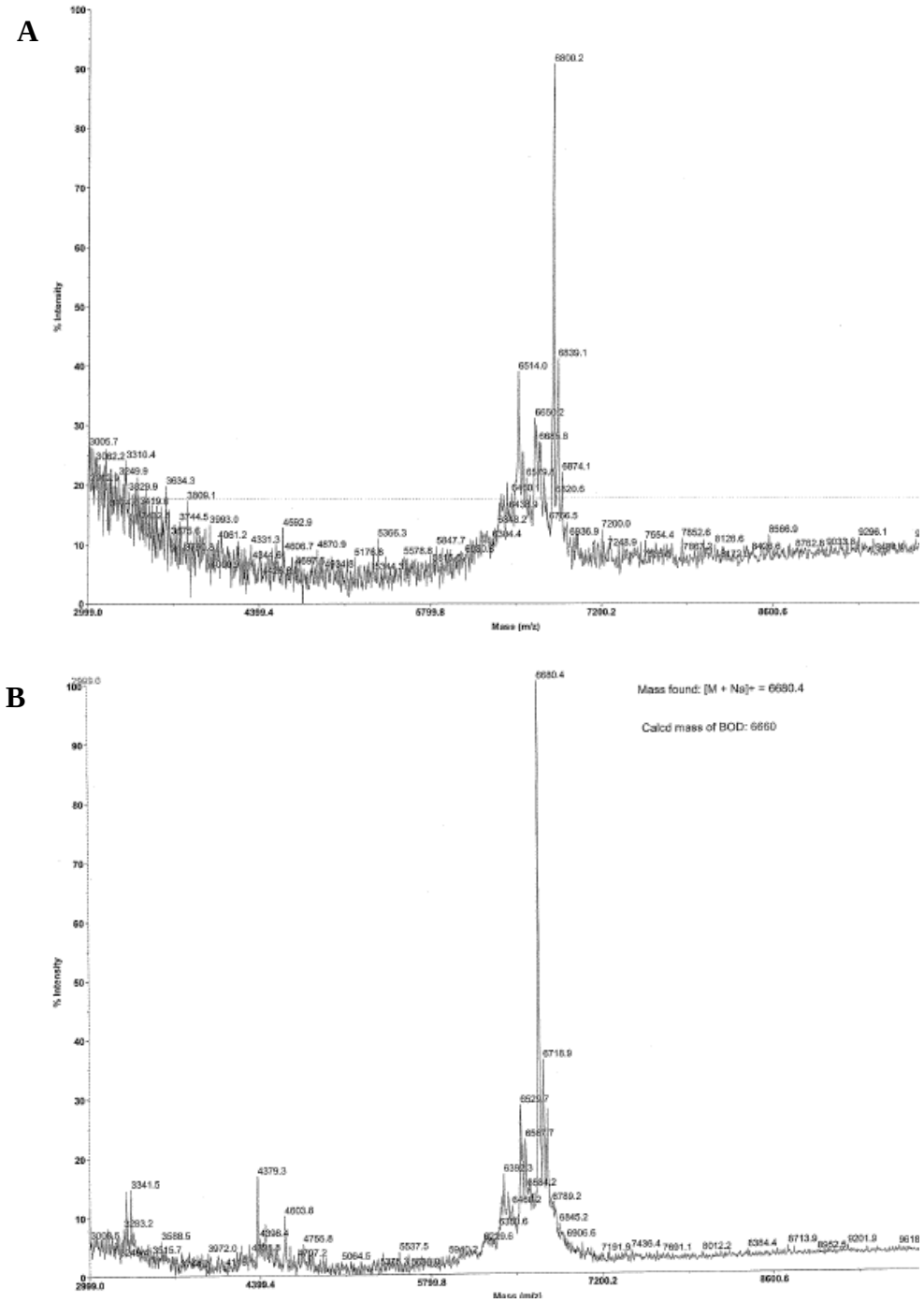

Figure 3-5. MALDI-TOF report of HPLC purified FA-sDNA and FL-sDNA. (A) The calculated mass of FA-sDNA is 6795 Da with MALDI-TOF generating 6800 m/z peak. (B) The calculated mass of FL-sDNA is 6660 Da with MALDI-TOF generating 6680 m/z peak.

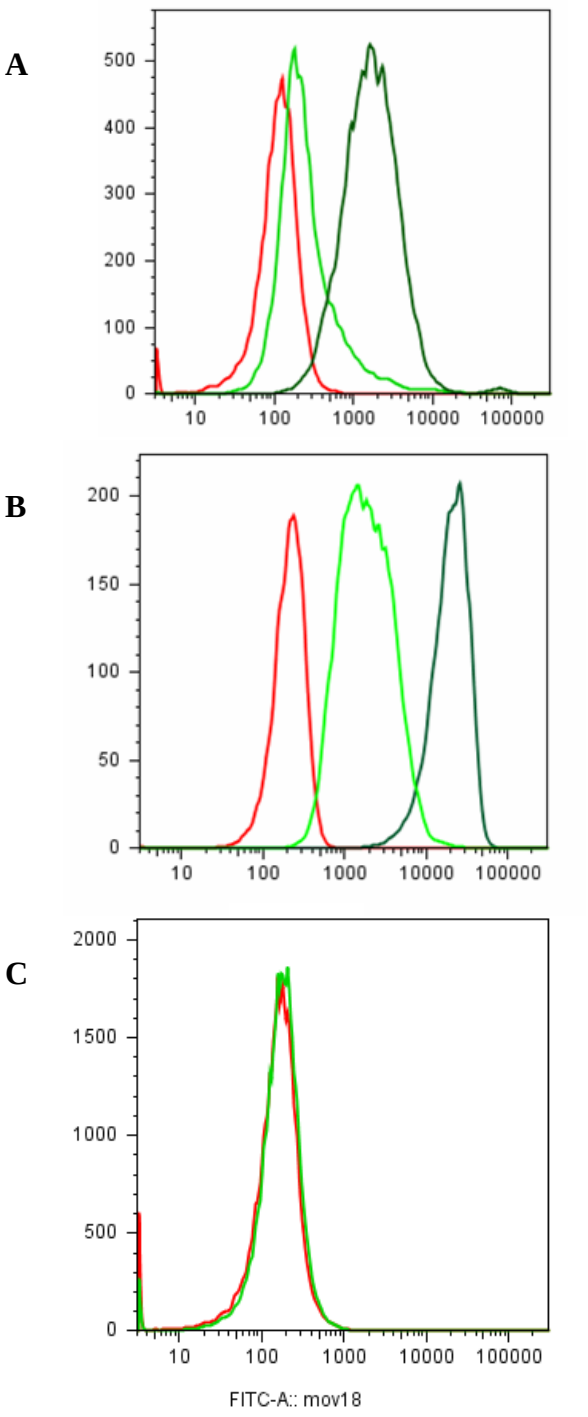

Figure 3-6. Flow cytometry analysis of folate receptor expression in conditioned OVCAR3 and KB cells. (A) Folate receptor expression in OVCAR3 cell line using FA-FL conjugate in light green and MOV18 antibody in dark green. (B) Folate receptor expression in KB cells. (C) No folate receptor expression is observed in non-conditioned KB cells.

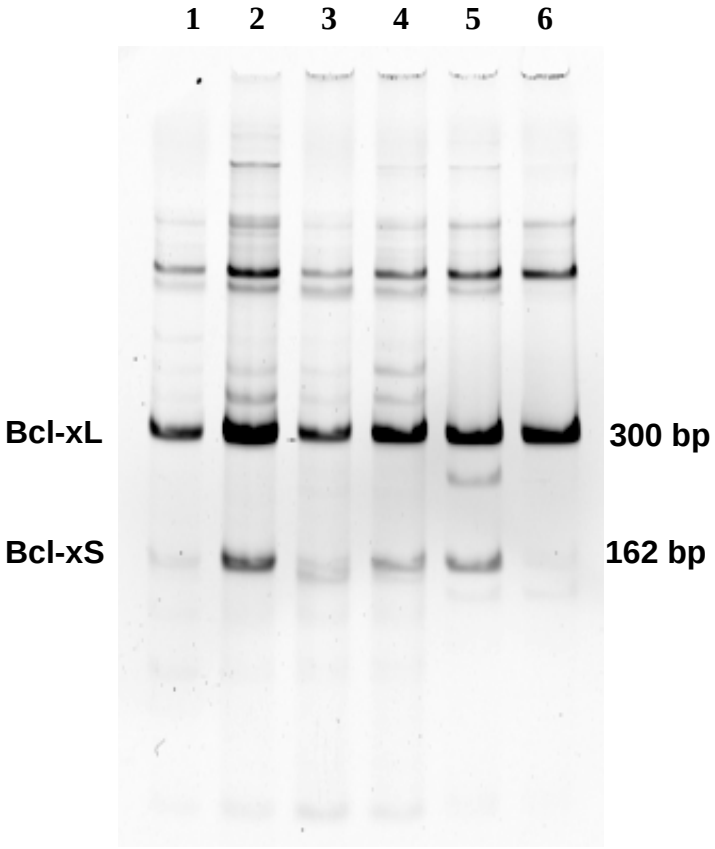

Figure 3-7. Complete 10% PAGE of PCR amplified Bcl-x mRNA. The 300 bp band corresponds to the Bcl-xL oncogene and 162 bp corresponds to the apoptotic Bcl-xS splice variant. Equal amounts of cellular mRNA were PCR amplified and equivalent volumes loaded into each lane. Band densities are proportional to the cellular expression level for each cell line. Lane 1 contains cellular mRNA from HELA cells, lane 2 from PC-3 cells, lane 3 from conditioned KB cells, lane 4 from conditioned OVCAR3 cells, lane 5 from CT-26 cells treated with SSO, while lane 6 contains non-treated CT-36 cellular mRNA.

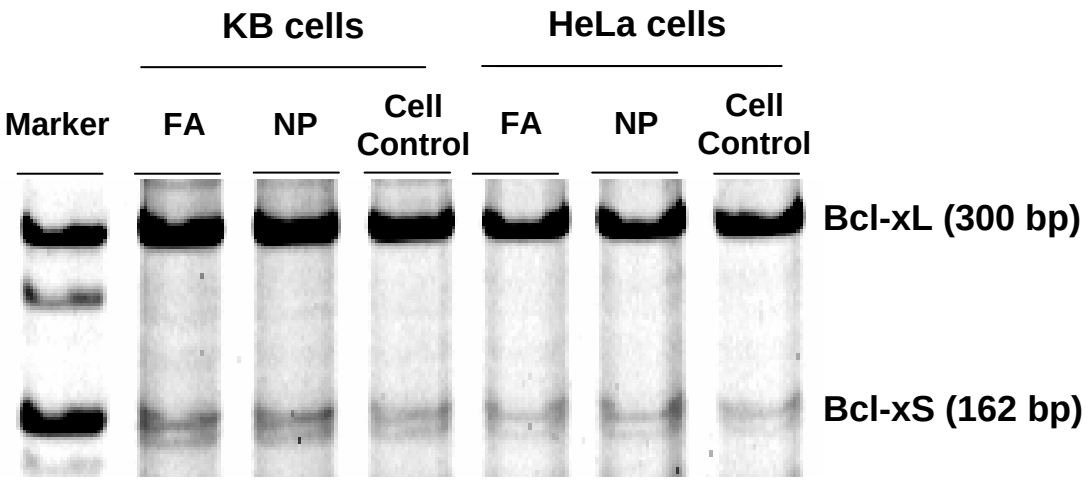

Figure 3-8. SSO-AuNP splicing efficiency was determined using PAGE. The marker contains 50/50 Bcl-xL and Bcl-xS controls. Folic acid targeted SSO-AuNP (FA) was no different than BODIPY labeled SSO-AuNP (NP) and slight shifting compared to untreated controls.

3.5 References

M. R. Alam, V. Dixit, H. Kang, Z. B. Li, X. Chen, J. Trejo, M. Fisher, and R. L. Juliano. Intracellular delivery of an anionic antisense oligonucleotide via receptor-mediated endocytosis. Nucleic Acids Res. 36:2764-2776 (2008).

A. Hachem and R. B. Gartenhaus. Oncogenes as molecular targets in lymphoma. Blood. 106:1911-1923 (2005).

S. H. Kang, M. J. Cho, and R. Kole. Up-regulation of luciferase gene expression with antisense oligonucleotides: implications and applications in functional assay development. Biochemistry. 37:6235-6239 (1998).

R. Kole, M. Vacek, and T. Williams. Modification of alternative splicing by antisense therapeutics. Oligonucleotides. 14:65-74 (2004).

S. L. Lin, S. Sukasweang, C. M. Chuong, S. Rasheed, and S. Y. Ying. D-RNAi (messenger RNA-antisense DNA interference) as a novel defense system against cancer and viral infections. Curr Cancer Drug Targets. 1:241-247 (2001).

D. R. Mercatante, C. D. Bortner, J. A. Cidlowski, and R. Kole. Modification of alternative splicing of Bcl-x pre-mRNA in prostate and breast cancer cells. analysis of apoptosis and cell death. J Biol Chem. 276:16411-16417 (2001).

D. R. Mercatante, J. L. Mohler, and R. Kole. Cellular response to an antisense-mediated shift of Bcl-x pre-mRNA splicing and antineoplastic agents. J Biol Chem. 277:49374-49382 (2002).

D. R. Mercatante, P. Sazani, and R. Kole. Modification of alternative splicing by antisense oligonucleotides as a potential chemotherapy for cancer and other diseases. Curr Cancer Drug Targets. 1:211-230 (2001).

B. Modrek and C. Lee. A genomic view of alternative splicing. Nat Genet. 30:13-19 (2002).
J. B. Opalinska and A. M. Gewirtz. Nucleic-acid therapeutics: basic principles and recent applications. Nat Rev Drug Discov. 1:503-514 (2002).

Z. Paroo, R. A. Bollinger, D. A. Braasch, E. Richer, D. R. Corey, P. P. Antich, and R. P. Mason. Validating bioluminescence imaging as a high-throughput, quantitative modality for assessing tumor burden. Mol Imaging. 3:117-124 (2004).

I. Habus, J. Xie, R.P. Iyer, W.Q. Zhou, L.X. Shen, and S. Agrawal. A mild and efficient solid-support synthesis of novel oligonucleotide conjugates. Bioconj. Chem. 9:283-291 (1998).

A. W. Peterson, R. J. Heaton, and R. M. Georgiadis. The effect of surface probe density on DNA hybridization. Nucleic Acids Res. 29:5163-5168 (2001).

S. Sabharanjak and S. Mayor. Folate receptor endocytosis and trafficking. Adv Drug Deliv Rev. 56:1099-1109 (2004).

P. Sazani and R. Kole. Modulation of alternative splicing by antisense oligonucleotides. Prog Mol Subcell Biol. 31:217-239 (2003a).

P. Sazani and R. Kole. Therapeutic potential of antisense oligonucleotides as modulators of alternative splicing. J Clin Invest. 112:481-486 (2003b).

G. Schmajuk, H. Sierakowska, and R. Kole. Antisense oligonucleotides with different backbones. Modification of splicing pathways and efficacy of uptake. J Biol Chem. 274:21783-21789 (1999).

H. Sierakowska, M. J. Sambade, D. Schumperli, and R. Kole. Sensitivity of splice sites to antisense oligonucleotides in vivo. RNA. 5:369-377 (1999).

J. Sudimack and R. J. Lee. Targeted drug delivery via the folate receptor. Adv Drug Deliv Rev. 41:147-162 (2000).

J. E. Wilusz, S. C. Devanney, and M. Caputi. Chimeric peptide nucleic acid compounds modulate splicing of the bcl-x gene in vitro and in vivo. Nucleic Acids Res. 33:6547-6554 (2005).

Q. Xu, B. Modrek, and C. Lee. Genome-wide detection of tissue-specific alternative splicing in the human transcriptome. Nucleic Acids Res. 30:3754-3766 (2002).

Chapter IV

ALBUMIN-BASED OLIGONUCLEOTIDE DELIVERY SYSTEM

Albumin is one of the most well studied and utilized proteins in animals due to its numerous physiological roles, which include maintenance of osmotic pressure, sequestration of xenobiotics and toxins, antioxidant activity, and as the transporter of essential fatty acids. This protein compromises roughly 60% of all serum proteins, with blood concentrations as high as 40 mg/ml in humans. Albumin is distributed throughout the body, with 60% of total albumin located in extravascular sites, making it the most abundant protein in the body. During its transit time through the human body, albumin will travel 15,000 times through circulation and 15 trips through extravascular sites (Peters. 1996). In one systemic pass, the protein will extravasate into interstitial space from circulation, drain into the lymphatics, and finally return to general circulation in 24 hours. With an average circulatory half-life of 19 days in humans with a 3.7% per day degradation rate, one molecule of albumin enjoys a very long 27 day life span.

The protein itself also serves as a nutrient, constituting a major amount of circulating nitrogen reserve in vertebrae animals. Albumin is also a major nutrient source for growing tumors (Kratz et al. 2000, Stehle et al. 1998). Proliferating tumor cells uptake larger amounts of albumin as a nutrient more rapidly than normal cells (Stehle et al. 1997, Kratz et al. 2002). The molecule is digested in the lysosome and resultant amino acids are used in de novo protein synthesis. The catabolism of albumin also supplies oncogenic cells with nitrates and essential fatty acids necessary for cell growth and division (Wunder et al. 1998). Recent

discoveries suggest upregulated albumin uptake is facilitated through binding to secreted protein acid and rich in cysteine (SPARC), an extracellular matrix glycoprotein overexpressed on cancer cells. Upon binding to SPARC, the gp60 surface receptor is recruited with intracellular caveolin-1 to form caveolae induced endocytosis (Desai et al. 2006, Porter et al. 1995). The vast quantity of endogenous albumin accompanied by passive accumulation near solid tumors mediated by the pathophysiology characterized by EPR, along with increased nutrient uptake in cancer cells augments the effectiveness of albumin as a drug delivery carrier for anti-cancer agents.

As pointed out above, albumin is the major transport protein of long-chain free fatty acids in both circulation and in extracellular fluids outside of vasculature (Peters. 1996). These fatty acids are an important source of cellular energy and precursor molecules that are converted to potent biological mediators such as hormones, essential building blocks for lipoproteins, and other cellular components (Kushlan et al. 1981). The protein has been shown to bind six fatty acids with high affinity, listed in **Figure 4-1** (Demant et al. 2002). Under normal physiological conditions, less than two fatty acid molecules are carried on albumin at a time, presumably at the binding sites of highest affinity. This leaves four other binding sites open on albumin throughout the body with unknown physiological relevance (Cistola. 1998). As more fatty acids are bound to albumin, the molecule is thought to be stabilized and half-life increases (Reed. 1988).

In 1998, the first clear X-ray crystal structure of 2.5 Å resolution was published exposing the unique architecture between binding of fatty acids onto albumin (Curry et al. 1998). This discovery revealed an asymmetric distribution of five myristic acid molecules on albumins surface. The FA binding sites displayed heterogeneous topology but all can be

described as deep hydrophobic pockets capped with cationic residues (Curry et al. 1999). This leads to the presumption that binding is influenced by interactions of hydrophobic amino acid residues lining the pocket to the acyl chain of fatty acids, since increasing chain length increases binding constants up to 18 carbons (Bhattacharya et al. 2000). Past studies also determined thermodynamic characteristics to further elucidate the mechanisms of fatty acid binding (Bojesen and Bojesen. 1992, Rose et al. 1994). Interestingly, thermodynamic parameters reveal an important contribution of electrostatic interactions between the fatty acid carboxylate anion and cationic amino acid residues. By conjugating a fatty acid while retaining the terminal anionic charge, the binding affinity to albumin could be preserved (Kurtzhals et al. 1995).

4.1 Depot and Circulation of Albumin Complexes versus Conjugates

The biological characteristics and innate function of albumin as a long circulating transporter has been widely exploited for delivering exogenous agents throughout the body for a sustained period of time (Kratz. 2008). In the first approach, chemotherapeutic agents are conjugated to directly to albumin. Here, the chemical conjugation is achieved in either two methods; attachment to random lysine residues on the surface or conjugation to free thiol of cysteine (Cys34) within the cleft of albumin.

Conjugation of peptides and proteins to the Cys34 have been shown to increase the half-life of the conjugated species mimicking that of non-modified albumin. Chemical conjugation involving a disulfide between a fragment antigen binding (Fab) fraction of antibody molecule and Cys34 of albumin increased the Fab residence time significantly greater than the Fab itself, while preserving its binding affinity (Smith et al. 2001).

Genetically engineered fusion proteins of albumin can also alter the pharmacokinetics of rapidly eliminated proteins. Interferon α-2b, an antiviral 19-kDa protein for the treatment of hepatitis C is rapidly cleared from the body with a half-life of two to three hours, requiring constant infusion to reach therapeutic concentrations. Fusion to recombinant albumin increases the half-life to 140 hours, far superior than current pegylated interferon-α with a half-lives ranging from 40-80 hours (Chemmanur and Wu. 2006). Similarly, ODNs conjugated to the Cys34 of albumin increased the stability of the oligomer in serum and increase uptake into cells (Bonfils et al. 1992).

Small chemotherapeutic agents have been covalently linked through the exposed ε-amine of lysine residues on the surface of albumin to enhance tumor targeting, reduce toxicity, and overcome drug resistance. To maximize drug load, albumin has been conjugated with up to 50 methotrexate (MTX) molecules then tested in rats to evaluate pharmacokinetics and disposition. As the load amount increased, accumulation at tumor site dramatically decreased along with increased liver uptake. The removal of these albumin conjugates from circulation is likely due to partial denaturation surrounding the modified lysines, causing conformational changes and recognition by scavenger macrophages in the liver (Schnitzer and Bravo. 1993, Stehle et al. 1997).

Due to increased elimination of conjugated albumin, only methotrexate-albumin conjugates in 1:1 molar ratios were observed to display significantly less liver uptake rate than higher MTX loaded conjugates. In the 1:1 conjugate, the drug loading is only in the range of 0.6%, 454 mw for methotrexate and 69 kDa for the protein. Also, results from murine studies with a 1:1 doxorubicin-albumin conjugates, synthesized at the Cys34 residue,

indicate successful accumulation in solid tumors and a higher antitumor effect compared to equimolar doses of doxorubicin (Kratz et al. 2000).

Many hydrophobic small drugs non-covalently bind to circulating albumin, causing sequestration of active agents and increased circulating half-life. Conjugation of cholesterol to oligonucleotides also causes protein binding and sustained circulation (Bijsterbosch et al. 2000, Rump et al. 1998). Recently, an albumin-based delivery platform, Abraxane® from Abraxis, has been FDA approved in 2005 for the treatment of metastatic breast cancer. This protein-bound paclitaxel drug delivery strategy does not utilize endogenous albumin but exploits partially denatured recombinant albumin microspheres to solubilize and retain the chemotherapeutic agent until the drug reaches the target solid tumor. In humans the protein-bound paclitaxel is a drug delivery strategy that increases the maximum tolerable dose while producing less dose variability and higher sustained concentrations compared to conventional paclitaxel. However, the complexation of the protein and formation of large nanoparticulates minimally altered the half-life of the conjugate to 21-27 hrs in humans compared to 20 hours for conventional paclitaxel, but much less than the natural half-life of human albumin (Gardner et al. 2008).

In the second approach, a drug molecule is modified with fatty acid such that this derivative becomes bound to albumin. An example will be insulin acylated with fatty acid for a slow release. The β-chain of insulin was shortened one amino acid at the N-terminus, to lysine (Lys29), and the ε-amine was coupled to myristic acid forming an amide bond to lysine (Kurtzhals et al. 1995). By serendipity, this conjugate retains the anionic charge from lysines free α-carboxylate, albeit at a further distance away from unmodified acyl chain. The association constant, K_A, of this conjugate toward human serum albumin (HSA) was

measured to be $2.4x10^5$ M^{-1}, or 500 fold lower binding than free palmitate (Kurtzhals et al. 1997). Increasing acyl chain length above 14 carbons did not increase binding affinity, which might suggest steric hindrance from the amide bond between the acyl chain and carboxylate anion. Nonetheless, binding to albumin was significant enough that 98% of all acylated insulin was bound to albumin in serum without pronounced peak activity after injection, unlike that of other sustained release insulin systems. The half-life of acylated insulin in pigs was measured at 14.3 hours, compared to native human insulin at 2 hours and sustained release Neutral Protamine Hagedorn at 10.5 hours (Markussen et al. 1996). This acylated insulin is labeled *insulin detemir* and is clinically approved as a very long acting insulin analog for the control of diabetes mellitus. This example shows that fatty acid conjugated to large molecular weigh therapeutic agents can bind and utilize the high affinity fatty acid binding sites on albumin as a carrier while masking it from degradation and elimination. However, *insulin detemir* does not take full advantage of the physiological transport of fatty acid, since both fatty acid anionic charge and unmodified acyl chain is necessary to bind to albumin with high affinity (Lambert. 2000).

4.2. Statement of Purpose

Development of a fatty acid-SSO delivery system which utilizes endogenous albumin as a carrier would be more efficient than administrating large doses of expensive SSO to overcome short circulating half-lives and drug transport barriers. This system would enhance clinical aspects of nucleic acid-based anti-cancer therapy by eliminating the need for constant infusion or hospital administration. The therapeutic index would also increase since more ODN accumulates at the tumor with fewer doses.

Fatty acid conjugates of a nucleic acid must preserve both ionic and hydrophobic interactions to bind with high affinity to albumin. This is under an assumption that the multi-anions from the nucleic acid will not interfere with the molecular interaction, depicted in **Figure 4-2**. This project focuses on the synthesis and characterization of therapeutically applicable fatty acid-DNA/albumin complexes, and preliminary in vitro characterization. The development of this delivery carrier system is separated into three stepwise objectives.

Aim1 **:** *Synthesize palmitic acid (PA) conjugates while preserving the free carboxylate and unmodified acyl chain.* A uniquely structured amino-fatty acid was synthesized in solution and also incorporated onto solid support. This α-amino fatty acid is the key ligand necessary to complex any oligonucleotide to albumin with high affinity.

Aim 2*:* *Measure apparent K_A and relevant thermodynamic parameters of PA conjugates with delipidated HSA using isothermal titration calorimetry (ITC).* The binding of PA to HSA must be preserved to maintain long circulatory half-life with the carrier.

Aim 3: *Develop and test an in vitro / in vivo model employing a syngeneic tumor cell line stably expressing inactive luciferase that is activated only after successful SSO delivery.* To test the feasibility of the delivery system utilizing SSO-705, stable transfection of B16 F10, a syngeneic cell line to C57BL/6, can be utilized for future in vitro and animal models

4.3 Materials and Methods

As stated in *Aim 1*, synthesis of the palmitic acid analog and conjugation to the oligonucleotide is the rate-limiting step for the development of an endogenous albumin based oligonucleotide carrier. Two techniques were developed to overcome the challenging chemistry, a solution-based and solid phase synthetic method. Analysis of binding utilizing ITC would distinguish thermodynamic properties based on affinity or avidity to albumin.

4.3.1 Materials

Custom synthesized 5'-amino-C6-poly(10) thymidine (dT_{10}) was purchased from IDT (Coralville, IA). The α-bromopalmitic acid (Cat. # 238422), sodium azide (cat. # S8032), *N,N'*-dicyclohexylcarbodiimide (DCC) (Cat. # D80002), *N*-diisopropylethylamine (DIEA) (Cat. # 550043), EDC (Cat. # 03450 and E7750), *NHS* (Cat. # 130672), succinic anhydride (Cat. # S-7626), Sephadex G-25 (Cat. # G25150), 4-(dimethylamino)pyridine (DMAP) (Cat. # 107700), Laura Broth (Cat. # L-3522), fatty acid-free bovine serum albumin (fraction V, Cat. # A-8806), *N,N,N',N'*-tetramethyl-*O*-(1*H*-benzotriazol-1-yl)uronium hexafluorophosphate (HBTU) (Fluka Cat. # 12804), silica gel grade 9385, pore size 60 Å, 230-400 mesh (Cat. # 227196), silica thin layer chromatography sheets (Cat. # Z193291), molecular sieves of 3A type, 8-12 mesh (Cat. # 208582), and various organic solvents were obtained from Sigma-Aldrich (Milwaukee, WI). The Wang resin was purchased from Advanced Chemtech in Louisville, KY (Cat. # SA5110) and used as is. Square 10x10 cm culture dishes (Cat. No. 08-757-11A) were obtained from Fisher Scientific (Pittsburgh, PA). The subcloning DH5α E. coli (Cat. # 18258) was purchased from Invitrogen (Carlsbad, CA). General cell culture media were obtained from Gibco (Grand Island, NY)

4.3.2 Synthesis of α-Aminopalmitic Acid

An amino (fatty) acid-like structure would preserve the necessary albumin binding properties and allow simple peptide synthesis methods to incorporate the ligand through the amino group (**Figure 4-3**). The α-aminopalmitic acid was previously synthesized but it is insoluble in almost all solvents of interest, which limits its utility as a ligand. This was confirmed three years later from newly available commercial α-aminopalmitic acid, which also displayed undesirable solubility characteristics. To increase solubility of the fatty acid ligand, the precursor α-bromopalmitate was *t*-butyl protected and converted to α-aminopalmitate in a three-step synthesis as summarized in **Figure 4-4**.

*t-Butyl Carboxylate Protection of α-Bromopalmitic Acid (Compound **1**)*

In an argon-purged 100 ml RBF, α-bromopalmitic acid (10 mmol, 3.353 gm) was dissolved in 5 ml of dichloromethane (DCM) containing activated molecular sieves (type 3A, 8-12 mesh) and catalytic amounts of DMAP (0.037 gm). To activate the reaction solution, DCC (12 mmol, 2.475 gm) dissolved in 5 ml of *t*-butanol (50 mmol) then added drop-wise through a chemical resistant stopper, while the solution was stirring. The mixture was further purged with argon and stirred at RT. The reaction was monitored via TLC (10% ethyl acetate, 90% hexane) with $(NH4)_2SO_4$ charring to follow the disappearance α-bromopalmitic acid at R_f 0.2 and appearance of new product at R_f 0.9. Five hours later the reaction mixture was passed through a glass sintered filter to remove dicyclohexyl urea and concentrated under vacuum, forming an oily residue. The oily solution was extracted six times with ethyl acetate (EtOAc):brine, vacuum concentrated, and further purified by flash silica gel chromatography. Purification of the butyl protected *α*-bromopalmitic acid was facile and

resulted in 80% recovery of Compound **1** (3.253 gm). Final analysis with a Varian GEMINI **300** ^{1}H-NMR (Palo Alto, CA) produced a clean chromatogram ($CDCL_3$, 300 mHz) δ 4.20 (1H, m), 2.10 (2H, m), 1.4 (9H, s), 1.3 (26H, m), 1.0 (2H , m).

*Gabriel Reaction for Synthesis of t-Butyl, α-phthalimidopalmitate (Compound **2**)*

In an argon purged 100 ml RBF, potassium phthalimide (4.0 mmole, 740.9 mg) was partially dissolved in 20 ml DMF containing 782.9 mg of **1** (2.0 mmole) with molecular sieves. The reaction mixture was purged with argon and stirred at RT overnight. The mixture was filtered through a 15 ml, 20M Kimax sintered glass filter to remove excess phthalimide and molecular sieves. The reaction solution was vacuum concentrated, extracted six times with EtOAc:brine, dried through calcium sulfate, and vacuum concentrated to dryness. Simple solvent extraction produced one spot on TLC at R_f 0.4 (10% EtOAc, 90% hexanes) with near complete recovery.

*Ing-Manske Reaction for Synthesis of t-Butyl α-Aminopalmitate (Compound **3**)*

Anhydrous hydrazine (100µl, 20 mmol) was added dropwise into a 25-ml RBF containing 2 mmole of **2** stirring in 10 ml anhydrous EtOH, and the reaction mixture was refluxed. The reaction was monitored with TLC following the disappearance of **2** at R_f 0.4 during the first five hours. The reaction mixture was passed through a glass sintered filter and concentrated under vacuum to produce whitish oil. After the phthalhydrazide precipitate was filtered off, the main product appeared at R_f 0.32 (40% ethyl acetate half-saturated with 28% NH_4OH, 60% hexanes) after $(NH_4)_2SO_4$ charring and development with ninhydrin, seen in **Figure 4-5**. The oil was repeatedly diluted with ethanol and concentrated until the smell of hydrazine disappeared. The product was dissolved in 4 ml *n*-propanol and purified by

flash silica gel chromatography using 5% propanol, 10% ethyl acetate saturated with NH_4OH, and 85 % hexanes as the mobile phase. Fractions with only product were pooled and evaporated to dryness revealing a dry white solid at 30% yield (183.2 mg). **Figure 4-6** shows the ^{1}H-NMR chemical shifts corresponding to **3** ($CDCl_3$, 300 mHz) δ 3.45 (1H, m), 1.7 (2H, m), 1.4 (9H, s), 1.3 (26H, m), 1.0 (2H, m).

4.3.3 Solid-Phase Chemistry of α-Aminopalmitic Acid-DNA (PA-dT_{10})

To overcome the limited solubility of α-amino-palmitic acid, the precursor α-amino-palmitic acid was also attached to solid support and conjugated to DNA, seen in **Figure 4-7**.

Synthesis of α*-Azidopalmitic acid (Compound **4**)*

Conversion of α-bromopalmitic acid to azidopalmitic acid was adapted from (Tornoe, et al. 2000). In a 100 ml RBF, α-bromopalmitic acid (14.3 mmol, 4.78 gm) and 1.44 gm of sodium azide (22.2 mmol, 1.5eq) was dissolved in 25 ml of DMF and stirred at RT while protected from light. The reaction was monitored via TLC for disappearance of the starting material, ending at 48 hours. The reaction was evaporated to dryness and excess sodium azide precipitated using hexanes. The suspension was filtered through a sintered glass filter, filtrate evaporated to dryness, dissolved in boiling methanol and quickly cooled via addition of wet ice to precipitate the product. The suspension was then centrifuged at 2500G at 4°C for an hour. The supernatant was gently decanted leaving 4.09 g of the white product (96% yield). (^{1}H NMR 300MHz: t, 3H δ 0.83 – 0.87; s, 25H, δ1.24; dm, 2H, δ1.58, δ1.72; dd, 1H, δ3.67 – 3.71)

Synthesis of Wang Resin-Bound α-Aminopalmitic Acid

Wang resin (430mg, 1mmol –OH) was swelled in a peptide synthesis vessel with DCM overnight. In a 100 ml RBF, 1.49 gm of α-azidopalmitic acid (5 mmol, 5 eq) and 1.90 gm of HBTU (5 mmol, 5 eq) was dissolved in 10 DMF containing 1.74 mL of DIEA (10 mmol, 10 eq). The reaction was stirred for 10 min at RT to produce the active ester. DCM was drained from the reaction vessel and activated α-azidopalmitic acid added to the resin. The reaction vessel was rocked overnight at RT. Approximately 15 hours later, the reaction vessel was drained and resin washed with 3 x 10 mL DMF followed by swelling in 5 ml of DCM for 2 hours. The resin-bound azide moiety was reduced via the Staudinger reaction (Malkinson et al. 2000) by adding 787 mg of triphenylphosphine (3 mmol, 3 eq) dissolved in 5 ml of tetrahydrofuran (THF) to the resin still wet with DCM. The reaction was rocked overnight at RT followed by the subsequent addition of 2 mL of dH_2O. The resin was allowed to rock for another 8 hours at RT, then washed with 10 mL methanol, then 10 mL of DCM. Gisin's procedure (Gisin. 1972) was performed on the resin to determine the loading efficiency of the reaction, which was found to be 44%.

Synthesis of PA-dT_{10} *Conjugate*

To the resin-bound α-amino palmitic acid (~200 µmol, 450 eq), added was 100 mg of succinic anhydride (1 mmol, 2250 eq) dissolved in a minimum of DMF which was then diluted four-fold in DCM. The reaction was monitored for completion via the ninhydrin test, occurring after 63 hours of rocking at RT. The resin was washed with DMF to remove excess succinic anhydride, then swelled in DCM for 2 hours. To the succinic acid modified resin was added 8.5 mg of EDC (4.25 µmol, 100 eq) dissolved in DMF containing 7.7 µl

DIEA. The resin was activated for 10 minutes at RT followed by the addition of 1.36 mg of dT_{10} DNA, of which 5'-end was aminohexyl modified (442.5 nmol, 1 eq), dissolved in 10 ml of DMF.

The resin was rocked overnight at RT and reaction monitored by testing the supernatant for ninhydrin activity the next day. Once completed the resin was washed with DMF then DCM. To cleave the conjugate, the resin was treated with 5% water in trifluoroacetic acid solution and rocked for two hours. The resin was treated again with water and fractions combined. The solution was vacuum concentrated and diluted in dH_2O. The DNA conjugate was G-25 desalted (refer to General Methods and Procedures **Section 2.2.2**), concentrated and HPLC purified using conditions as follows: 5 ml/min linear gradient; % buffer B, 0–10%/5 min, 10-40%/5 min, 40%/5 min, and 40-100%/5 min. Pump A contained 0.1 M TEAA while pump B contained only acetonitrile. The eluent was continuously monitored at 260 nm. Collected product was concentrated, desalted, and lyophilized.

4.3.4 Preliminary Binding Analysis of PA-dT_{10} to Albumin

Binding experiments were carried out at 25°C using a VP–ITC calorimeter from MicroCal (Northampton, MA, USA). All samples were degassed before loading into the instrument. The reference cell was loaded with H_2O and sample cell loaded with 15 μM of delipidated bovine serum albumin in 0.1 M borate buffer. The pipette injector was loaded with 150 μM **PA-dT_{10}**. The instrument was set to inject an initial volume of 2 μl with 4 μl subsequent aliquots spaced 240 seconds apart for the rest of the study. The initial starting

power reference was set for 15 mV. In **Figure 4-8**, Origin 8.0 (Microcal Software) was used to analyze the titration heat profiles.

4.3.5 Stable Transfection of B16 F10 cell line with Luc-705 Plasmid

Murine B16 F10 adherent cell line of unknown passage was graciously obtained from Dr. Fan Yuan at Duke University and grown in DMEMH supplemented with 10% FBS and 1% pen/strep.

Gene Amplification

Plasmids EGFP-654 and Luc705 containing aberrant splicing reporter genes graciously supplied by Dr. Ryszard Kole (UNC Lineberger Cancer Center) were amplified using standard E. coli cloning technique. DH5α strain of E. coli was transformed with 100 ng of either plasmid using established heat shock techniques. The transformed bacterium was incubated in a cabinet shaker at 37°C for one hour. A sample of the bacterial medium was drawn and streaked onto Laura Broth (LB)/agarose plates containing 50 μg/ml ampicillin antibiotic for selection. Colonies were grown overnight in a 37°C incubator. The next day, one visibly large, isolated colony was arbitrarily chosen from each plate and scrapped off using a 1000 ul pipet tip. The colony was inoculated into sterile test tubes containing 3 ml of Laura Broth media with antibiotics and rocked incubated in a shaker at 37°C for 6 hours. A 500 ul sample from each tube was diluted into sterile 1L flasks containing 500 ml LB media with antibiotics.

Each flask was incubated in a shaker at 37° C for 18 hours. The medium was then centrifuged at 6,000g for 15 minutes to pellet the colony. Plasmid was extracted from the

colony following protocols using the Endofree Plasmid Maxi Kit® from Qiagen (Cat. # 12362 , Valencia, CA). Overall yield was estimated by multiplying absorbance at 260 nm by a factor of 50 to give plasmid concentration in ug/ml. The plasmid purity was assessed by UV absorbance ratios at 260 nm/280 nm and by agarose electrophoresis utilizing ethidium bromide to visualize dsDNA (data not shown).

Stable Cotransfection using EGFP-N1 and Luc705 plasmid

All transfection was carried out in-house using Lipofectamine Plus® as suggested by the manufacturer (Invitrogen Cat. # 18324, Carlsbad, CA). The B16 F10 cells were harvested, counted, and seeded into a 6-well plate at ~$5x10^4$ cells per well with serum containing media one day prior to cotransfection. To prepare for transfection, 2 μg of Luc705 and 1 ug of EGFP-N1 was mixed and precomplexed with 18 μl of PLUS® reagent by gentle rocking at RT for 15 minutes. The recommended volume of Lipofectamine reagent (12 μl) was diluted with Dulbecco's modified high-glucose Eagle's medium (DMEMH) and added to each plasmid mixture. The solution is gently rocked at RT for 15 minutes. This prepares enough DNA/lipid complex of each plasmid for 3 wells. An aliquot of the plasmid complex is added to each well containing 1 ml of DMEMH and incubated for 5 hours. After the 5 hour incubation, serum is added with media to bring the final concentration to that of normal growth medium. The DNA complex containing media was replaced the next day with complete growth media.

Selection of Stably Expressing EGFP-N1 Gene

Two days after transfection, cells from each well were harvested and diluted into 10x10 cm square dishes. Stably transfected cell lines were selected using 1600 μg/ml Geneticin (G418) containing growth medium for 5 days and maintained with 400 μg/ml G418 containing growth medium for 15 days. These concentrations were based on previous non-transfected B16 cell survival studies with G418. Shown in **Figure 4-9**, the G418-resistant, EGFP expressing colonies were transferred from the dish to a 12-well plate using a 200 μl plastic pipette under a Nikon TMS inverted microscope (Melville, NY) at 40x magnification. Each clone was separately propagated and froze in liquid nitrogen until needed for in vitro studies.

4.4 Results and Discussion

Initial synthesis and experiments focused primarily toward developing a fatty acid ligand conjugated to oligonucleotides, while preserving its affinity and avidity to complex with albumin, depicted in **Figure 4-2**. The α-amino palmitic acid molecule is an ideal molecule, resembling an amino acid and a fatty acid analog with free amino moiety to tether the ligand to DNA.

4.4.1 Solution-Phase Synthesis of α-Amino Palmitic Acid

Prior synthesis of α-aminopalmitic acid would precipitate during the Ing-Manske reaction (data not shown), with a complexion and texture similar to scrambled egg white. The product was not soluble in a battery and combination of organic solvents, heat, or aqueous media. To overcome the limiting solubility, the carboxylate was initially protected

with a hydrophobic t-butyl group, compound **1**, in order to alter solubility long enough to attach to the oligonucleotide of choice.

The Gabriel reaction was used for SN_2 substitution of the bromo moiety for a phthalimide derivative. Due to limited solubility of the reactant potassium phthalimide, a large volume of DMF as a solvent was necessary for complete disappearance of **1** on TLC. The intermediate **2** was not analyzed further and used as is for the next reaction. Synthesis of the final product using the Ing-Manske reaction utilizes ethanolic hydrazine at reflux to produce phthalhydrazide byproduct along with the primary amine. The remainder of **1** (t-butyl α-bromo palmitate) and **3** (t-butyl α-amino palmitate) was archived in 2003 and stored in the desicator. The ligand was never attached to any oligonucleotide.

4.4.2 Solid-Phase Synthesis of PA-dT_{10}

As shown in **Figure 4-6**, the α-aminopalmitic acid was synthesized on solid support to overcome solubility issues in solution chemistry and for ease of purification. As a DNA probe for ITC binding analysis, 5' amino-modified dT_{10} was conjugated to the α-amino palmitic acid while attached to Wang resin. As described in **Section 4.3.3**, starting material α-bromopalmitic acid was converted to **4**. Compound **4** was activated with HBTU and conjugated to the Wang resin. The azide moiety was reduced to an amine and reacted to succinic anhydride. The succinic acid was activated with HBTU and 5' amino-C6-dT_{10} introduced to the resin. Cleavage of PA-dT_{10} was performed using 1 N NaOH for 15 minutes at RT and HPLC purified. The PA-dT_{10} was water-soluble and purified by HPLC in **Section 4.3.2**. The peak corresponding to 2-[4-(hexylamino)-4-succinamidyl] palmitic acid-dT_{10} product eluted at 13.8 min compared with the starting material eluting around 2.6 min. The

HPLC fractions were pooled, concentrated, G-25 desalted, and used as is for ITC analysis. The final concentration was determined at A_{260} using ε_{260} value of 8.16 x 10^4 $M^{-1}cm^{-1}$ and absorbance 260/280 ratio to analyze purity.

4.4.3 Preliminary ITC Study of PA-dT_{10}

To determine the binding affinity of one PA-dT_{10} to BSA with multivalent binding sites, less than 1:1 ligand to albumin concentration were used to theoretically saturate the highest affinity binding site. Since a small fraction of secondary and tertiary binding will alter the heat evolved, large concentrations of both ligand and albumin were utilized in the experiment to increase the signal-to-noise ratio and fit a sigmoid curve to the first theoretical binding site. The sample cell loaded with 15 μM of delipidated bovine serum albumin in 0.1 M borate buffer. The pipette injector was loaded with 150 μM PA-dT_{10}. Total injections was limited to less than 1:2 PA-dT_{10} molecule to albumin protein to isolate only the highest affinity binding site on albumin. This proved very difficult, since the binding of each fatty acid to albumin site has similar but less affinity, resulting is a sloped-stepwise curve with sequential binding. Data analysis from the single ITC experiment, in **Figure 4-8**, did produce a binding curve and K_A determined to be 1.23 x 10^6 M^{-1}, or 5-fold higher affinity than that of insulin detemir but still 100-fold less than free palmitate, listed in **Figure 4-1**.

4.4.4 Cotransfection of B16 F10 cell line with EGFP

Cotransfection of EGFP-N1 plasmid is necessary since the Luc-705 plasmid does not contain a mammalian antibiotic resistance gene and therefore cannot be selected alone. The EGFP-N1 plasmid contains a Geneticin resistance cassette and its cellular fluorescence was

used to physically separate transfected cells for individual cloning. Cells stably cotransfected with EGFP (510 nm emission, 488 nm excitation) will also express the Luc-705 gene. These cells strongly fluoresce under a Zeiss LSM 10 inverted fluorescent microscope (Thornwood, NY) and large colonies were marked on the bottom of the dish with a marker. Isolated colonies were transferred to individual wells and propagated for cryogenic storage. During propagation with G418 selection media, the fluorescence intensity became heterogeneous, likely due to loss of gene activity causing cell death. This caused dramatic differences in growth rate between wells, with two colonies disappearing during propagation. The highest density colonies were also the most homogeneous and were cryogenically stored until needed.

4.5 Conclusion and Future Studies

With only one ITC study, optimization of protein and ligand concentrations and the injection volume is necessary to obtain higher quality data, and further binding studies with PA-dT_{10} must be repeated. Initial results show a marked, but expected decrease in affinity for albumin when comparing PA-dT_{10} to that of free palmitic acid. Compared to insulin detemir, the PA-dT_{10} possesses 5-fold higher affinity than the clinically approved insulin conjugate, which may further prolong circulation half-life in humans. To elucidate the affect of charge interactions in binding to albumin, PA-dT_{10} analogs are currently being synthesized without anionic charge or with a cationic charge. Utilizing the current solid phase synthetic scheme shown in **Figure 4-7**, alterations in cleavage condition can produce the desired analogs depicted in **Figure 4-10**. The solid phase chemistry presented in **Section 4.3.3** and will be continuously studied in the principal investigator's lab in the future.

Luc-705 splice expression was never used in the present study, because it was decided to use an endogenous oncogenic slicing variant Bcl-xL expressed in many human and immortalized cell lines. Discussed in **Chapter III**, the discovery and characterization of the Bcl-xL oncogene offers a viable therapeutic target for clinical applications that negated the utility of the Luc-705 expression system to test for splice shifting strategies using endogenous albumin as a carrier.

Currently, an ongoing focus in the Cho lab is to characterize the importance of ionic interactions to modulate albumin binding. Incremental increases in binding affinity should be directly related to prolonged circulation of any ODN conjugated to the α-aminopalmitic acid ligand. Indeed, preliminary binding studies does reveal a decrease or loss of binding affinity when the anionic charge is removed or altered, as shown in **Figure 4-11**. Understanding the mechanism of protein binding may alter and enhance future fatty acid analogs manufactured in the lab for upcoming pharmacokinetic studies in the rodent model.

K_1 (10^8 M^{-1})	K_2(10^7 M^{-1})	K_3(10^7 M^{-1})	Literature
1.04	4.60	2.90	Bojesen, 1992
1.53	12.2	7.50	Richeri *et al*, 1993
1.48	3.40	3.40	Rose *et al*., 1994

Figure 4-1. Range of albumin binding affinity, K_A, values obtained for palmitate at the three highest binding sites at 37º C using three different techniques. The values were used as reference to analyze loss of affinity for the PA-dT_{10} conjugate.

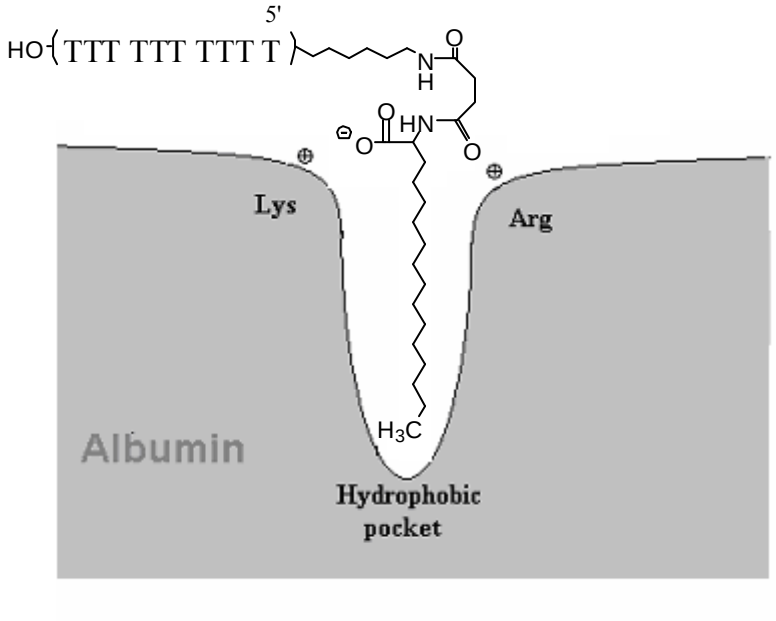

Figure 4-2. Schematic illustration of albumin binding of PA-dT_{10}. The α-aminopalmitic acid is bound in the pocket of albumin while the oligonucleotide extends out of the protein surface. Note that this construct preserves the free carboxylate, allowing electrostatic interactions toward cationic charges lining the hydrophobic pockets of albumin.

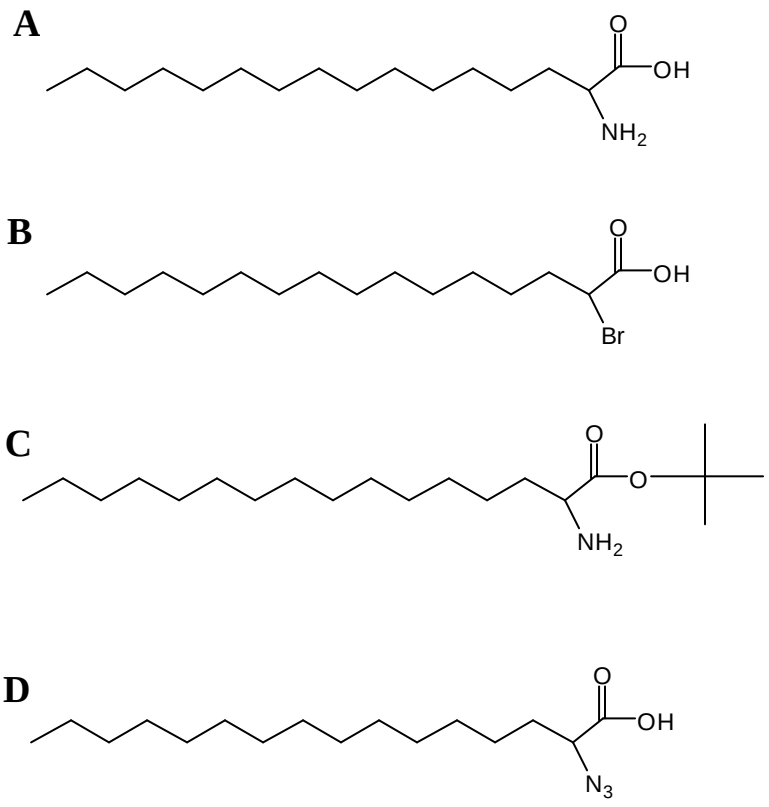

Figure 4-3. List of palmitic acid derivatives purchased or synthesized. (A) The α-aminopalmitic acid was previously synthesized but is insoluble in almost all solvents of interest, which limits its utility as a ligand. (B) The α-bromopalmitic acid is commercially available ((Aldrich cat. # 238422) and used as the starting material. (C) Structure of t-Butyl, α-Aminopalmitate, **3**, the final product from solution synthesis described in **Section 4.3.2**. (D) The α-azidopalmitic acid synthesized in solution prior to attachment to Wang resin.

Step 1: t-Butyl Protection via DCC Coupling

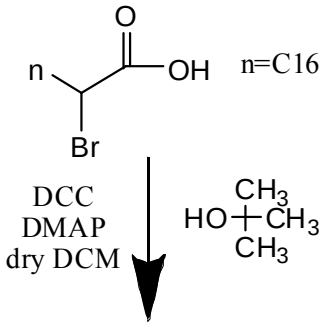

Step 2: Gabriel Synthesis

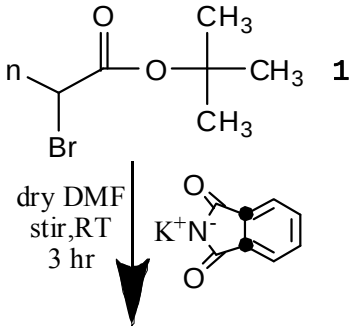

Step 3: Ing-Manske Procedure

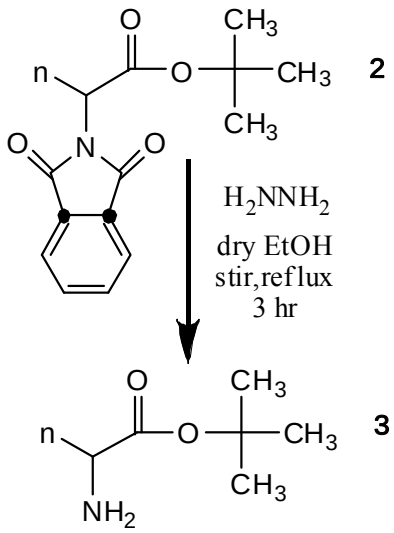

Figure 4-4. Synthetic scheme for t-butyl α -aminopalmitate (**3**) from commercially available α-bromopalmitic acid. The three step synthesis from **Section 4.3.2** is outlined along with the intermediate.

Step 1: t-Butyl Protection via DCC Coupling: t-Butyl protection of bromopalmitic acid was synthesized using DCC (1:1.2) as a coupling agent. A catylatic amount of DMAP will be added the dry DCM. The reaction mixture was stirred at RT and followed via TLC (10% EtoAc/90% Hexanes) until PA reactant spot disappeared. The reaction mixture was filtered to remove DCU and then extracted 6x in ethyl acetate/brine. The organic phase was dried, then concentrated under pressure. The crude product was passed through a 1.5'x20' silica gel (230-400 mesh) column for separation of 2-bromo t-butyl palmitate, 1 . A sample of the product was analyzed and verified via 400 mHz proton NMR.

Step 2: Gabriel Synthesis: Displacement of the bromide ion by phthalimide was followed via TLC until compound 1 reactant spot disappears. The excess potassium phthalimide was filtered and filtrate dried, concentrated under vacuum then extracted 6x in ethyl acetate/brine.

Step 3: Ing-Manske Procedure: The phthalimide intermediate is cleaved using excess hydrazine under reflux conditions (65°C) in ethanol. The reaction was followed via TLC (5% propanol/10% NH4OH sat. ethyl acetate/85% hexanes) until Compound 2 dissappeared. The precipitate was filtered off and the filtrate dried, then evaporated under vacuum. Solvent extraction, column chromatography and NMR validation is same as step 1. The product was stored in an amber vial, under argon in a desiccator until needed.

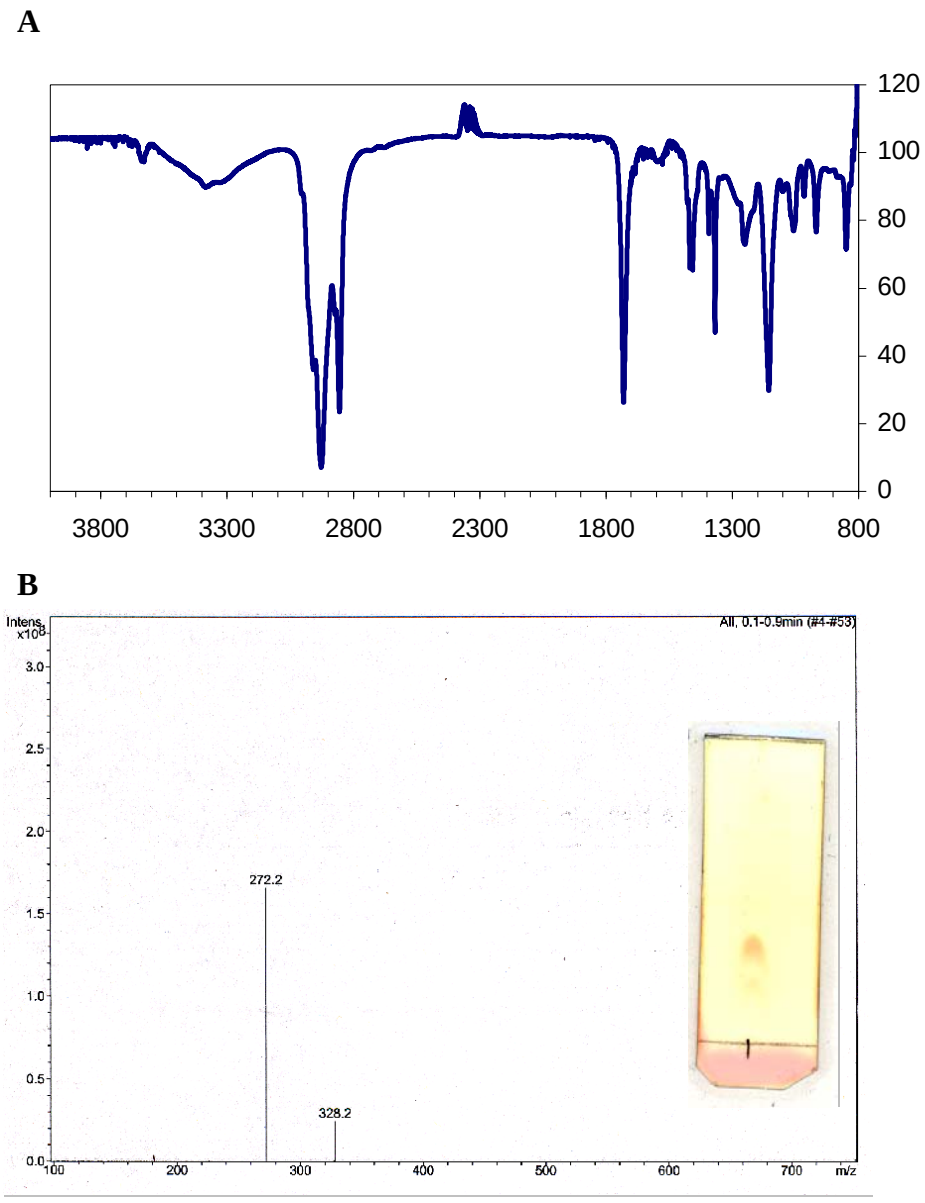

Figure 4-5. Analysis of t-butyl aminopalmitate (**3**) using FT-IR and ESI-MS^n spectroscopy. (A) FT-IR spectrum identifying the double stretching of a primary amine at 3200-3500 cm^{-1}.(B) Mass spectrum from ESI-MS^n identifies two molecules. The 328 m/z corresponds to compound **3** mass of 327+1H while the 272 m/z match to deprotected aminopalmitic acid at 271+1H. Although the sample was purified, as seen in the TLC insert, the t-butyl ester may be labile during electrospray ionization.

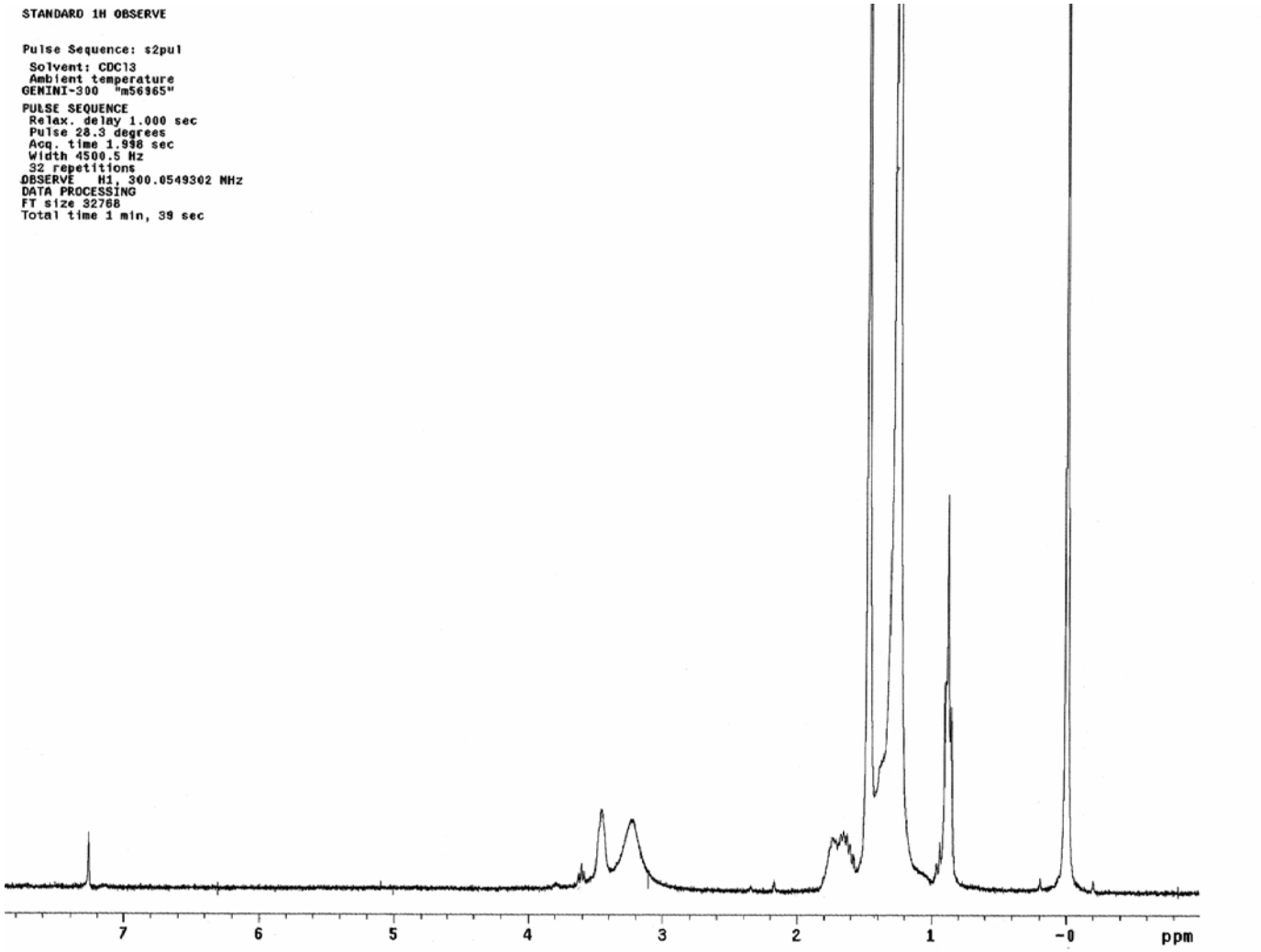

Figure 4-6. ^{1}H-NMR spectra of compound **3**. All chemical shifts were identified ($CDCL_3$, 300 mHz) δ 3.45 (1H, m), 1.7 (2H, m), 1.4 (9H, s), 1.3 (26H, m), 1.0 (2H, m).

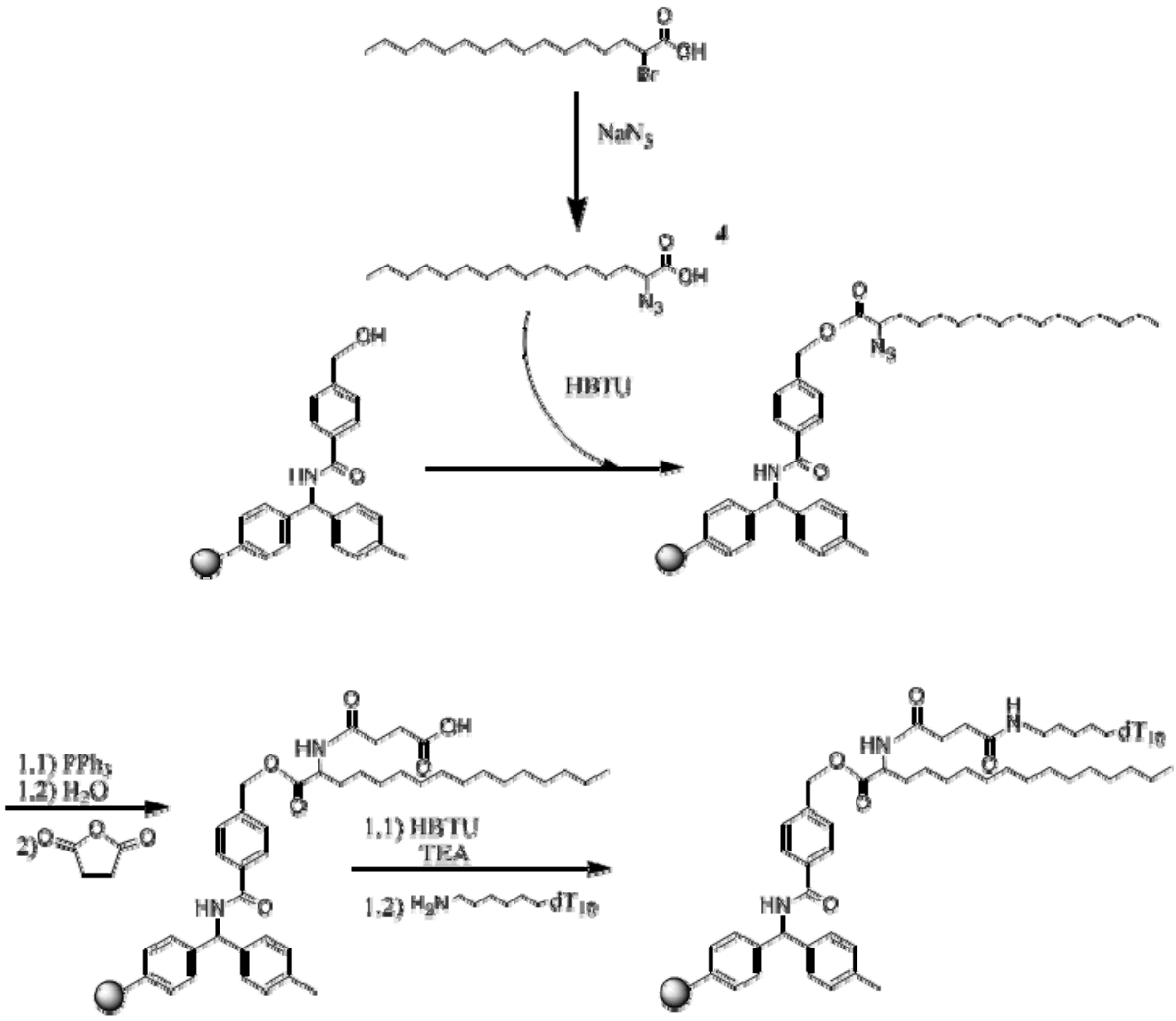

Figure 4-7.General solid phase synthesis of PA-dT_{10} conjugate. As described in Section **4.3.3**, starting material α-bromopalmitic acid was converted to 4 with 96% yield. Compound **4** was activated with HBTU and conjugated to the Wang resin with 44% loading efficiency determined using the Gisin procedure. The azide moiety was reduced to an amine and reacted to succinic anhydride until ninhydrin tested negative. The succinic acid was activated with HBTU and 5' amino-C6-dT_{10} introduced to the resin. Cleavage of PA-dT_{10} was performed using 1 N NaOH for 15 minutes at RT and HPLC purified. Multiple batch yields ranged from 10-15% of final product based on available free amine immobilized on Wang resin.

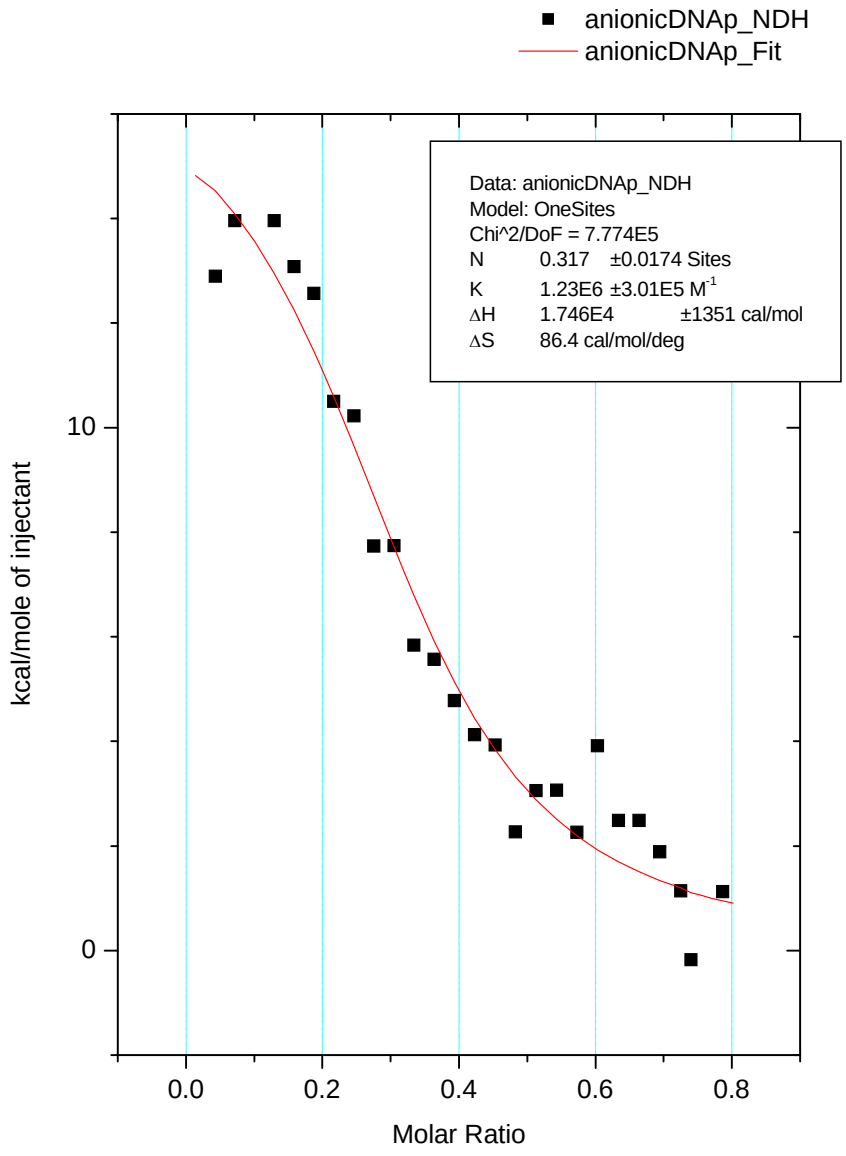

Figure 4-8. Binding analysis of PA-dT_{10} conjugate to delipidated bovine albumin using ITC. The experimental K_A was 1.23 x 10^6 M^{-1}, roughly 100 fold less than that of free palmitic acid.

Well 1

Well 2

Well 3

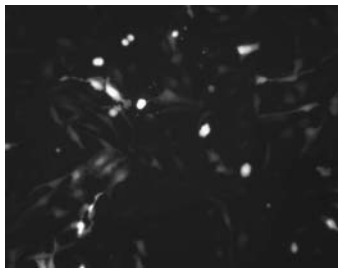

Well 4

Well 9

Well 10

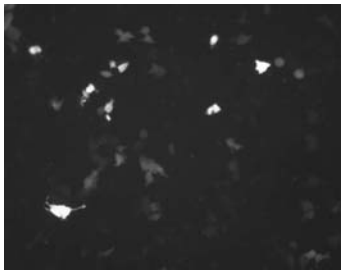

Well 11

Figure 4-9. Stably cotransfected B16 F10 cells were cloned in a 12-well plate containing 400 μg/ml of G418 selection antibiotic. Two colonies were lost during propagation and three lost EGFP fluorescence. The highest density colonies in well nine and ten were also the most homogeneous and were cryogenically stored until needed.

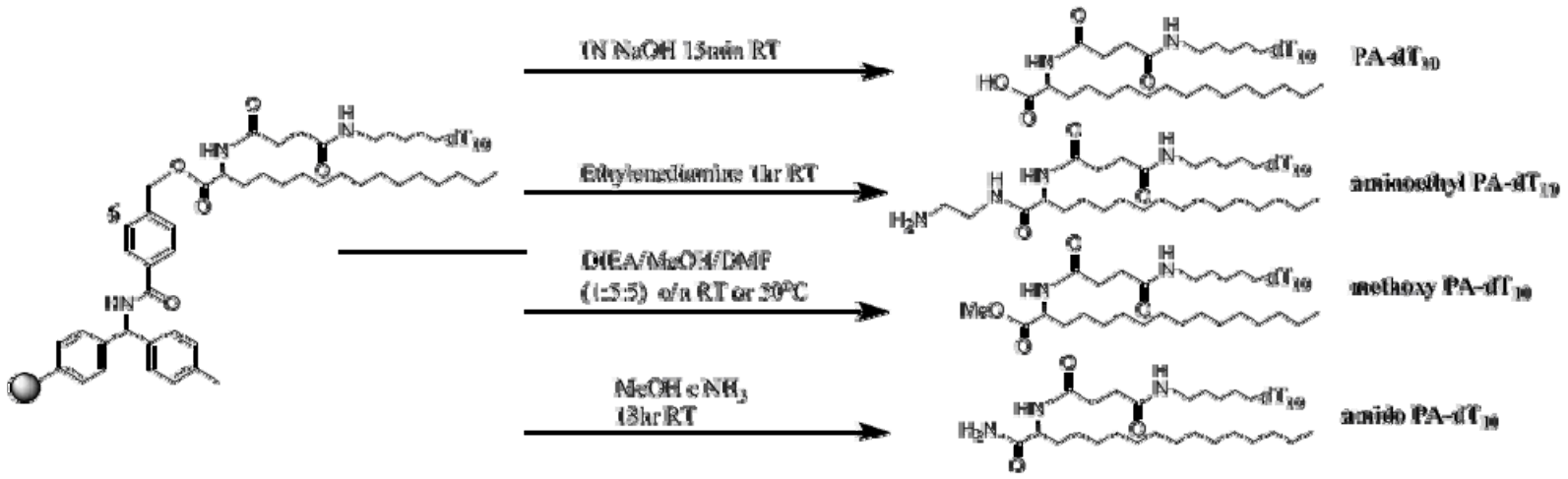

Figure 4-10. Analogs produced from alterations in cleavage conditions. The PA-dT_{10} is cleaved from the resin with NaOH treatment. The cationic analog, aminoethyl PA-dT_{10} is produced using ethylene diamine treatment. Two analogs without charge are produced using ammonium saturated methanol or diisopropylethylamine treatment to produce amido PA-dT_{10} or methoxy PA-dT_{10}.

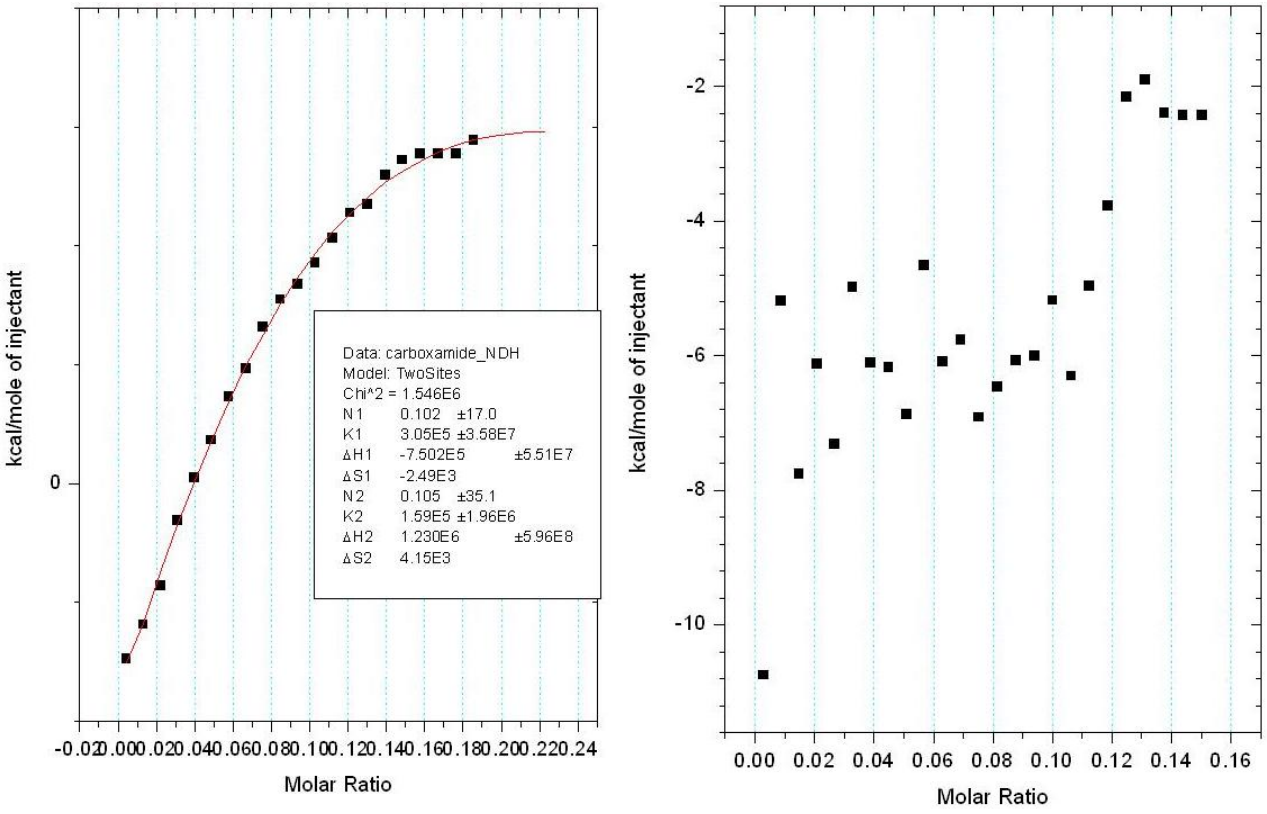

Figure 4-11. Preliminary binding analysis of (A) amido-PA-dT_{10} and (B) aminoethyl-PA-dT_{10} to delipidated bovine albumin. The experimental K_A for amido-PA-dT_{10} was 3.05 x 10^5 M^{-1}. Computer regression using Origin® 8.0 software could not fit a binding curve for aminoethyl-PA-dT_{10}.

4.6 References

A. A. Bhattacharya, T. Grune, and S. Curry. Crystallographic analysis reveals common modes of binding of medium and long-chain fatty acids to human serum albumin. J Mol Biol. 303:721-732 (2000).

M. K. Bijsterbosch, E. T. Rump, R. L. De Vrueh, R. Dorland, R. van Veghel, K. L. Tivel, E. A. Biessen, T. J. van Berkel, and M. Manoharan. Modulation of plasma protein binding and in vivo liver cell uptake of phosphorothioate oligodeoxynucleotides by cholesterol conjugation. Nucleic Acids Res. 28:2717-2725 (2000).

I. N. Bojesen and E. Bojesen. Water-phase palmitate concentrations in equilibrium with albumin-bound palmitate in a biological system. J Lipid Res. 33:1327-1334 (1992).

E. Bonfils, C. Depierreux, P. Midoux, N. T. Thuong, M. Monsigny, and A. C. Roche. Drug targeting: synthesis and endocytosis of oligonucleotide-neoglycoprotein conjugates. Nucleic Acids Res. 20:4621-4629 (1992).

A. T. Chemmanur and G. Y. Wu. Drug evaluation: Albuferon-alpha--an antiviral interferon-alpha/albumin fusion protein. Curr Opin Investig Drugs. 7:750-758 (2006).

D. P. Cistola. Fat sites found! Nat Struct Biol. 5:751-753 (1998).

S. Curry, P. Brick, and N. P. Franks. Fatty acid binding to human serum albumin: new insights from crystallographic studies. Biochim Biophys Acta. 1441:131-140 (1999).

S. Curry, H. Mandelkow, P. Brick, and N. Franks. Crystal structure of human serum albumin complexed with fatty acid reveals an asymmetric distribution of binding sites. Nat Struct Biol. 5:827-835 (1998).

E. J. Demant, G. V. Richieri, and A. M. Kleinfeld. Stopped-flow kinetic analysis of long-chain fatty acid dissociation from bovine serum albumin. Biochem J. 363:809-815 (2002).

N. Desai, V. Trieu, Z. Yao, L. Louie, S. Ci, A. Yang, C. Tao, T. De, B. Beals, D. Dykes, P. Noker, R. Yao, E. Labao, M. Hawkins, and P. Soon-Shiong. Increased antitumor activity, intratumor paclitaxel concentrations, and endothelial cell transport of cremophor-free,

albumin-bound paclitaxel, ABI-007, compared with cremophor-based paclitaxel. Clin Cancer Res. 12:1317-1324 (2006).

E. R. Gardner, W. L. Dahut, C. D. Scripture, J. Jones, J. B. Aragon-Ching, N. Desai, M. J. Hawkins, A. Sparreboom, and W. D. Figg. Randomized crossover pharmacokinetic study of solvent-based paclitaxel and nab-paclitaxel. Clin Cancer Res. 14:4200-4205 (2008).

B. F. Gisin. The monitoring of reactions in solid-phase peptide synthesis with picric acid. Anal Chim Acta. 58:248-249 (1972).

F. Kratz, R. Muller-Driver, I. Hofmann, J. Drevs, and C. Unger. A novel macromolecular prodrug concept exploiting endogenous serum albumin as a drug carrier for cancer chemotherapy. J Med Chem. 43:1253-1256 (2000).

F. Kratz, A. Warnecke, K. Scheuermann, C. Stockmar, J. Schwab, P. Lazar, P. Druckes, N. Esser, J. Drevs, D. Rognan, C. Bissantz, C. Hinderling, G. Folkers, I. Fichtner, and C. Unger. Probing the cysteine-34 position of endogenous serum albumin with thiol-binding doxorubicin derivatives. Improved efficacy of an acid-sensitive doxorubicin derivative with specific albumin-binding properties compared to that of the parent compound. J Med Chem. 45:5523-5533 (2002).

F. Kratz. Albumin as a drug carrier: Design of prodrugs, drug conjugates and nanoparticles. J Control Release. (2008).

P. Kurtzhals, S. Havelund, I. Jonassen, B. Kiehr, U. D. Larsen, U. Ribel, and J. Markussen. Albumin binding of insulins acylated with fatty acids: characterization of the ligand-protein interaction and correlation between binding affinity and timing of the insulin effect in vivo. Biochem J. 312 (Pt 3):725-731 (1995).

P. Kurtzhals, S. Havelund, I. Jonassen, and J. Markussen. Effect of fatty acids and selected drugs on the albumin binding of a long-acting, acylated insulin analogue. J Pharm Sci. 86:1365-1368 (1997).

M. C. Kushlan, J. L. Gollan, W. L. Ma, and R. K. Ockner. Sex differences in hepatic uptake of long chain fatty acids in single-pass perfused rat liver. J Lipid Res. 22:431-436 (1981).
D. M. Lambert. Rationale and applications of lipids as prodrug carriers. Eur J Pharm Sci. 11 Suppl 2:S15-27 (2000).

J. P. Malkinson, R. A. Falconer, and I. Toth. Synthesis of C-terminal glycopeptides from resin-bound glycosyl azides via a modified Staudinger reaction. J Org Chem. 65:5249-5252 (2000).

J. Markussen, S. Havelund, P. Kurtzhals, A. S. Andersen, J. Halstrom, E. Hasselager, U. D. Larsen, U. Ribel, L. Schaffer, K. Vad, and I. Jonassen. Soluble, fatty acid acylated insulins bind to albumin and show protracted action in pigs. Diabetologia. 39:281-288 (1996).

P. L. Porter, E. H. Sage, T. F. Lane, S. E. Funk, and A. M. Gown. Distribution of SPARC in normal and neoplastic human tissue. J Histochem Cytochem. 43:791-800 (1995).

R. G. Reed. Ligand-binding properties of albumin Parklands: Asp365----His. Biochim Biophys Acta. 965:114-117 (1988).

H. Rose, M. Conventz, Y. Fischer, E. Jungling, T. Hennecke, and H. Kammermeier. Long-chain fatty acid-binding to albumin: re-evaluation with directly measured concentrations. Biochim Biophys Acta. 1215:321-326 (1994).

N. L. Rosi, D. A. Giljohann, C. S. Thaxton, A. K. Lytton-Jean, M. S. Han, and C. A. Mirkin. Oligonucleotide-modified gold nanoparticles for intracellular gene regulation. Science. 312:1027-1030 (2006).

E. T. Rump, R. L. de Vrueh, L. A. Sliedregt, E. A. Biessen, T. J. van Berkel, and M. K. Bijsterbosch. Preparation of conjugates of oligodeoxynucleotides and lipid structures and their interaction with low-density lipoprotein. Bioconjug Chem. 9:341-349 (1998).

J. E. Schnitzer and J. Bravo. High affinity binding, endocytosis, and degradation of conformationally modified albumins. Potential role of gp30 and gp18 as novel scavenger receptors. J Biol Chem. 268:7562-7570 (1993).

B. J. Smith, A. Popplewell, D. Athwal, A. P. Chapman, S. Heywood, S. M. West, B. Carrington, A. Nesbitt, A. D. Lawson, P. Antoniw, A. Eddelston, and A. Suitters. Prolonged in vivo residence times of antibody fragments associated with albumin. Bioconjug Chem. 12:750-756 (2001).

G. Stehle, H. Sinn, A. Wunder, H. H. Schrenk, J. C. Stewart, G. Hartung, W. Maier-Borst, and D. L. Heene. Plasma protein (albumin) catabolism by the tumor itself--implications for tumor metabolism and the genesis of cachexia. Crit Rev Oncol Hematol. 26:77-100 (1997).

G. Stehle, A. Wunder, G. Hartung, and H. Sinn. Albumin synthesis rates in cachectic cancer patients with an ongoing acute-phase protein response. Ann Surg. 228:720 (1998).

C. W. Tornoe, P. Davis, F. Porreca, and M. Meldal. Alpha-azido acids for direct use in solid-phase peptide synthesis. J Pept Sci. 6:594-602 (2000).

A. Wunder, G. Stehle, H. H. Schrenk, G. Hartung, D. L. Heene, W. Maier-Borst, and H. Sinn. Antitumor activity of methotrexate-albumin conjugates in rats bearing a Walker-256 carcinoma. Int J Cancer. 76:884-890 (1998).

Chapter V

CONCLUSION

The present dissertation describes two distinct macromolecular carrier systems to deliver therapeutic oligonucleotides to solid tumors. The focus of **Chapter I** is to present a snapshot of the current and applied delivery strategies using various nanoparticles, along with existing difficulties in utilizing nucleic acid-based medicine as viable therapies in humans. In **Chapter II**, the development of a colloidal gold-based carrier is explored utilizing oligonucleotides as a modular linker to hybridize an array of targeting ligands or therapeutic oligonucleotides. **Chapter III** is the continuation of developing a gold colloid based delivery system using therapeutic oligonucleotides and studying the splice shifting affects in human nasal-pharyngeal derived KB carcinoma. Finally, **Chapter IV** starts a new project developing a system to utilize long circulating endogenous albumin as carriers for oligonucleotide delivery to tumors.

Development of colloidal gold-based oligonucleotide carriers is an offshoot to the first study published in *Science* with anti-sense oligonucleotide complexed to gold nanoparticles and effectively knocking down translation of the target mRNA (Rosi et al. 2006). In this system, the oligonucleotide is stably complexed to gold through four thiols, strategizing that targeted mRNA translation is sterically inhibited by gold conjugate through avidity, without releasing the oligonucleotide from the gold surface. The approach used in **Chapter II** is to conjugate the gold particle with non-therapeutic oligonucleotides and hybridize siRNA or

targeting ligands to these oligomers. The complementary ligands were incorporated with PEG to increase systemic stability of the gold nanoparticle, as seen in TNFα-conjugated gold nanoparticles (Paciotti et al. 2004). To analyze the loading efficiency of complementary ligands, BODIPY FL was linked to a PEG_{900} through a disulfide linker as a probe to measure the maximal number of targeting ligand and therapeutic oligonucleotides available for 10-nm gold particles. The low availability of payload, approximately six binding sites, disfavored further development using this strategy. To overcome the low cargo capacity seen in **Chapter II**, the therapeutic oligomer SSO against Bcl-xL was directly conjugated to the surface of gold nanoparticles, providing a larger carrier capacity of 60 to each 10 nm gold nanoparticle. Since thiol exchange occurs in the reductive environment of the cytosol, the therapeutic SSO should release and exert a pharmacologic response without further modifications (Hong et al. 2006). The therapeutic oligomer would also act as the modular linker to hybridize a targeting ligand for active uptake into targeted cancer cells. Folic acid was chosen for its ability to endocytose and release into the cytosol of folate receptor expressing cancer cells (Yang et al. 2006). **Chapter III** successfully developed a gold nanoparticle based carrier incorporating 60 splice shifting oligonucleotides as the modular linker hybridized to seven folic acid targeting ligands. This system was tested in KB cells conditioned to overexpress the folate receptor, but was not able to significantly alter expression of the Bcl-xL oncogene. The preliminary study revealed very limited splice correction using the folic acid targeting SSO-AuNP, which warrants further studies to elucidate why a pharmacologic response did not occur in the cell culture.

Overall, the successful synthesis of oligonucleotide ligands hybridized to AuNP provides a flexible opportunity to analyze and modify the DNA based modular gold

nanoparticle in order to increase cargo capacity. Utilizing the methods stated in **Section 5.2** holds much promise in developing a 10 to 50 nm sized macromolecular delivery carrier, whether the core scaffold is gold, polymer, or biological-based. The key ingredients are there to modify any system for active targeting and controlled release. The methodology developed in this dissertation is proven by multiple analytical methods and should be applicable for other nanoparticle carriers as well.

The albumin based delivery strategy developed in **Chapter IV** is unlike that of the above approaches, as the carrier is an endogenous protein, which appears to act as a nutrient for cancer cells (Stehle et al. 1997). Six high affinity fatty acid binding sites have been characterized on albumin, offering a natural binding mechanism to tether oligonucleotides via fatty acid linkers (Curry et al. 1999). Described in **Chapter IV,** a palmitic acid analog, α-aminopalmitic acid (compound **3)**, was successfully synthesized which retains the hydrophobic and ionic charge interactions necessary to bind tightly to albumin. The linker was conjugated via the amino group to a probe oligonucleotide (PA-dT_{10}) and binding analyzed using an isothermal titration calorimeter to measure the binding constant between the PA-dT_{10} and that of fatty acid free bovine serum albumin. Preliminary results confirm binding in the order of $1x\ 10^6\ M^{-1}$ association constant, roughly 100-fold than that of free palmitic acid. While significantly less than the free fatty acid, the PA-dT_{10} possess higher affinity than the current clinically approved albumin binding strategy utilized *in insulin detemir*. Ongoing studies to characterize the importance of ionic interactions may develop an enhanced fatty acid analog with greater affinity to albumin. The rationale to maximize binding affinity should lead to sustained circulation mimicking that of endogenous albumin, with a half-life of 19 days in humans. No further discussion is necessary regarding the

albumin based delivery system. This project has been passed to the next generation of graduate students and has progressed rapidly with renewed ambition and soon to be published results.

5.1 References

S. Curry, P. Brick, and N. P. Franks. Fatty acid binding to human serum albumin: new insights from crystallographic studies. Biochim Biophys Acta. 1441:131-140 (1999).

R. Hong, G. Han, J. M. Fernandez, B. J. Kim, N. S. Forbes, and V. M. Rotello. Glutathione-mediated delivery and release using monolayer protected nanoparticle carriers. J Am Chem Soc. 128:1078-1079 (2006).

G. F. Paciotti, L. Myer, D. Weinreich, D. Goia, N. Pavel, R. E. McLaughlin, and L. Tamarkin. Colloidal gold: a novel nanoparticle vector for tumor directed drug delivery. Drug Deliv. 11:169-183 (2004).

N. L. Rosi, D. A. Giljohann, C. S. Thaxton, A. K. Lytton-Jean, M. S. Han, and C. A. Mirkin. Oligonucleotide-modified gold nanoparticles for intracellular gene regulation. Science. 312:1027-1030 (2006).

G. Stehle, H. Sinn, A. Wunder, H. H. Schrenk, J. C. Stewart, G. Hartung, W. Maier-Borst, and D. L. Heene. Plasma protein (albumin) catabolism by the tumor itself--implications for tumor metabolism and the genesis of cachexia. Crit Rev Oncol Hematol. 26:77-100 (1997).

J. Yang, H. Chen, I. R. Vlahov, J. X. Cheng, and P. S. Low. Evaluation of disulfide reduction during receptor-mediated endocytosis by using FRET imaging. Proc Natl Acad Sci U S A. 103:13872-13877 (2006).

Appendix I. Concentration Dependant Uptake of FITC-PEG-Folate (FL-FA)

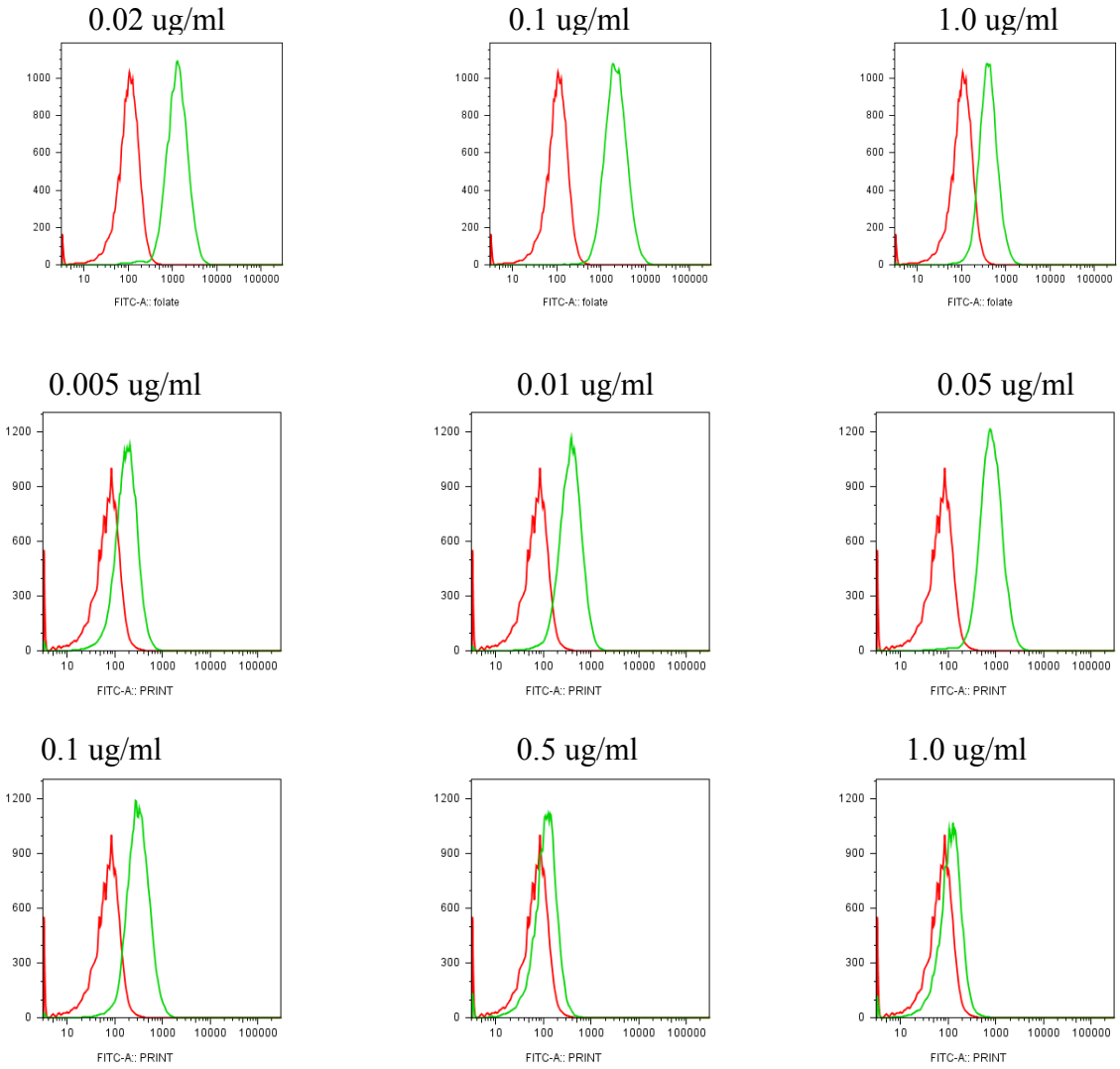

Initial folate receptor validation techniques used 0.02, 0.1 and 1.0 ug/ml of FL-FA as a positive control. The 0.1 ug/ml concentration showed the highest uptake from the past flow studies, seen in the first row. Further studies reveal concentration dependant binding in cell culture and possible down-regulation of folate receptor at higher concentrations. The highest FL-FA fluorescence was observed at 0.05 ug/ml conc. Overall, FL-FA concentration at 0.01-0.1 ug/ml yield best results. This correlates to folate concentrations from 2.6 to 26 nM.